Role of P2Y12 Receptor-mediated ADP Signalling at Microglia in the Phagocytosis of Neurons

Michiko O. Inouye

Dissertation submitted for the degree of

Master of Philosophy in Biological Science

at the University of Cambridge, Department of Biochemistry

Wolfson College

June 2018

Abstract

Despite the prevalence of neurodegenerative disorders such as Parkinson's and Alzheimer's diseases, surprisingly little is known about the molecular mechanisms governing widespread neuronal loss observed in these conditions. Recent studies, however, have linked heightened microglial phagocytosis of live neurons under inflammatory stimuli such as amyloid-β and lipopolysaccharide (LPS) to this loss. The ADP-specific microglial receptor P2Y12 has been implicated in long-range communication between neurons and microglia, as well as in microglia chemotaxis preceding phagocytosis, but the direct role of this receptor in phagocytosis of live neurons has not been addressed. In addition, P2Y12 antagonists have already been established in the clinic as treatments for thrombosis, and whether these inhibitors could further serve a neuroprotective purpose by preventing phagocytosis was speculated. Upon examining the effect of P2Y12 inhibition using the competitive antagonist PSB0739, and P2Y12 genetic knockdown on phagocytosis of neuroblast-like, naïve PC12 targets by LPS-activated BV-2 microglia through a combination of flow cytometry and microscopy analyses, I show that P2Y12 perturbation does not affect microglial phagocytosis of neuronal targets under LPS stress. However, P2Y12 disruption led to significant decreases in phagocytosis of bead and neuronal targets under unstimulated conditions, which suggested that P2Y12 plays an important role in the phagocytic mechanisms of resting microglia. Additionally, fluorescent calcium response assays yielded significant decreases in acute calcium response to ADP in P2Y12-inhibited and knockdown cells, confirming that P2Y12 plays a major role in calcium mobilization due to ADP treatment in BV-2 microglia. Furthermore, examination of the role of ADP on the regulation of P2Y12 mRNA expression using reverse transcription-quantitative polymerase chain reaction (RT-qPCR) led to the finding that P2Y12 expression is reduced in response to high concentrations of ADP. These findings highlight the novel ideas that 1) the P2Y12 receptor has functional roles in phagocytosis of basal microglia besides cell migration, and 2) persistent imbalance of ADP in the extracellular environment affects P2Y12 expression, which may underlie inflammatory stimuli-induced P2Y12 downregulation in the transition from resting to highly phagocytic, disease-associated microglia.

Acknowledgements

First and foremost, I would like to thank my supervisor, Professor Guy Brown for this rare and highly fruitful experience conducting research on microglial phagocytosis and learning techniques of RT-qPCR, calcium assays, flow cytometry and microscopy at his laboratory. I am grateful for his supervision and guidance throughout my year as an MPhil Student. Thank you so much to all members of the laboratory, Dr. Miguel Burguillos, Dr. Mar Puigdellívol Cañadell, Dr. Anna Vilalta, David Allendorf, Tom Cockram, and Claire Butler for their advice on research direction and technical skills, as well as for their continuous support. I also greatly appreciate the valuable feedback from my advisor, Professor Svetlana Khoronenkova. I would like to extend a big thank you to the other two members of my Graduate Thesis Panel, Professor Sarah Lummis and Professor Aviva Tolkovsky, for their advice during the middle of my thesis period. Lastly I would like to thank my parents and friends for their support.

Declaration

This dissertation is the result of my own work and includes nothing which is the outcome of work done in collaboration except where specifically indicated in the text. It is not substantially the same as any that I have submitted, or, is being concurrently submitted for a degree or diploma or other qualification at the University of Cambridge or any other University or similar institution except as specified in the text. I further state that no substantial part of my dissertation has already been submitted, or, is being concurrently submitted for any such degree, diploma or other qualification at the University of Cambridge or any other University or similar institution except as specified in the text. This thesis does not exceed the word limit (20,000 words) for the MPhil dissertation set by the Degree Committee for the Faculty of Biology at the University of Cambridge.

TABLE OF CONTENTS

List of Abbreviations

A2A Adenosine A2A receptor

Aβ Amyloid-beta

ADP Adenosine diphosphate

AIDS Acquired Immune Deficiency Syndrome

Akt Protein kinase B

ALS Amyotrophic Lateral Sclerosis

AMP Adenosine monophosphate

AMPK Adenosine monophosphate-activated protein kinase

ANOVA One-way analysis of variance

ATP Adenosine-5'-triphosphate

BSA Bovine serum albumin

BV-2 Immortalized mouse microglial cell line infected with v-raf/v-myc containing retrovirus

C Celsius

Cathepsin B Cysteine protease B

CD11B/CD29 Integrin alpha M β_1

CD39 NTPDase1

CD73 5'-nucleotidase

Cox2 Cyclooxygenase 2

cRGDfV Cyclo(Arg-Gly-Asp-D-Phe-Val)

CytD Cytochalasin D

dH_2O Distilled water

DMEM Dulbecco's modified eagle's medium

DMSO Dimethyl sulfoxide

dNTP Deoxynucleotide triphosphates

DTT Dithiothreitol

EC_{50} Half maximum effective concentration

ER Endoplasmic reticulum

ERK Extracellular signal-regulated kinase

FBS Fetal bovine serum

FL1 Flow cytometer interference filter, detects 533±30nm, green channel

FL3 Flow cytometer interference filter, detects >670nm, red channel

FSC Forward scatter

Gal3 Galectin-3

GABA Gamma-aminobutyric acid

gDNA Genomic deoxyribonucleic acid

GPCR G protein-coupled receptor

h hour(s)

HS Horse serum

HSD honestly significant difference (from Tukey's test)

IB4 Isolectin-B4-Alexa-Fluor-488

Iba1 Calcium binding adapter molecule 1

IFN-γ Interferon gamma

IL-1β Interleukin 1-beta

iNOS Nitric oxide synthase

InsP3 Inositol 1,4,5-triphosphate

IRF8 Interferon regulatory factor 8

JNK1/2 c-Jun N-terminal kinase 1 and 2

Ki Inhibitor constant

LPS Lipopolysaccharide

LRP Lipoprotein receptor-related protein

MAPK Mitogen-activated protein kinase

MerTK Proto-oncogene tyrosine protein kinase MER

Mfge8 Milk fat globule-EGF factor 8

2MeSADP 2-methylthio-ADP

min minute

mRNA Messenger ribonucleic acid

NFκB Nuclear factor kappa-light-chain-enhancer of activated B cells

NMDA N-methyl-D-aspartate

NO Nitric oxide

NPP1 Pyrophosphatase

ns not significantly different

NT Non-target siRNA-transfected

P2Y12 Purinergic 2Y receptor 12

P2X7 Purinergic 2X receptor 7

PBS Phosphate buffered saline

PC12 Cell line derived from pheochromocytoma of rat adrenal medulla

PFA Paraformaldehyde

PGC-1α Peroxisome proliferator-activated receptor gamma coactivator 1-alpha

PHOX Nicotinamide adenine dinucleotide phosphate oxidase complex

PI3K Phosphoinositide-3-kinase

PKC Protein kinase C

PLC Phospholipase C

PMA Phorbol 12-myristate 13-acetate

PSB0739 1-Amino-9,10-dihydro-9,10-dioxo-4-[[4-(phenylamino)-3-sulfophenyl]amino]-2-anthracenesulfonic acid sodium salt

PtdSer Phosphatidylserine

PU.1 PU-box binding transcription factor

s seconds

SEM Standard error of the mean

SIP Sample Injection Port

siRNA Small interfering ribonucleic acid

SIRT1 Sirtuin 1

SSC Side scatter

STS Staurosporine

RNA Ribonucleic acid

RNAi RNA interference

RPMI Roswell park memorial institute medium

RT-qPCR Reverse transcription quantitative polymerase chain reaction

TAMRA 5-(and 6)-carboxytetramethylrhodamine succinimidyl ester

TLR Toll-like receptors

TNF-α Tumor necrosis factor alpha

TREM-2 Triggering receptor expressed on myeloid cells 2

Trypsin-EDTA Trypsin- ethylenediaminetetraacetic acid

TYROBP (aka DAP12) Tyrosine kinase-binding protein

UDP Uridine diphosphate

Unt Untreated

VNR Vitronectin receptor

% w/v Percent of weight of solution in the total volume of solution

Introduction

Neurodegenerative diseases are marked by widespread neuronal loss, which is likely mediated by pathological stimulus-induced microglial phagocytosis of neurons

Neurodegenerative disorders are broadly characterized by a progressive and drastic loss of neurons in the brain and/or the spinal cord, which leads to disability in movement (i.e. Parkinson's disease, motor neuron disease, spinocerebellar ataxia) or cognitive decline including memory loss (i.e. Alzheimer's disease, Huntington's disease). As most fully matured and differentiated neurons lack the ability to self-renew or proliferate, such a severe decrease in the number of live and functional neurons in the central nervous system is irreversible, rendering affected patients disabled for an entire lifetime. Although the existence of many of these disorders has been known for over a decade, they present difficult hurdles in medicine today, as there is no established cure or definite method of prevention. For these reasons, there is an urgency to better understand the mechanisms underlying this neuronal loss, which must be explored at the molecular level in order to realistically achieve safe, precise, and purposeful clinical treatments to help affected individuals.

Contrary to expectation, despite the widespread loss of neurons in neurodegenerative disorders, this decrease is not necessarily accompanied by greater neuronal cell death, which suggests that neuronal loss is mediated by a mechanism other than apoptosis. This finding has been demonstrated in studies of Alzheimer's disease. For example, Alzheimer's disease-associated lesions were found to have very few numbers of neurons with morphological characteristics of apoptosis, such as cell shrinkage and blebbing (Stadelmann et al., 1998). In transgenic Alzheimer's disease mouse models, caspase-3 activation due to soluble amyloid-beta was observed, but there was no evidence of actual neuronal cell death (D'Amelio et al., 2011). These studies therefore imply that a non-neuronal cell type is facilitating removal of live neurons.

Recent studies have elucidated the ability of microglia to eliminate live and viable neurons by ingestion when activated by an external stimulus, which may explain this neuronal loss. Microglia, first identified by Ramon y Cajal in 1913 and further studied by Pio del Rio Hortega, are recognized as the resident immune cells of the central nervous system. Like macrophages, they have the unique ability to engulf particles (from 0.5μm, to as large as 20μm in diameter via IgG-opsonization) in their surroundings by a process termed phagocytosis (Kreutzberg, 1996; Cannon and Swanson, 1992). Phagocytosis is necessary and beneficial to a certain extent, for instance to facilitate neurodevelopment through clearance of immature neurons and glia to remove redundant synaptic connections (Marin-Teva et al., 2004, Paolicelli et al., 2011, Schafer et al., 2012, Cunningham et al., 2013), as well as to protect neurons from potentially harmful substances such as foreign pathogens (Brown and Neher, 2014). However, in the presence of pathological stimuli, microglia become

activated to an excessive degree, causing them to ingest surrounding neurons at heightened levels, even those which are healthy and viable (Neher et al., 2011). This stimuli-induced phagocytosis results in widespread neuronal and synaptic loss as observed in neurodegenerative diseases.

Strikingly, amyloid-beta (Aβ) has been identified as one such stressor, in which low (nanomolar) concentrations of Aβ were found to indirectly kill neurons through inducing microglial phagocytosis (Neniskyte et al., 2011). Aβ has strong implications in neurodegenerative diseases, as insoluble Aβ accumulation is recognized as one of the hallmarks of the Alzheimer's disease phenotype (Wyss-Coray and Rogers, 2012), and thus this finding of Aβ-induced microglial activation is seminal in linking the induced phagocytosis mechanism to neurodegeneration. Indeed, other studies have suggested the link between microglial phagocytosis and neurodegenerative diseases other than Alzheimer's, namely frontotemporal dementia (Kao et al., 2011), Parkinson's and Amyotrophic Lateral Sclerosis (ALS) (Cunningham et al., 2013; Rogers et al., 2007; Dewil et al., 2007), as well as acquired immune deficiency syndrome (AIDS) dementia (Marker et al., 2012). Similarly, lipopolysaccharide (LPS), a major constituent of bacterial cell walls and a potent inflammatory activator of microglia, was also found to increase phagocytosis of live neurons (Neher et al., 2011), and thus it has been used to investigate microglial phagocytosis in the context of neurodegenerative disease. Importantly, these studies give support to the idea that neurodegenerative disorders involve a pathological stimulus like Aβ or LPS which operates as the inducer of microglial activation. Consequently, this activation drives excessive phagocytosis of neurons, leading to widespread neuronal loss.

The molecular mechanisms governing Aβ and LPS-induced microglial phagocytosis of neurons have been studied thoroughly

The molecular pathways governing Aβ and LPS-induced microglial phagocytosis of neurons have been extensively studied. For simplification, these mechanisms may be summarized by the following sequence: 1) initial recognition of external stimulus and inflammatory activation of microglia, 2) interaction of activated microglia with neuronal targets via ligand-receptor binding, and 3) cytoskeletal rearrangements causing final engulfment. It is important to bear in mind, however, that due to the multitude of signalling factors involved in all three of these steps of phagocytosis, most likely much of the molecular pathways underlying these events occur concurrently.

Regarding the first step, the recognition of Aβ and LPS are mediated by Toll-like receptors (TLR) on microglia cell surfaces. Specifically, Aβ can activate both TLR2 and TLR4 receptors (Reed-Geaghan et al., 2009) while LPS selectively activates TLR4 on microglia (Fitzgerald et al., 2003) through binding of TLR4-associated proteins. It should be noted that, because Aβ can activate two different receptors while LPS can only activate one, the signalling pathways of Aβ-mediated phagocytosis are likely more complex than that of LPS. TLR activation is followed by protein kinase

C (PKC) activation in the cytosol (Combs et al., 1999). The activated PKCs phosphorylate cytosolic subunits of the NADPH oxidase complex (PHOX), which results in the assembly of the whole complex on the microglial cell membrane (Gao et al., 2012; Combs et al., 1999). Active PHOX releases superoxide, while also initiating a complex intracellular signalling pathway which includes phosphoinositide-3-kinase (PI3K) activation, protein kinase B (Akt) phosphorylation, activation of the mitogen-activated protein kinase (MAPK) superfamily (including p38, extracellular signal-regulated kinase (ERK), c-Jun N-terminal kinase 1 and 2 (JNK1/2)), which ultimately serves to activate nuclear factor kappa-light-chain-enhancer of activated B cells (NF-κB) (Saponaro et al., 2012; Kaminska et al., 2009). NF-κB , upon activation, can translocate into the nucleus and act as a transcription factor, which facilitates transcriptional upregulation of inflammation-associated genes, such as those encoding cysteine protease B (cathepsin B), interferon gamma (IFN-γ), tumor necrosis factor (TNF-α), interleukin 1-beta (IL-1β), nitric oxide synthase (iNOS), and cyclooxygenase 2 (Cox2) (Kaminska et al., 2009). These transcriptional upregulations lead to large production of these proteins and release of inflammatory cytokines, notably cathepsin-B, TNF-α, and nitric oxide (NO) in high quantities (Perry and Holmes, 2014).

Although TLR2 and 4 have been recognized as the microglial surface receptors responsible for initiating the Aβ and LPS-mediated signalling pathway described above, the binding of Aβ and LPS to the microglial transmembrane receptor, triggering receptor expressed on myeloid cells 2 (TREM-2), has been reported, suggesting the involvement of TREM-2 in the mechanism (N'Diaye et al., 2009; Jonssen et al., 2013; Zhao et al., 2018; Jones et al., 2014; Guerreiro et al., 2013). TREM-2 has been identified as a significant risk factor for Alzheimer's disease due to its function in facilitating microglial phagocytosis (Hickman and El Khoury, 2014). The signalling downstream of TREM-2 is understood to involve phosphorylation of tyrosine kinase-binding protein (TYROBP, also known as DAP12) and similar to the TLR pathway, leads to the activation of NF-κB and production of reactive oxygen species (Charles et al., 2008).

As a consequence of these signalling pathways and transcriptional changes, a salient phenotypic change has been noted in microglia upon Aβ and LPS exposure. In contrast to the inactive form, characterized by a small cell body with highly branched processes, active microglia take on an amoeboid cell shape, in which their processes are partially retracted to the cell body (Hanisch and Kettenmann, 2007; Ransohoff and Perry, 2009). Besides changes in appearance, activated microglia also exhibit behavioural changes in which they become more motile and proliferate more rapidly, in addition to becoming highly phagocytic (Gomez-Nicola and Perry, 2015). Thus, upon examination of this first step, we find that just the initial binding activity of Aβ and LPS to microglial surface receptors launches a series of intricate signalling cascades, which ultimately widely affects the transcriptional profile of these cells; these changes are clearly manifested in terms of morphological and behavioural differences from the resting state.

Next, regarding the second step of the sequence, these activated microglia recognize and come into contact with neuronal targets by means of ligand-receptor interactions. There are a few different combinations of these interactions that have been elucidated in relation to both Aβ and LPS-induced phagocytosis of live neurons (it should be noted that only the mechanisms associated specifically with phagocytosis of live-but-stressed neurons, distinct from that of apoptotic neurons or bacterial targets, are indicated below).

One recognized combination is the interaction among phosphatidylserine (PtdSer), milk fat globule-EGF factor 8 (Mfge8), and vitronectin receptor (VNR) (Neher et al., 2011; Neniskyte and Brown, 2013; Neniskyte et al., 2011). In activated microglia, released NO (as a result of iNOS upregulation) and superoxide (from activated PHOX) react with one another to produce peroxynitrite (Bal-Price et al., 2002), which subsequently stresses neurons to reversibly expose PtdSer, a phospholipid normally facing the cytosolic side of the cell membrane. Active microglia release the opsonin Mfge8, which binds to PtdSer on the neurons. Mfge8 (now bound to neuronal PtdSer) further binds to the microglia surface receptor VNR, thereby acting as a bridging protein facilitating contact between neurons and microglia (Fuller and Van Eldik, 2008; Akiyama et al., 1991).

Calreticulin and lipoprotein receptor-related protein (LRP) interactions, as well as Proto-oncogene tyrosine protein kinase MER (MerTK) and Galectin-3 (Gal3) interactions also underlie microglia-neuron binding preceding phagocytosis (Fricker et al., 2012). The former is characterized by neuronal exposure of calreticulin, which is recognized by LRP expressed on the microglia cell surface. For the latter, activated microglia are found to release Gal3 along with neuraminidase; Gal3 binds to MerTK expressed on the microglial cell surface, while neuraminidase desialylates both microglial and neuronal surfaces. The desialylation enables the released Gal3 (already bound to microglial MerTK) to bind neurons, and thus allows microglia-neuron contact (Nomura et al., 2017). Further, MerTK-PtdSer interactions via the opsonin Gas6 has been suggested in the phagocytosis of stressed neurons, presenting another interaction mechanism (Neher et al., 2012).

Upon direct interaction between neurons and microglia, the process of engulfment is initiated. It is generally understood that ligand-receptor binding at the microglia membrane as described above, subsequently activates small GTPases such as Rac, which acts together with calcium binding adapter molecule 1 (Iba1), promoting rapid actin polymerization (Ohsawa et al., 2000; Kanazawa et al., 2002) and allowing quick reshaping of the microglial cytoskeleton to position the cell for phagocytosis. Nevertheless, actual engulfment can only occur upon formation of what is termed the “phagocytic cup” in microglia, which describes a crown-like structure rich in F-actins, forming around the target cell. The phagocytic cup formation is regulated by the interaction between uridine diphosphate (UDP) released by stressed neurons, and microglial P2Y6 receptors, which initiates a downstream signalling pathway involving activation of phospholipase C (PLC) and intracellular calcium release (Koizumi et

al., 2007; Neher et al., 2014). This UDP-P2Y6 interaction has been described as the "final engulfment signal" which orchestrates the final step of phagocytosis of live neuronal targets.

Taken together, close examination of Aβ and LPS-mediated phagocytosis of live neurons has highlighted a clear sequence of events, beginning with initial signal recognition of Aβ and LPS by microglia surface receptors, followed by a myriad of downstream signalling cascades. The conglomeration of various factor activations and upregulation of inflammation-associated genes transforms the microglia to a highly phagocytic phenotype. Upon activation, microglia bind surrounding neurons by ligand-receptor interactions, which facilitates intracellular pathways that lead to cytoskeletal rearrangements and final engulfment.

Initial microglia-neuron interactions via ADP-P2Y12 signalling in phagocytosis mechanism is of interest

To explore ways of intercepting the above-mentioned mechanisms to prevent neuronal loss in the presence of stimuli such as Aβ and LPS, it may be most effective and simple to focus on the first interactions between neurons and microglia. More specifically, it is worth examining early communication and asking what can be done to prevent microglia from contacting neurons and registering them as phagocytic targets in the first place. The neuron-microglia interactions mentioned above (PtdSer-Mfge8-VNR, Calreticulin-LRP, MerTK-Gal3, UDP-P2Y6) all likely occur when microglia are already relatively close in proximity to the target neuron. Even the UDP-P2Y6 interaction, which involves a low molecular weight nucleotide which can be thought to easily travel long distances in the extracellular environment, has been found to in fact be a spatiotemporally restrictive signalling mechanism (Koizumi et al., 2013). Given that activated microglia change to an amoeboid morphology and become motile, it is reasonable to assume that in most cases of microglial phagocytosis of neurons, microglia begin at a distance from the target neuron, and upon moving toward the neurons, recognize the aforementioned signals at the neuronal surfaces, which leads into the phagocytosis sequence. Thus, to gain a fuller picture of Aβ and LPS-induced microglia phagocytosis of neurons, the mechanisms governing microglial chemotaxis preceding engulfment are highly relevant and must also be considered. In other words, a crucial question to ask is: do the molecular mechanisms underlying microglial movement have direct implications for phagocytosis?

One potentially important point of connection between microglia movement and phagocytosis is extracellular adenosine-5'-triphosphate (ATP) signalling. In the presence of Aβ, neurons have been found to release ATP, which serves as an early alerting signal to microglia (Inoue 2006; Potucek et al., 2006; Di Virgilio et al., 2009). Further, ATP is understood to be a very potent chemoattractant and an important find-me signal (Dibaj et al., 2010; Elliott et al., 2009; Chekeni et al., 2010). Indeed, in comparison to UDP which is also released by stressed neurons, ATP exhibits much higher diffusion and leakage (Koizumi et al., 2007); thus ATP plays an important role in long-range communication

between microglia and neurons in the presence of inflammatory stimuli, which promotes microglia movement toward neuronal targets.

Studies have elucidated various mechanisms of neuronal ATP release, the principal mode being through vesicular release via exocytosis upon being packaged together with principal neurotransmitters such as gamma-aminobutyric acid (GABA) (Pankratov, 2006). Furthermore, neuronal ATP release has been found in association with N-methyl-D-aspartate (NMDA) receptor activation due to changes in ionic gradient and neuronal membrane depolarization (Dissing-Olesen et al., 2014). ATP release via pannexin-1 channels, as well as via volume-sensitive anion channels has been reported, although the latter mechanism has been linked with osmotic swelling and hypoxia-affected neurons (Lazarowski, 2012). Continuing with this last point, it is important to recognize that neuronal ATP release has principally been understood in relation to apoptosis and injury, and therefore it should be noted that it is still somewhat vague whether live-yet-stressed neurons (distinct from apoptotic neurons) exhibit this phenomenon, and at what concentrations ATP is released by stressed neurons.

However, in considering the stability of ATP, it may be more precise and worthwhile to look at ADP signalling instead to understand the early interactions between neurons and microglia in the context of phagocytosis. It is well-understood that ADP is more stable in aqueous environments in comparison to ATP not only in general terms based on their chemical structure -- lower entropy, resonance stabilization, and higher hydrogen bond formation with water. Given this greater stability of ADP, it is reasonable to assume that ADP signalling at microglia may be more relevant in long-range communication and the chemotaxis-phagocytosis sequence than ATP. Indeed, microglia have membrane-bound ectonucleotidases NTPDase1 (CD39) and pyrophosphatase NPP1 which rapidly degrade ATP (Lim et al., 2018).

In order to study ADP signalling mechanisms between microglia and neurons, it is necessary to direct our attention toward P2Y12, the major ADP-binding receptor of microglia. P2Y12 is categorized as a Gi/o protein-coupled receptor (Haynes et al., 2006). It is 342 amino acids long, and the secondary structure is characterized by 7 hydrophobic transmembrane domains that are connected by 3 extracellular and 3 intracellular loops (von Kugelgen et al., 2006). In human P2Y12, the ADP binding site is understood to be bordered by transmembrane helices 3, 5, 6, and 7 and specifically Tyr105, Glu188, Arg256, Tyr259, and Lys280 are important in the interaction (Schmidt et al., 2012). In addition, its affinity to ADP is high in comparison to ATP, with an EC_{50} (half maximum effective concentration) of approximately 100nM (Abbracchio et al., 2006). It is understood to localize at the surface of microglia, having been found exclusively on the surface of ramified microglia in vivo (Haynes et al., 2006). It should also be noted that P2Y12 is microglia-specific; it has been shown through transcriptomic studies that microglia are the only cell type in the brain that express P2Y12

(Zhang et al., 2014) and this selectivity has also been observed in rat brains through in situ hybridization and immunohistochemistry (Sasaki et al., 2003). Due to this specificity, P2Y12 has been proposed to be an identifier of microglia that distinguishes it from other myeloid cells (Hickman et al., 2013).

Importantly, ADP-mediated P2Y12 activation has an established role in microglia process extension and migration. Specifically, P2Y12 receptor activation has been shown to cause microglia to extend their processes toward injured neurons (Haynes et al., 2006) or hyperactive neurons releasing ATP (Dissing-Olesen et al., 2014). P2Y12 activation has been shown as a requirement for ADP-induced cell migration in rat microglia (De Simone et al, 2010). Moreover, P2Y12 activation by ADP induces membrane ruffling in microglia, which is a morphology characteristic of chemotactic microglia (Honda et al., 2001). Regarding the specific molecular mechanisms underlying P2Y12-mediated chemotaxis, ADP binding to P2Y12 causes a conformational change in the receptor, which initiates a downstream pathway involving inhibition of adenylate cyclase by Gα, as well as Gβγ-mediated activation of phospholipase C (PLC), release of calcium ions from inositol 1,4,5-triphosphate (InsP3)-sensitive stores, PI3K activation, and Akt phosphorylation (Irino et al., 2008). The mechanism of activation is further tied to an efflux of potassium ions, as there is crosstalk between P2Y12 and potassium channels on microglia (Swiatkowski et al., 2016). These signalling reactions ultimately result in the activation of integrin alpha M β_1 (CD11B/CD29), a cell adhesion molecule which mediates interactions with the extracellular matrix, as well as actin filament remodelling (Ohsawa et al., 2010), which together is understood to facilitate microglial chemotaxis. A summary of this downstream sequence is illustrated below (Introduction Figure 1).

To recapitulate, the earliest communication that occurs between Aβ and LPS-activated microglia and neurons likely takes the form of ADP-P2Y12 interactions, which presently has solely been tied to microglia chemotaxis. Even though microglial migration frequently precedes engulfment of neuronal targets, a possible direct role of P2Y12 in microglial phagocytosis of neurons has not been addressed. It is therefore worth investigating whether P2Y12 is linked to phagocytosis, and if that is the case, P2Y12 could be a novel target for preventing neuronal loss in neurodegenerative diseases. Importantly, as P2Y12 is expressed in platelets and has an established role in platelet aggregation (Hollopeter et al., 2001; Foster et al., 2001), there are already P2Y12 antagonists available which have been used in the clinic to treat thrombosis. For example, clopidogrel has been available for over 20 years in the clinic and has been proven to be an effective treatment for myocardial infarction and stroke (CAPRIE Steering Committee study, 1996). It is identified as a pro-drug, which must be metabolized by cytochrome P450 enzymes in the liver to produce active metabolites which bind P2Y12. It has been suggested to bind covalently to the Cys17 and Cys270 residues of the P2Y12 receptor, thereby irreversibly and competitively blocking agonist binding. Importantly, the metabolite of clopidogrel has been reported to permeate the blood-brain-barrier, and thus has promise of

neurological applications (Sipe et al., 2016). Other irreversibly-P2Y12 binding prodrugs exist, including ticlopidine and prasugrel, which have been used in the clinic. Ticagrelor and cangrelor are newer P2Y12-targeting treatments which do not require activation in the liver, and are reversibly binding, allosteric inhibitors of P2Y12 (Nawarskas and Clark 2011; Wallentin et al., 2009). Thus, if P2Y12 is indeed linked to phagocytosis, there is a clearly foreseeable and realisable clinical application in place, in which these antagonists may be used as neuroprotective agents for patients with neurodegenerative disorders.

P2Y12 expression regulation has important implications

In addition to examining whether P2Y12 inhibition could serve a neuroprotective purpose, another question that is important to ask is how P2Y12 expression is regulated in microglia. As mentioned earlier, the transition of microglia to the highly phagocytic phenotype in the presence of pathological stress is facilitated by a cascade of intracellular signalling events and genome-wide alterations in the gene expression profile of these cells. Interestingly, the gene encoding P2Y12 is one of the genes whose expression is largely altered upon activation. Specifically, deep RNA-sequencing of individual microglia over the course of inflammatory activation led to the finding that large genomic changes during the transition to the activated state occur in two stages, which are distinguished by whether or not they are directed by TREM2: 1) TREM2-independent transcriptional changes, characterizing "primed" microglia, poised for excessive inflammation and phagocytosis, and 2) TREM2-dependent transcriptional changes, characterizing aggressive and inflammatory microglia (Keren-Shaul et al., 2017). In the study, P2Y12 downregulation was found to occur in the first, TREM2-independent stage of activation. This finding not only establishes that P2Y12 downregulation is involved in the process of inflammatory activation and that this downregulation is not mediated by TREM2, but also it suggests that whatever is regulating P2Y12 expression, acts immediately upon stimulus exposure.

There are other studies that highlight the relevance of P2Y12 expression regulation in understanding microglia behaviour, specifically in relation to migration. For instance, P2Y12 expression was found to dramatically decrease following morphology change and migration to target cells following local injury (Haynes et al., 2006). In addition, P2Y12 downregulation has been associated with aging, as P2Y12 gene expression was decreased in human microglia associated with increased age (Galatro et al., 2017). Together, these studies indicate that change in P2Y12 expression is key in directing microglial morphology and motility upon inflammatory activation, and could have important implications for age-related neurological disorders.

Aims

In this thesis, I aim to determine whether the ADP-binding microglial receptor, P2Y12, plays a direct role in microglial phagocytosis of neurons, distinct from microglial migration, in conditions where a pathological stimulus (in this case, LPS) is present (Introduction Figure 2), and to determine if P2Y12 inhibition using the competitive and reversibly-binding antagonist PSB0739 (Methods Figure 12) can serve a neuroprotective purpose. Additionally, I seek to further elucidate the mechanism of P2Y12 expression regulation, mainly by asking if P2Y12 activation itself by addition of its agonist ADP, alters the expression of P2Y12. Answers to these questions could potentially bring to light ideas for novel therapeutic strategies to treat neurodegenerative disorders through preventing neuronal loss by microglial phagocytosis.

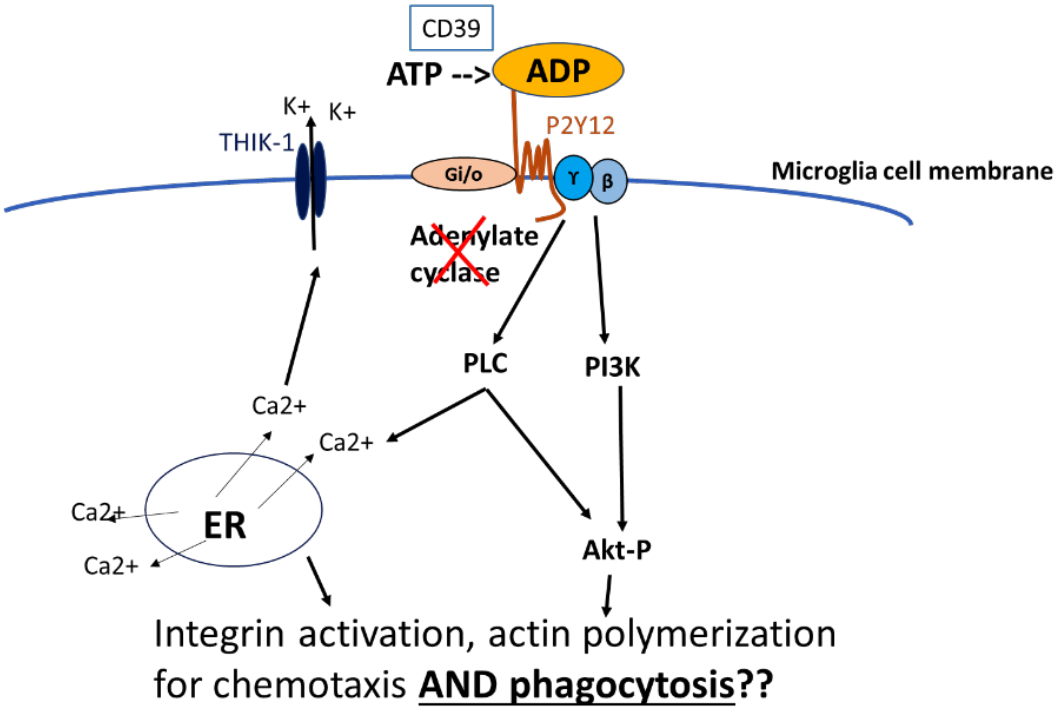

Introduction Figure 1. Downstream pathway from P2Y12 activation. Extracellular ADP, one of the degradation products of extracellular ATP via enzymatic activity of the ectonucleotidase CD39, bind and activate P2Y12 receptors localized on the cell membranes of microglia. P2Y12 is a Gi/o-coupled receptor, and thus activation leads to the inhibition of adenylate cyclase (and subsequent downregulation of cAMP, mediated by the Gα subunit), as well as activation of PI3K and Akt phosphorylation (mediated by Gβ), and PLC pathway (mediated by Gγ). PLC activation leads to IP3-dependent intracellular calcium release and THIK-1-dependent potassium efflux. Together these signalling pathways downstream of P2Y12 activation facilitate integrin activation and actin polymerization understood to mediate cell adhesion and chemotaxis mechanisms. The link to phagocytosis, however, has not been made.

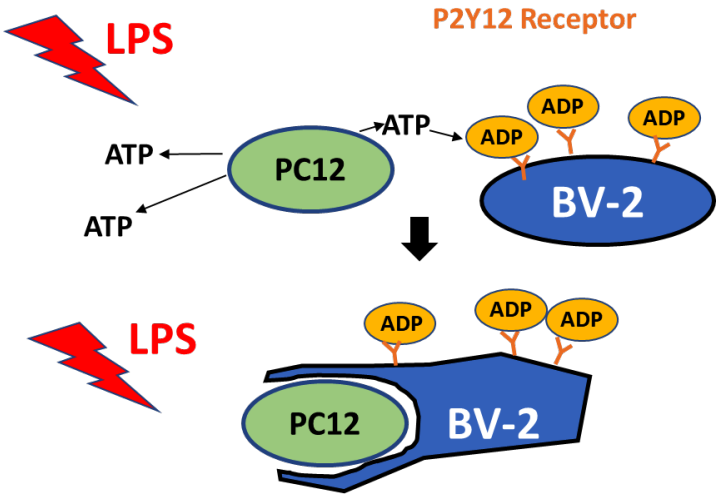

Introduction Figure 2. Starting hypothesis of the project. The present project seeks to determine whether the microglial P2Y12 receptor has direct implications in the phagocytosis of live neurons under LPS-activation, distinct from its established role in chemotaxis, using the immortalized microglial cell line BV-2 and neuroblast-like naïve rat pheochromocytoma PC12 cells. The hypothesis is that LPS stimulus activates BV-2 microglia causing transformation to a phagocytic phenotype, and also induces ATP release from PC12. The ATP released is degraded to ADP and detected by the microglia via their P2Y12 receptors, which subsequently facilitates phagocytosis.

Materials and Methods

Reagent Table

Reagent or Resource	Source	Identifier
6-well plate	Starlab	CC7682-7506
24-well plate	Starlab	CC7682-7524
96-well plates (Black-walled)	Costar	3603
96-well plates, polystyrene (Clear, v-bottom)	Costar	3897
96-well FlexStation pipette tips clear	Molecular Devices	9000-0912
ADP	Sigma	A2754
Calcium Assay Kit	BD Biosciences	640176
Cyclo(Arg-Gly-Asp-D-Phe-Val) (cRGDfV)	Sigma	C6581
Cytochalasin D from *Zygosporium mansonii*	Sigma	C8273
0.1M DTT	Thermo Fisher	Y00147
Dulbecco's Modified Eagle's Medium	Thermo Fisher	41966-029
Fetal Bovine Serum (FBS)	Thermo Fisher	A3160801
5x First Strand Buffer	Thermo Fisher	S6142
Fluospheres Polystyrene Microspheres 1.0µm Red fluorescent (Excitation/Emission: 580/605nm)	Thermo Fisher Scientific	F13083 Lot 1755723
Gentamicin sulphate	Melford Laboratories	G38000-1
bisbenzimide H 33342 trihydrochloride (Hoechst 33342) (Excitation/Emission: 346/460nm)	Sigma	14533
Horse Serum	Thermo Fisher	16050122
Green-fluorescent Isolectin-B4-Alexa-Fluor-488 from *Griffonia simplicifolia (*IB4) (Excitation/Emission: 495/519)	Invitrogen	I21411
Lipofectamine 2000	Thermo Fisher	11668019
Lipofectamine 3000	Thermo Fisher	L3000015
Lipopolysaccharide from *Salmonella enterica* serotype typhimurium	Sigma	L6143
Monarch Total RNA Miniprep Kit	NEB	T2010S
OptiMEM	Thermo Fisher	51985026
Paraformaldehyde	Sigma	P6148
PBS	Thermo Fisher	10010015
Poly-L-Lysine	Sigma	P8920
1-Amino-9,10-dihydro-9,10-dioxo-4-[[4-(phenylamino)-3-sulfophenyl]amino]-2-anthracenesulfonic acid sodium salt (PSB0739)	Tocris	3983 batch no. 3

Random Hexamer Primer	Thermo Fisher	Y02321
Reverse Transcriptase Superscript RNaseH	Thermo Fisher	18064-022
Red-fluorescent 5-(and 6)-carboxytetramethylrhodamine succinimidyl ester (TAMRA) (Excitation/Emission: 549/573nm)	Biotium	90022
siRNA (Control): siGENOME Non-Targeting siRNA #2, Target Sequence: UAAGGCUAUGAAGAGAUAC	Dharmacon	SO-2695037G D-001210-02-20
siRNA (P2Y12) Silencer Select Sequence (5'->3') GGACGUAACAAAAUGUUCUtt (sense) AGAACAUUUUGUUACGUCCtt (antisense)	Life Technologies	P/N 4390771 ID# s89185 Lot# ASO2AXQS
Staurosporine	Sigma	S5921
Trypan blue	Sigma	T8154
Trypsin Ethylenediaminetetraacetic acid (Trypsin/EDTA)	Thermo Fisher	25300054

Primer List

Name	**Forward sequence (5'-> 3')**	**Reverse sequence (3'-> 5')**
β-Actin	CCACACCCGCCACCAGTTCG	CCCATTCCCACCATCACACC
IL-6	GACAAAGCCAGAGTCCTTCAGA	AGGAGAGCATTGGAAATTGGGG
P2Y12	ATAACGTGCTACCCGACCTG	GCAGAGACTTCAGCAAGGCA

Detailed Descriptions of Experimental Methods

BV-2 Cell Culture

BV-2 is an immortalized microglial cell line originally obtained from primary mouse microglia, that has been stably transfected with a v-raf/v-myc carrying retrovirus (Blasi et al 1990; Bocchini et al 1992; Henn et al 2009). The BV-2 cells used here were a gift from Dr. Miguel Burguillos at the Cambridge Institute for Medical Research. The cells used for experiments were all under a passage number of 30 (where passage number indicates the number of times the cells are exposed to trypsin for detaching and split into new flasks with fresh medium, also known as the subculture number).

The BV-2 cells were maintained in Dulbecco's modified Eagle's medium (DMEM) supplemented with 10% Fetal Bovine Serum (FBS) and 0.001% broad-spectrum antibiotic Gentamicin, which prevents protein synthesis in both Gram-negative and Gram-positive bacteria. Cells were grown in 10mL of this media in T75 ($75cm^2$) cell culture flasks, at 37^o C and 5% CO_2. Typically for each passage, cells were harvested with 0.5% Trypsin- ethylenediaminetetraacetic acid (Trypsin-EDTA)

for 5 min in 37^{o} C, split at a 1:20 dilution (a cell count of approximately 1.25 x 10^5 – 1.50 x 10^5) using fresh 37^{o} C pre-heated 10% FBS DMEM. The cells were maintained at 37^{o} C and grown to a density of approximately 2.5~3.0 x 10^6 cells total after three days, at which point they were split again.

Additionally during each passage, cells were counted and their viability was determined by obtaining a 10µl sample of cell suspension, combining with 10µl of 0.4% Trypan blue, mixing and loading onto a haemocytometer. Cells mounted on the haemocytometer were counted manually by microscopy to determine cell concentration. The number of Trypan blue-stained cells was noted to confirm at least 85% cell viability before each passage and seeding for experiments.

PC12 Cell Culture

Naïve rat pheochromocytoma cells (PC12) (Greene and Tischler 1976) were maintained in RPMI-1640 medium supplemented with 10% horse serum (HS), 5% FBS (both filter-sterilized before addition), and 1/1000 Gentamicin in untreated T75 cell culture flasks. These neuroblast-like cells were kept in suspension at 37^{o} C and 5% CO_2 in 10mL of this PC12 media in T75 cell culture flasks. Typically for each passage, cells were grown to a density of approximately 4.5~5.0 x 10^6 cells total at 37^{o}C before being split at a 1:10 dilution (cell count 4.5~5.0 x 10^5) to be passaged again after 3 days. The cells were maintained in suspension. The passage number of the PC12 cells for experiments was between 3-25 (following 25 subcultures, the cells which are normally floating began to adhere to the flask, indicating abnormality in their adhesion properties). At least 85% cell viability was determined using trypan blue and counting the number of blue-stained cells using the haemocytometer before seeding for experiments.

RNA interference in BV-2

2.0 x 10^4 BV-2 cells were seeded per well in a 6-well plate in 10% FBS DMEM media for 24 h. The following day, non-target siRNA and P2Y12 siRNA were diluted in OptiMem (per well: 3µl siRNA (20µM) to 62.5µl OptiMem). Lipofectamine dilutions in OptiMem were also made (per well: 3.75µl lipofectamine to 62.5µl OptiMem). Diluted lipofectamine was added to each siRNA sample at a 1:1 ratio (this lipofectamine is necessary for the transfection, as it serves to create liposomes which enclose the siRNA in vesicles that can permeate the cell membrane). The seeded cells were taken out of the incubator, the DMEM was aspirated and replaced with 625µl OptiMem. 125µl of the diluted siRNA-lipofectamine was added drop-wise to the respective wells. The cells treated with siRNA-lipofectamine were incubated for 3 h at 37^{o}C, during which liposomes would form with the siRNA enclosed, which can then be introduced into the BV-2 cells. After the incubation, the wells were washed three times with 10% FBS DMEM, and left in 37^{o}C overnight. The following day, the wells were washed with PBS and the cells were detached mechanically by resuspension with a P1000 pipette. The detached cells were transferred to 15mL tubes and pelleted by spinning 1.0 x 10^3 xg for 5

min. At this point the cells were counted, and re-seeded for RT-qPCR analysis, phagocytosis, and/or calcium experiments.

RT-qPCR

For running RT-qPCR on untreated cells, 3.0 x 10^5 sample cells were seeded in one well per sample in a 6-well plate, in 2mL total volume of 0.5% FBS DMEM supplemented with Gentamicin (1/1000 dilution) and incubated overnight. The following day, cells were detached from the well surfaces mechanically by thorough resuspension with P1000 pipette, transferred to Eppendorf tubes and pelleted by spinning at 2.0 x 10^3 xg for 5 min. For RT-qPCR analysis of siRNA-transfected cells, 24 h after transfection, cells were counted and seeded at 3.0 x 10^5 cells per well in 2mL total volume of 10% FBS DMEM (high serum in order to promote the growth of transfected cells, which are more vulnerable to cell death than untreated cells), left to incubate for 24 h so that RNA extraction occurred 48 h after transfection. For experiments examining P2Y12 expression changes upon LPS activation, ADP, or PSB0739 treatment, cells were seeded at 3.0 x 10^5 overnight in 0.5% FBS DMEM, after which the treatments were added and incubated for another 24-48 h as indicated (thus for these experiments, the cell number at the RNA extraction step was higher). Primary cDNA used for the comparison of expression levels to BV-2 was obtained from cortical microglia of C57BL6 (P1-4) mice, 48 h post-transfection with non-target siRNA control. This primary mouse cDNA sample was prepared by Dr. Miguel Burguillos.

RNA extraction was performed using the Monarch Total RNA Miniprep Kit, following the protocol outlined beginning with cell lysis, then removal of gDNA, binding of RNA onto RNA purification column, washing with RNA priming buffer and twice with RNA wash buffer, then eluting in 50µl volume of nuclease-free water.

The concentration of RNA was quantified by nanodrop, and reverse transcription was performed taking 1µg of the RNA sample and adding nuclease-free water to a total volume of 9µl in PCR tubes. If any one of the samples in a group of samples to be compared with one another had a low concentration such that it was not possible to take 1µg of RNA in 9µl, the maximum possible amount in 9µl volume was obtained for that sample, and all other samples were adjusted accordingly to that lowest amount with nuclease-free water. Per tube, 1µl of 240ng Random Hexamer Primer, and 1µl of 10mM dNTPs were added to the 9µl samples, and the tubes were incubated at 65^0C for 5 min, then placed directly on ice. 4µl of 5x Reverse Transcription Buffer and 2µl 0.1M DTT (final concentration 10mM) were added per tube and incubated for 2 min on the bench at room temperature (~25^0C). 1µl reverse transcriptase enzyme was added to each sample and the following program was set on the thermocycler: 25^0C 10 min, 42^0C 50 min, 70^0C 15 min, 4^0C hold.

Following reverse transcription, all cDNA samples were diluted 1:5 to 200ng, but if the concentrations of RNA were low to begin with, no dilution was performed. Primer pairs were

combined at 5µM dilutions in nuclease-free water. The reaction recipe per sample (25µl volume) was: 2x Sybr Green Mix 12.5µl, H_2O 9.5µl, 2µl of primer (5µM forward and reverse combined), and 1µl cDNA. cDNA combined with H_2O were loaded to respective qPCR tube strips first, followed by mixes of primer and Sybr Green on top. All samples were loaded in triplicate qPCR tubes. qPCR was run on the 72-well rotor Qiagen GeneQ machine, with the following program: 95^0C 10m, [95^0C 10s, 60^0C 15s, 72^0C 20s] 40 cycles, 55^0C-95^0C melt.

For analysis, the efficiency of each primer was determined by first ensuring that the resulting amplification values were above 1.6, the takeoff point was within a cycle range of 18-30, and that the melt curve suggested specificity of the primer. It should be noted that even before ordering primers, the primer sequences were always entered into the "In-Silico PCR" function on UCSC Genome Browser (https://genome.ucsc.edu/) to observe the exact location of the target, and to determine the specificity of the primer at this step (to check if the primer mapped to a single location on the genome). When choosing among different primers, the primer that met all of the above criteria, and also preferably spanned an exon-exon junction to select for cDNA, was the one that was ultimately used. In terms of qPCR analysis, comparative quantitation values for the beta-actin (used as a reference for all analyses) were averaged among triplicates per sample. Each comparative quantitation value for genes tested (IL6 and P2Y12 primers) were divided by this beta-actin average to obtain individual values of IL6 or P2Y12 mRNA expression relative to beta-actin. Further, the mean of these technical replicates (the mean fold change in mRNA level from beta-actin) was calculated and used for analysis for a single experiment.

Calcium Assays

For the calcium assays, a modified version of the protocol indicated in the BD Biosciences Calcium Assay Kit was followed. Prior to the assays, cells were seeded at 5.0 x 10^4 cells per well in at least 7 columns of a 96-well black-walled plate, in 500 µl total volume of 0.5% FBS DMEM supplemented with 1/1000 gentamicin and incubated at 37^0C overnight. The next day, roughly equal cell densities and viability of the cells were confirmed by examining cell populations and cell morphologies in each well under a light microscope. Next, calcium indicator (solubilized in DMSO and aliquoted prior to the experiment) supplied in the Calcium Assay Kit in non-Phenol Red DMEM and 1X Signal Enhancer (prepared by diluting 10X Signal Enhancer in Calcium Assay Buffer provided in kit) for calcium assay was prepared, in which the calcium indicator was first diluted 1:1000 in Signal Enhancer, and this enhancer-indicator solution was further diluted 1:2 with non-phenol red DMEM. At this point the incubated cells were taken out, the cell media was removed from all wells and replaced with 100µl of the prepared calcium dye-containing solution. The plate was returned to the 37^0C incubator for 1 h to allow the cells to incorporate the calcium-sensitive dye, which allows immediate fluorescence emission from the cells upon induction of intracellular calcium responses, which can subsequently be detected by the Flexstation following treatment injection. The plate was

then transferred to room temperature (~25^{0}C), shielded from light for 20 min. During these incubations, treatments to be injected into the individual wells for the assay were prepared and loaded at 275µl total volume per well in one column of a clear 96-well V-bottom 0.3mL plate. The treatments were prepared at 10x concentration of the final desired concentrations, as the treatments were to be diluted 1:10 upon addition to the cells (i.e. for 100µM ADP treatment, 1mM ADP solutions were loaded in the compound plate). The ADP dilutions were prepared fresh from stock before each use and diluted in PBS. In terms of setting the program for the Flexstation 3, the settings were adjusted using the SoftMax Pro software such that treatments for each column of cells were taken from the same single column prepared in the compound plate. Additionally, the program was set to allow 30s of background reading before injection, followed by 2min 30s reading, for a total recording time of 3min per sample. Rate was set at 1 (~16 µl/s), 10µl volume for treatment addition, excitation at 525nm (within green spectrum), sensitivity at 5, reading length of 180s, interval of 5s, reads number 37. Other settings were as follows: reads/well: 5; automix: off; calibrate: on; PMT (photomultiplier tube): medium; settle time: off; log time: 0; end time: 180; RFU (relative fluorescence units) min: 0; RFU max: 20000; Vmax (maximum velocity) points: 37/37; assay plate type: 96-well Greiner blk/clr btm; assay plate fluid initial volume 100 µl; transfers: 1; pipette height: 90 µl; volume: 10.0 µl; compound source: Costar 96 Vbtm 0.3ml; No triturate; autocalibrate: on; autoread: off.

For the PSB0739 time course experiment, the inhibitor (prepared at 10mM dilution in PBS) was added along with the calcium-sensitive indicator-DMEM-enhancer solution at a final concentration of 10µM prior to the 1h incubation at 37^{0}C and 20min incubation at room temperature, for the 1h 20min time point. For the 20m time point, the inhibitor was directly added to the cells immediately following the 1h 37^{0}C incubation such that the cells were treated with the inhibitor for the entirety of the 20min room temperature incubation. For the 10min time point, the inhibitor was added to the cells 10min into the room temperature incubation. As controls, alongside the inhibitor additions for 20min and 10m time points, in parallel another set of wells were treated at these times with PBS. Since all experiments followed the sequence of 1h incubation at 37^{0}C, then 20min incubation at room temperature regardless of inhibitor treatment length, the temperature alterations before the assay should be consistent across all time course samples. It should be noted, however, that reconstituted PSB0739 has a blue colour, which raises some concern regarding possible interference in fluorescence detection by the Flexstation, although preliminary experiments where cells were injected with PSB0739 only showed little changes in fluorescence emission, similar to the vehicle (PBS treatment) condition.

For measuring the calcium responses in LPS-stressed and untreated cells, cells were seeded at 5.0 x 10^4 cells per well in at least 7 columns of a 96-well black-walled plate, in 500 µl total volume of 0.5% FBS DMEM supplemented with 1/1000 Gentamicin and incubated at 37^{0}C for at least 12 h. The media was removed from all of the wells and replaced with either 500 µl of fresh 0.5% FBS DMEM

with 100ng/ml LPS or 0.5% FBS DMEM with PBS. The cells were further incubated for 12-16 h at 37^0C, followed by addition of the calcium sensitive-dye.

For analysis of the calcium data (Methods Figure 1), the results of each treatment condition were examined separately (every time the number of technical replicates was $\geq$4, where "technical replicates" means the number of wells of the same treatment condition within a single run on the Flexstation). A line graph of the raw values (fluorescence emission units) per time point was plotted (Methods Figure 1A). For every sample, a dip in the fluorescence was observed immediately following the injection of the treatment by the Flexstation (at t=33s). This "minimum" fluorescence value was subtracted from each subsequent fluorescence value recorded for the time points following injection, to observe specifically the rises in calcium due to the treatments for each technical replicate (Methods Figure 1B). In general where there was a calcium response, a clear peak and decay were observed in the range of 0-45 seconds following treatment injection, so the x-axis was adjusted to take into account only the fluorescence emission units corresponding to this range of time (Methods Figure 1C). The data for each technical replicate were combined to generate average fluorescence values at each time point for a single experiment (Methods Figure 1D). For consistent comparisons across independent replicate experiments, average values for each experiment were normalized to the maximum value recorded for the ADP only condition of the experiment (thus the y-axis values after normalization are no longer in in terms of arbitrary fluorescence units (AFU)). After two or three independent replicate experiments (where "independent replicate" means the same experimental procedure was performed either with a different batch of cells or conducted on a different day), all average curves were combined to obtain "grand averages" of calcium response values corresponding to each time point following treatment injection (Methods Figure 1E). A composite graph of all of the grand average curves for each treatment was generated for the final figure (Methods Figure 1F). The calcium response value corresponding to the peak of the curves was determined and plotted as bar graphs to directly compare the calcium response for each treatment condition quantitatively (Methods Figure 1G).

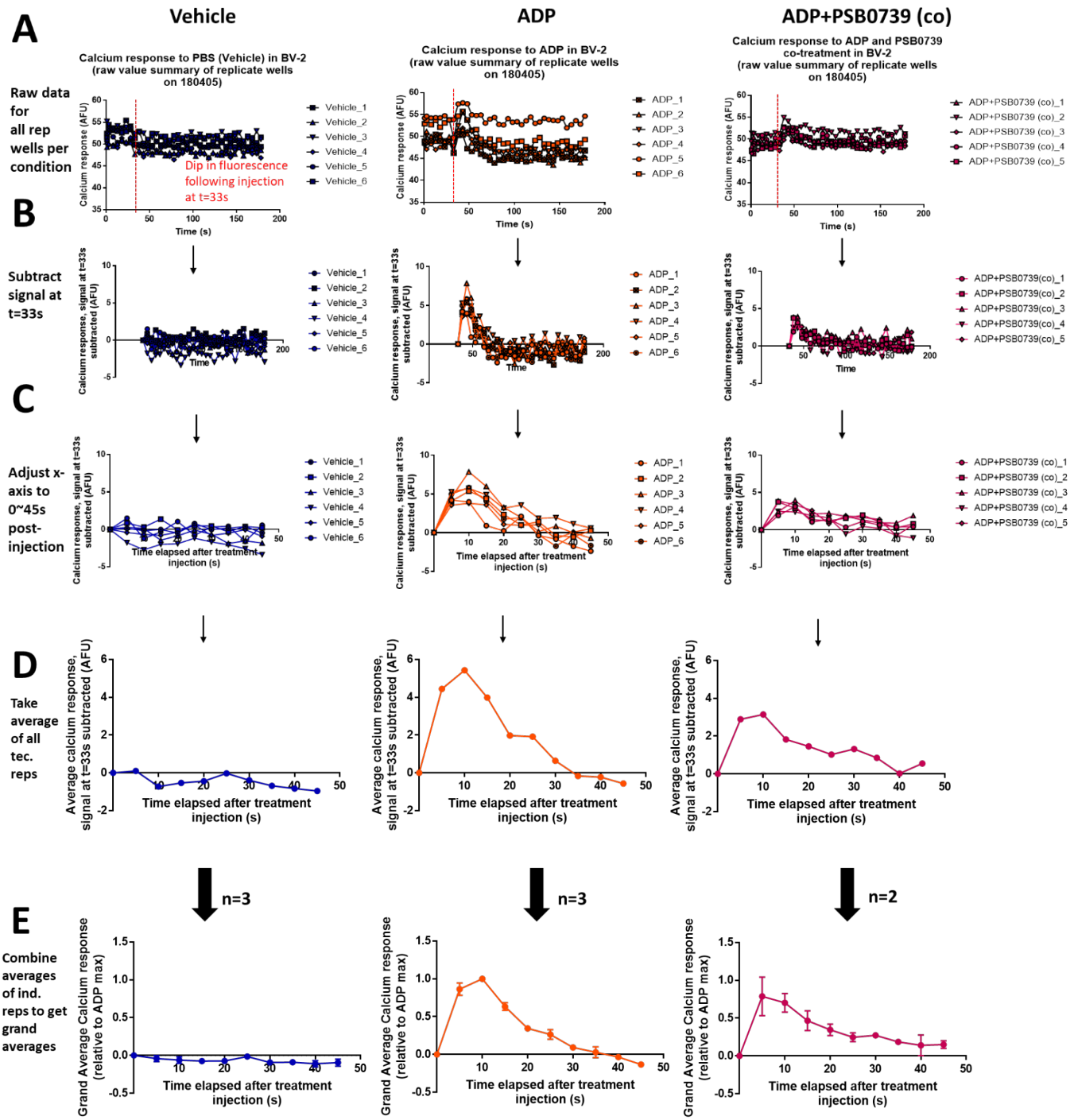
A
Vehicle
ADP
ADP+PSB0739 (co)
Raw data for all rep wells per condition
Calcium response to PBS (Vehicle) in BV-2 (raw value summary of replicate wells on 180405)
Calcium response to ADP in BV-2 (raw value summary of replicate wells on 180405)
Calcium response to ADP and PSB0739 co-treatment in BV-2 (raw value summary of replicate wells on 180405)
Dip in fluorescence following injection at t=33s
Calcium response (AFU)
Time (s)
Vehicle_1
Vehicle_2
Vehicle_3
Vehicle_4
Vehicle_5
Vehicle_6
ADP_1
ADP_2
ADP_3
ADP_4
ADP_5
ADP_6
ADP+PSB0739 (co)_1
ADP+PSB0739 (co)_2
ADP+PSB0739 (co)_3
ADP+PSB0739 (co)_4
ADP+PSB0739 (co)_5
B
Subtract signal at t=33s
Calcium response, signal at t=33s subtracted (AFU)
Time
C
Adjust x-axis to 0~45s post-injection
Time elapsed after treatment injection (s)
D
Take average of all tec. reps
Average calcium response, signal at t=33s subtracted (AFU)
E
Combine averages of ind. reps to get grand averages
n=3
n=3
n=2
Grand Average Calcium response (relative to ADP max)

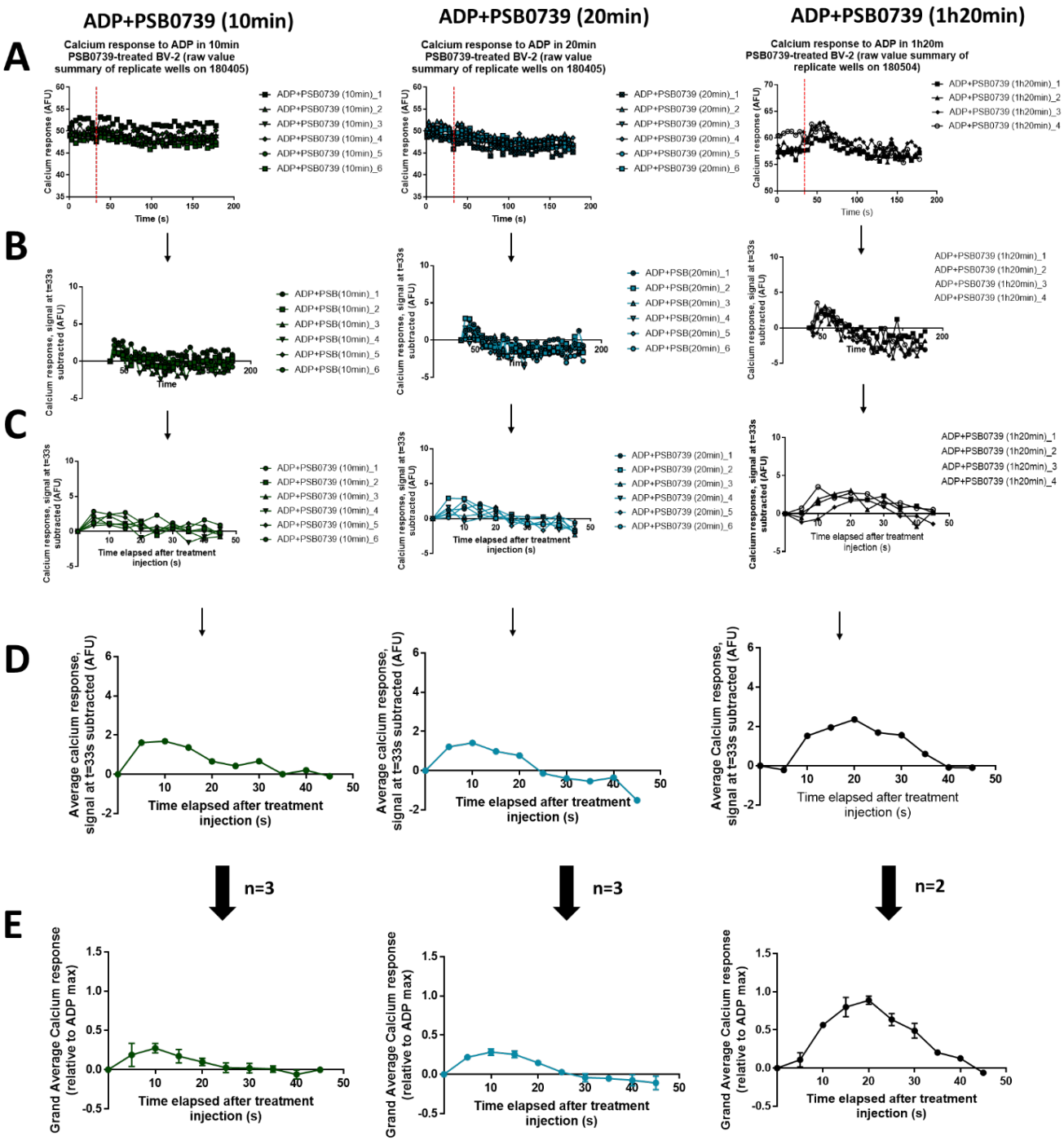
ADP+PSB0739 (10min)
ADP+PSB0739 (20min)
ADP+PSB0739 (1h20min)
A
B
C
D
E
Calcium response to ADP in 10min PSB0739-treated BV-2 (raw value summary of replicate wells on 180405)
Calcium response to ADP in 20min PSB0739-treated BV-2 (raw value summary of replicate wells on 180405)
Calcium response to ADP in 1h20m PSB0739-treated BV-2 (raw value summary of replicate wells on 180504)
Calcium response (AFU)
Time (s)
ADP+PSB0739 (10min)_1
ADP+PSB0739 (10min)_2
ADP+PSB0739 (10min)_3
ADP+PSB0739 (10min)_4
ADP+PSB0739 (10min)_5
ADP+PSB0739 (10min)_6
ADP+PSB0739 (20min)_1
ADP+PSB0739 (20min)_2
ADP+PSB0739 (20min)_3
ADP+PSB0739 (20min)_4
ADP+PSB0739 (20min)_5
ADP+PSB0739 (20min)_6
ADP+PSB0739 (1h20min)_1
ADP+PSB0739 (1h20min)_2
ADP+PSB0739 (1h20min)_3
ADP+PSB0739 (1h20min)_4
Calcium response, signal at t=33s subtracted (AFU)
Time
ADP+PSB(10min)_1
ADP+PSB(10min)_2
ADP+PSB(10min)_3
ADP+PSB(10min)_4
ADP+PSB(10min)_5
ADP+PSB(10min)_6
ADP+PSB(20min)_1
ADP+PSB(20min)_2
ADP+PSB(20min)_3
ADP+PSB(20min)_4
ADP+PSB(20min)_5
ADP+PSB(20min)_6
Time elapsed after treatment injection (s)
Average calcium response, signal at t=33s subtracted (AFU)
Average Calcium response, signal at t=33s subtracted (AFU)
n=3
n=3
n=2
Grand Average Calcium response (relative to ADP max)

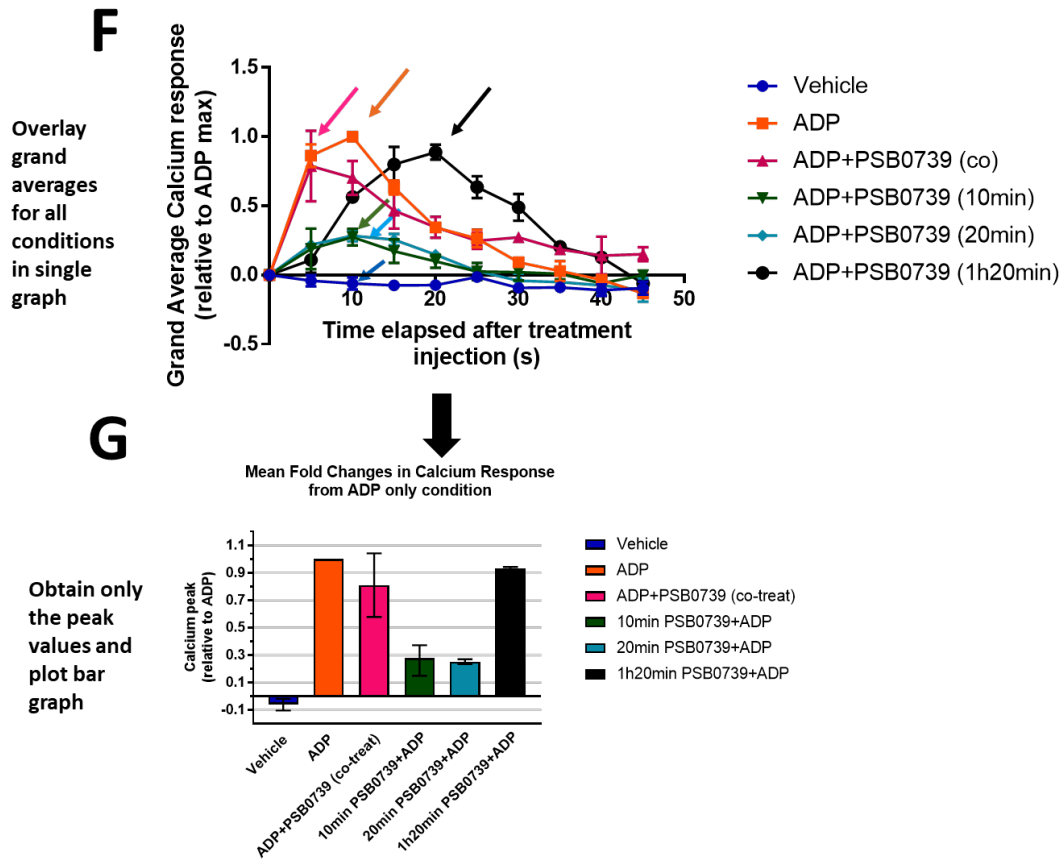

Methods Figure 1. Step-by-step outline of adjustments made to raw curves for calcium data analysis (part of PSB0739 time course experiment shown as example). The process of calcium response analysis from initial raw values obtained for Vehicle, ADP, ADP and PSB0739 co-treatment, ADP treatment to 10min PSB0739 pre-treated cells, ADP treatment to 20min PSB0739 pre-treated cells, and ADP treatment to 1h 20min PSB0739 pre-treated cells for one independent experiment (either from 180405 or 180504) are illustrated, followed by graphs combining this data with that of other independent replicate experiments to obtain grand averages. **A:** Raw data obtained directly from the Flexstation for each technical replicate per condition (where "technical replicate" means identical wells run on the plate) for one experiment. Y-axis represents arbitrary fluorescence units (AFU) indicating calcium release, and x-axis represents time elapsed since the start of the recording (treatment is injected at t=30s and recording continues until t=180s). The number of technical replicates is different across conditions as a result of discarding noticeable outliers. Note that there is a dip in the calcium response immediately following the injection of treatment. **B:** The "minimum" fluorescence value at t=33s was subtracted from each subsequent fluorescence value to observe specifically the rises in calcium following treatments. **C:** X-axis was adjusted to examine only the range of 0-45s following treatment injection. **D:** The average fluorescence at each time point among technical replicates was calculated to generate average calcium curves. **E:** After two or three independent replicate experiments, all average curves were combined to generate "grand average" calcium curves upon normalizing each value to maximum of ADP condition. Here, data = mean ± S.E.M. where n=3, and mean with range where n=2. **F:** All grand average curves were overlayed in a single graph. **G:** Values corresponding to the peak of the curves (indicated by coloured arrows) were plotted as bar graphs. Data = mean ± S.E.M. where n=3, and mean with range where n=2 (co-treatment and 1h20min samples).

Bead Phagocytosis Assays *(Methods Figure 2)*

1.0 x 10^5 BV-2 cells were seeded in 500µl total volume of 0.5% FBS DMEM per well in a 24-well plate for 24 h to allow the cells to adhere to the surface of the wells. Beads used for this phagocytosis assay were 1.0µm red-fluorescent polystyrene microspheres suspended in distilled water with 0.02% anti-fungal and anti-septic agent thimerosal ($1x10^{10}$ beads/ml, 0.552% w/v beads). The concentration was converted to w/v by the following calculations: The beads are 1µm in their diameter; the density of polystyrene is 1.055g/cm^3; volume per bead = (4/3) x 3.14 x (0.5µm) ^{3} = 0.523 μm^3; 0.523 μm^3 = 0.523 x 10^{-12} cm^3; mass of one bead = 0.523 x 10^{-12} cm^3 (1.055g/cm^3) = 0.552 x 10^{-12} g; $1x10^{10}$ beads/ml, so 0.552 x 10^{-12} (10^5) g/ml = 0.552 x 10^{-2} g/ml, which is the concentration of beads in the bottle in g/ml; 1µl = 0.001ml, which means that the concentration of beads in the bottle in % is 0.552%. These are carboxylate-modified beads that have a high density of carboxylic acids on their surfaces to allow covalent coupling of primary amine groups of microglial surface proteins to these carboxyl groups exposed on the beads (thus non-specific to any one type of surface receptor). The red fluorescent dye is contained within the bead core instead of the surface, which make the possibility of quenching fluorescence difficult.

For the first experiments testing the effect of exogenous ADP, the following treatments were added in triplicate wells for 1h at 37^0C: 1) 0.0012% w/v 1um beads, 2) 0.0012% w/v beads and 100µM ADP together, 3) only H_2O and no beads. All dilutions were made in dH_2O. All treatments were added quickly and dropwise in a circular motion as evenly as possible on top of the seeded cells. As mentioned above, the BV-2 seeding and co-incubation period with the beads were all conducted in low serum (0.5% FBS) medium. The low-serum environment was created with the intention of synchronizing the cell cycles of the samples, and preventing over-stimulation of signalling pathways promoting the growth and survival of the cells during the experiment, which could interfere with measurements of phagocytosis with ADP treatment. Furthermore, high serum has been known to immediately promote phagocytosis at high levels in microglia (Bohlen et al 2017).

After the 1h incubation, the media was aspirated and replaced with ice-cold PBS pH 7.2 to wash out free beads. The center of the wells were quickly observed and imaged at 10x magnification under the Leica DMI6000 microscope (brightfield setting, 10x0.3 dry lens, magnification of 1, single image mode, acquisition mode XY) to check cell morphology and apparent phagocytosis using the Leica Application Suite. Cells were harvested with 0.5% trypsin in PBS for 5 min in 37^0C, quenched with 10% FBS DMEM to inactivate the trypsin, transferred to 1.5mL eppendorfs and pelleted by spinning at 2.0 x 10^3 xg for 5 min. The cells were fixed in 4% paraformaldehyde for 15 min on the shaker, after which they were pelleted and the supernatant removed. The pellet was resuspended in 50µl ice-cold PBS and kept on ice before running on BD Accuri C6 Flow Cytometer.

The Flow Cytometer was used referring to the manual instructions (https://www.bdbiosciences.com/documents/BD_Accuri_C6Flow_Cyto_Instrument_Manual.pdf). The flow cytometer works in that negative pressure is applied to suck the prepared cell suspension in PBS out of the sample tube, which is diluted with the sheath fluid (deionized water with bacteriostatic concentrate solution) and is run through a 200µm ID quartz capillary (of variable core diameter depending on pressure setting), where the cells are passed as a single file of particles. The minimum detectable particle size is 0.5µm, and the "medium" pressure settings used for experiments is 35µL/min, 16 µm sample core diameter. The cells passed through is exposed to lasers in two directions, one in the forward direction (0^o, ±13) and another in the side direction (90^o, ±13), giving rise to two different scatter patterns, the forward scatter (FSC) and the side scatter (SSC). The forward scatter gives an indication of cell size, and the side scatter gives an indication of the cell complexity or granularity (material contained within the cell). Lasers within the machine operate at wavelengths of 488nm (20mW, Solid State Blue Laser) and 640nm (14.7mW, Diode Red Laser). FL1 interference filter is used for capturing green fluorescence (533 ± 30nm) and FL3 optic filter for red fluorescence (>670nm) which are emitted by fluorescently-labelled cells in response to laser excitation.

The method of flow cytometry analysis is outlined below (Methods Figure 3). The untreated (BV-2 only) samples were run first before all of the other samples with unlimited settings for cell count, medium fluidics speed (35µl/min), and size threshold setting at 80,000 FSC as done in previous studies using BV-2 (such as Hornik et al, 2016) (anything passing through the Sample Injection Port (SIP) that yields a forward scatter of <80,000 is not counted as an event and therefore will not show up as a dot on the plot). The clear peak of cell population observed in the log plot for SSC (side scatter; measure of granularity) vs. FSC (forward scatter; measure of size) plot was gated (in other words, the peak was outlined with a polygonal drawing to analyse only the enclosed points for analysis) to select for BV-2 cells (as opposed to cell debris and free beads). All subsequent samples were run with the setting limit of 10,000 events (points on the plot, indicative of cell population) within this gate, in order to analyse 10,000 BV-2 cells for each condition. Each sample was thoroughly mixed by pipetting before placement onto the flow cytometer. SSC vs. FL3 (Methods Figure 2) (>670nm, detects red fluorescence) plot was created. For analysis, a vertical line was drawn on this SSC vs. FL3 plot just adjacent to the cell population to set a FL3 threshold to eliminate the background red signal detected for cells that had not phagocytosed any beads. With the CFlow Plus software, the % of events on the right of the FL3 gate (indicative of Red-fluorescent BV-2) out of all events in the plot, as well as the mean FL3 intensity of all of the events past this threshold were used to measure bead phagocytosis. The mean FL3 analysis method allows one to determine the differences in the number of beads phagocytosed by cells (greater number of ingested beads yields greater FL3 intensity per cell). Thus, for analysis, % FL3+ events and mean FL3 were used as two ways to quantify bead phagocytosis.

In a later independent experiment, incubations with beads were shortened to 30 min and the pelleted samples were all immediately analysed on the flow cytometer without fixation, in order to eliminate the possibility of ADP degradation and cell death during the previous 1-h incubations.

Where the effect of P2Y12 knockdown on bead phagocytosis was tested, NT and P2Y12 siRNA-transfected cells 24h post-transfection were seeded for 24h incubation before the addition of beads with or without ADP. In other words, the assay was performed on the cells 48 h after transfection.

Where the effect of LPS stress and PSB0739 treatment on phagocytosis was tested, following initial seeding of the cells in 0.5% FBS DMEM for 24h, the media was replaced with new 0.5% FBS DMEM either supplemented with 100ng/ml LPS or with PBS, and the cells were incubated for another 24h. Where applicable, PSB0739 (diluted in PBS) was added to the wells for a final concentration of 10µM and all other wells were treated with PBS as a control. Where applicable, 10min later, ADP (100µM) was added, along with beads (0.0012% w/v) for 1h incubation. One more 24-well plate with an entirely identical set of treatments was incubated in parallel for 1h on ice, covered in aluminium foil. Following the incubation, the plates were imaged, and cells were detached simultaneously. Treatments were all done in triplicate. For these experiments where there was an identical set of samples done in cold conditions, the % FL3+ events given by the cold incubation was subtracted from the signal of the corresponding condition incubated in 37^0C, in order to distinguish ingesting events from binding events. When taking the replicate averages across three independent experiments, the % FL3+ readings (upon subtraction of cold signal) were relatively consistent. However, the mean FL3 values often varied across different days, perhaps due to unintentional variation in the concentration of beads which were added. For this reason, the average of mean FL3 across independent replicates were obtained following normalization to the Control sample.

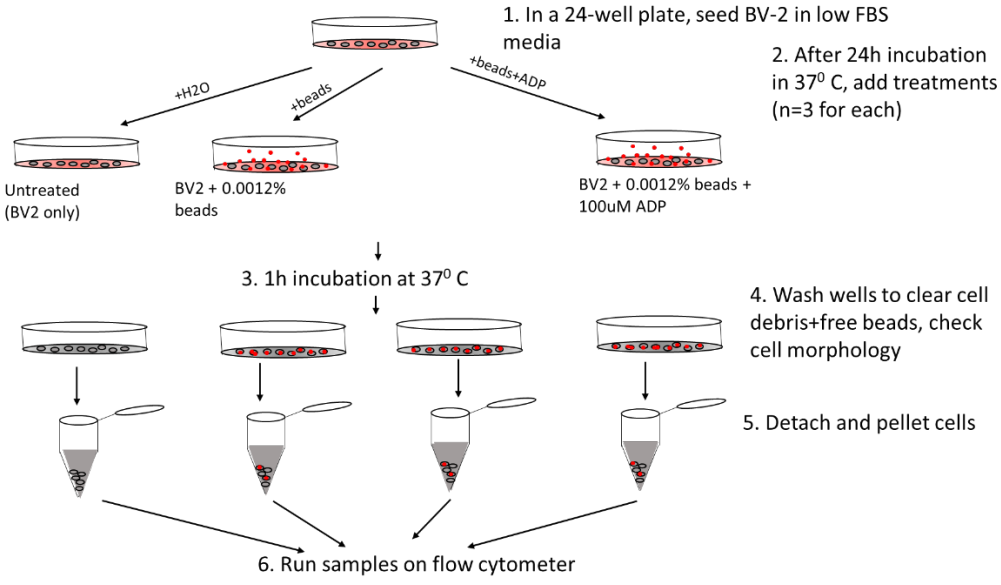

Methods Figure 2. Schematic diagram of 1µm Bead-BV-2 Phagocytosis Assay with ADP treatment.

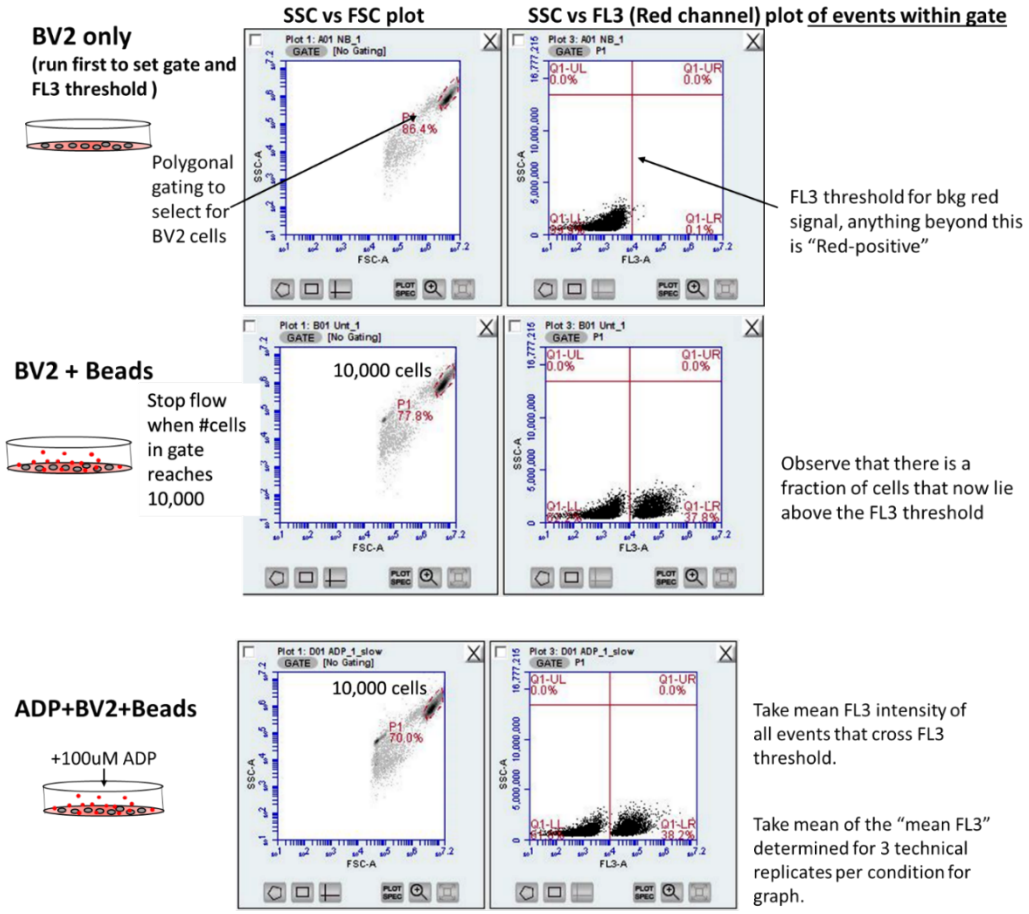

Methods Figure 3. SSC vs. FSC gating and SSC vs. FL3 plots for the conditions tested for the Bead-BV-2 Phagocytosis Assay.

PC12 Phagocytosis Assays *(Methods Figure 4)*

BV-2 seeding and treatments before co-incubation

5.0 x 10^4 BV-2 cells were seeded in 500µl of 0.5% FBS DMEM (pre-heated to 37°C) per well in 24-well plates and incubated at 37° C for 24 h to adhere. Following the incubation, the DMEM was replaced with warm PC12 medium (10% HS, 5% FBS, 1/1000 gentamicin in RPMI) for all wells (media was not replaced for early trials of the experiment). For the necessary wells, Lipopolysaccharide from Salmonella enterica serotype typhimurium (LPS) from Sigma was added at a concentration of 100ng/ml and all wells were incubated at 37° C for another 23 h dropwise in a circular motion evenly on top of the cells. Where necessary, after the incubation, P2Y12 antagonist was added at a concentration of 10µM dropwise evenly on top of the cells in a circular motion. Likewise, where necessary, negative controls Cyclo(Arg-Gly-Asp-D-Phe-Val) (cRGDfV, final concentration 50µM) and Cytochalasin D (CytD) (1µM final concentration) were added. The wells were incubated for one h at 37C. There was no replacement of the medium or washing off of the LPS.

During this one-h incubation, PC12 cells were counted and pelleted. The pellet of cells was stained with red-fluorescent 5-(and 6)-carboxytetramethylrhodamine succinimidyl ester (TAMRA, 580nm emission wavelength, amine-reactive fluorescent label) at a concentration of 50μM in PBS for 15 min in a tube covered in foil at room temperature. Following the 15-min incubation, the stained PC12 cell pellet was spun down at 2.0 x 10^3 xg for 5 min, washed with ice-cold PBS in the dark, spun again, and finally resuspended in cold 500μl 0.5% FBS PC12 medium (for the first trials of the experiment, 0.5% FBS BV-2 medium was used). The TAMRA-stained PC12 cells were covered in foil until immediately before use.

Co-incubation of BV-2 with PC12 cells

Immediately after the 1h antagonist (and phagocytosis inhibitors cRGDfV, CytD) incubation, the TAMRA-stained PC12 were mixed vigorously by pipetting to thoroughly break up clumps and 3.0 x 10^5 cells were added dropwise, in a circular motion directly on top of the seeded BV-2 cells evenly throughout the entire area of the well (because I was interested in phagocytosis distinct from migration, the target neurons were added directly on top of the microglia so they were already contacting one another). For the control wells that did not receive the PC12, PC12 medium was added (0.5% FBS BV-2 medium was used during the first trials of the experiment). One 24-well plate was placed in the 37 ^{o} C incubator, and as a negative control for phagocytosis, another one of the 24-well plates was covered in aluminium foil and placed on ice. These plates were incubated in their respective temperatures (37^o C and temperature on ice ~10^o C) for 2 h 45 min.

IB4-Alexa 488 (green fluorescence) staining of BV-2, transfer of suspension for PC12 recovery analysis, and brief imaging of attached cells

Immediately following the co-incubation of BV-2 and PC12, the 37^o C plate was transferred to ice and BV-2 cells in all wells were specifically stained using the green-fluorescent Isolectin-B4-Alexa-Fluor-488 (IB4) at a final concentration of 2μg/mL for 15 min (emission wavelength 488nm). IB4 is a glycoprotein that is part of a family of isolectins isolated from the seeds of the African legume *Griffonia simplicifolia*, and is selective for terminal a-D-galactosyl residues on microglia surfaces. Following IB4 staining, the suspension in the wells were transferred to either 1) fresh eppendorfs for PC12 recovery analysis with flow cytometry, or 2) poly-L-lysine coated 24-well plates for PC12 recovery analysis with microscopy (specifics detailed below). After the suspension removal, the wells were washed once with ice-cold PBS (this step was skipped for the later experimental replicates). The center of the wells were quickly observed and imaged at 10x magnification under the Leica DMI6000 microscope for imaging of the adhered (BV-2) cells. In addition to observing the cell morphology following the co-incubation, successful staining of the IB4 and TAMRA was determined through the green and red channels.

Harvest of attached (BV-2) cells

Cells were harvested with 0.5% trypsin in PBS, quenched with DMEM, and transferred to eppendorfs. The wells were washed once more with ice-cold PBS and added to the eppendorfs. The harvested cells were pelleted by spinning at 2.0 x 10^3 xg for 5 min. The cells were fixed in 50µl 4% PFA for 15 min on the shaker, after which they were pelleted and the supernatant removed. The pellet was resuspended in 50µl ice-cold PBS and kept on ice before running on BD Accuri C6 Flow Cytometer (the machine is maintained at room temperature, ~25^{o}C).

Flow cytometry analysis for phagocytosis by BV-2 of TAMRA-labelled PC12

BV-2 only samples were run first before all other samples with unlimited cell count settings, medium fluidics speed (35µl/min, 16µm core), and threshold setting at 80,000 FSC. The clear peak observed in the log plot for SSC vs. FSC plot was gated using the polygonal drawing feature on the CFlow Plus software to select for BV-2 cells (10^5.5~$10^{6.5}$ SSC, $10^{6.2}$~$10^{7.2}$ FSC). All subsequent samples were run with the setting limit of 10,000 events within this gate as done previously in Hornik et al 2016. Each sample was thoroughly mixed by pipetting before placement onto the flow cytometer. However, upon running a sample containing only PC12, the SSC vs. FSC plot yielded a clear peak within the gate made from the BV-2 only sample, indicating that both cell types yield the same size and granularity ranges by this flow method (Methods Figure 5). To distinguish BV-2 cells based on their IB4 (green) label instead and to eliminate any background green fluorescence emitted by the IB4 (green)-negative PC12 cells, SSC vs. FL1 (detects 533±30nm, green channel) was plotted for a PC12 only sample and a FL1 threshold was created (~$10^{5.2}$ FL1) such that any events past this threshold would be determined as IB4 (green)-positive, and thus definitively BV-2 cells (for later experimental replicates, the event limit was set to 10,000, not from the FSC vs. SSC gating, but for the number of events that were IB4 positive in order to increase the sample size) (Methods Figure 6).

Furthermore, in order to accurately distinguish the BV-2 cells that were TAMRA (red)-positive (phagocytosis of TAMRA-labelled neurons) from TAMRA-negative (no phagocytosis), SSC vs. FL3 (detects >670nm, red channel) was plotted for a BV-2 only sample and a FL3 threshold was created (~$10^{4.5}$), such that any recorded cells that pass this threshold would be determined as TAMRA (red)-positive, and thus the BV-2 cells that have phagocytosed TAMRA-labelled PC12s (Methods Figure 7). For the analysis, the number of events past this threshold (indicative of BV-2 cells that are TAMRA (red)-positive) out of the total number of BV-2 cells was calculated and this proportion was used as a measure of phagocytosis (Methods Figure 8). This proportion of red-positive BV-2 counts was used as opposed to mean FL3 intensity of red-positive BV-2 cells as in the ADP-beads experiment because most BV-2 (even those that are untreated) are capable of ingesting multiple beads within the incubation period and the intensity provides a measure of the extent of phagocytosis, whereas BV-2 do not consume multiple PC12 and thus the difference in overall phagocytosis is more easily probed

with the proportion of BV-2 that have eaten a PC12 versus not. In other words, in these experiments only the % FL3+ events was used to determine phagocytosis, as it was assumed that BV-2 could only phagocytose one PC12 cell at maximum over the 3 h period.

PC12 recovery analysis with flow cytometry

For analysing PC12 recovery by flow cytometry, the supernatant from all wells were transferred to fresh eppendorfs on ice and covered in aluminium foil. The recovered cells were pelleted, and the pellet was resuspended in 50µl ice-cold PBS and kept on ice before running on BD Accuri C6 Flow Cytometer. The pellet was not fixed as PC12 cells have a tendency to clump together, and so flow cytometry of recovered PC12 was always performed on the day of the experiment. Since the aim was to determine the total number of PC12 in the recovered suspension, all 50µl of each sample was run on the flow cytometer (volume limit set for 50µl, unlimited cell count and collection time, medium fluidics, 80,000 FSC threshold). Using a PC12 only sample, the peak for FSC vs. SSC was gated. To distinguish PC12 cells based on their TAMRA (red) label and to eliminate any background red fluorescence emitted by TAMRA-negative BV-2 cells, a sample of only BV-2 cells was run on the flow cytometer, and SSC vs. FL3 (red channel) was plotted. An FL3 threshold was made (~$10^{4.5}$ FL3) such that any events past this threshold would be determined as TAMRA (red)-positive, indicative of PC12 cells (in other words, the threshold was adjusted such that there were no cells in the BV-2 only sample that surpassed it) (Methods Figure 9). Thus, for analysis, the number of events counted past the FL3 threshold (by the "event count" feature of the flow cytometer) was used as a measure of the number of PC12 cells in the suspension (Methods Figure 10).

PC12 recovery analysis with microscopy

For analysing PC12 recovery by microscopy, the supernatant from all wells were transferred to poly-L-lysine coated 24-well plates. To avoid using the outer wells, these samples were divided on two 24-well plates, using only the middle wells. For coating the wells beforehand, enough poly-L-lysine to coat the entirety of the wells (~300µl) was added, the plates were incubated at 37C for 5 min, and the poly-L-lysine was completely removed and left in the hood for a few min to air-dry before being placed back at 37C until they were needed for suspension transfer. For later replicates of the experiment, the suspension was first transferred to fresh eppendorfs, and clumps of PC12 cells were thoroughly dissociated before transfer to the wells to break up aggregates which become a source of large variability among technical replicates in the counting data. Following transfer of the supernatant to the coated wells, an equal volume of warm PC12 medium was added (530µl). The wells were incubated for 1.5 h in 37^{o} C to allow for the recovered cells to adhere.

Following the incubation, the media was removed carefully with a pipette (as opposed to aspiration). The cells were fixed with 300µl of 4% PFA, the plate was covered with aluminium foil and placed on the shaker for 15 min at room temperature (~25^{o} C). The wells were washed with ice-cold PBS three

times. After the third wash, 290µl of PBS and 10ul of nuclear stain Hoechst33342 (for a final working concentration of 4µg/ml, excitation/emission wavelength 361/497nm) was added, the plate was covered and incubated at room temperature for 20 min. The wells were washed with PBS three times and taken to the Leica DMI6000 microscope for imaging.

An overview of the analysis method for PC12 recovery by microscopy is indicated in the diagram below (Methods Figure 11). One image was taken at the center of the well for all wells to get a sense of the overall density of each sample. Four microscopic fields (each $1.9x10^5$ μm^2) at 20x magnification per well in 3 wells per condition were imaged for a single experiment. The four microscopic fields were obtained such that there was one image for each of the following off-center (but not on the edge) locations of the well: upper left, lower left, upper right, and lower right. A system was in place where the microscope was positioned at the edges of the individual well first and the positioning knobs were turned in the same fashion (i.e. two and a half turns on the fast setting) to obtain each off-center position for consistency of analysis among all wells. Images for red (for detecting TAMRA stain) and blue (for detecting Hoechst stain) channels were obtained for each field. The red channel (detecting TAMRA stain) and the blue channel (detecting Hoechst stain) were overlayed, and the number of PC12 cells were counted for each image. The counts were added for the four images taken for each well. The average of this sum was calculated for the three technical replicates per condition.

Staurosporine-stressed PC12 Phagocytosis Assays

For experiments testing whether P2Y12 knock-down or inhibition affects phagocytosis of staurosporine-stressed PC12 in the absence of LPS, 5.0×10^4 BV-2 were seeded for in 0.5% FBS DMEM in two 24-well plates (an additional plate for cold incubation) for 24 h. In parallel, in a 6-well plate, PC12 cells were seeded in PC12 medium (10% HS, 5% FBS, 1/1000 Gentamicin) supplemented with 10nM concentration of staurosporine or in PC12 medium with supplemented with PBS and DMSO (as the staurosporine stock was in DMSO, which was further diluted in PBS before addition to the PC12 medium). The PC12 were incubated at 37^0C for 24 h. Following the incubation, PC12 from both stressed and unstressed conditions were separately pelleted and stained with TAMRA. Where applicable, PSB0739 was added directly to the necessary wells with seeded BV-2 for 10m before the addition of 3.0×10^5 TAMRA-labelled PC12 directly on top of the cells. As explained above, these co-cultures were incubated at either 37^0C or on ice for 3 h. PC12 recovery was analysed by microscopy, and the adhered BV-2 were analysed for phagocytosis on the flow cytometer (calculating % FL3+ events, subtracting the signal given by the cold incubation conditions).

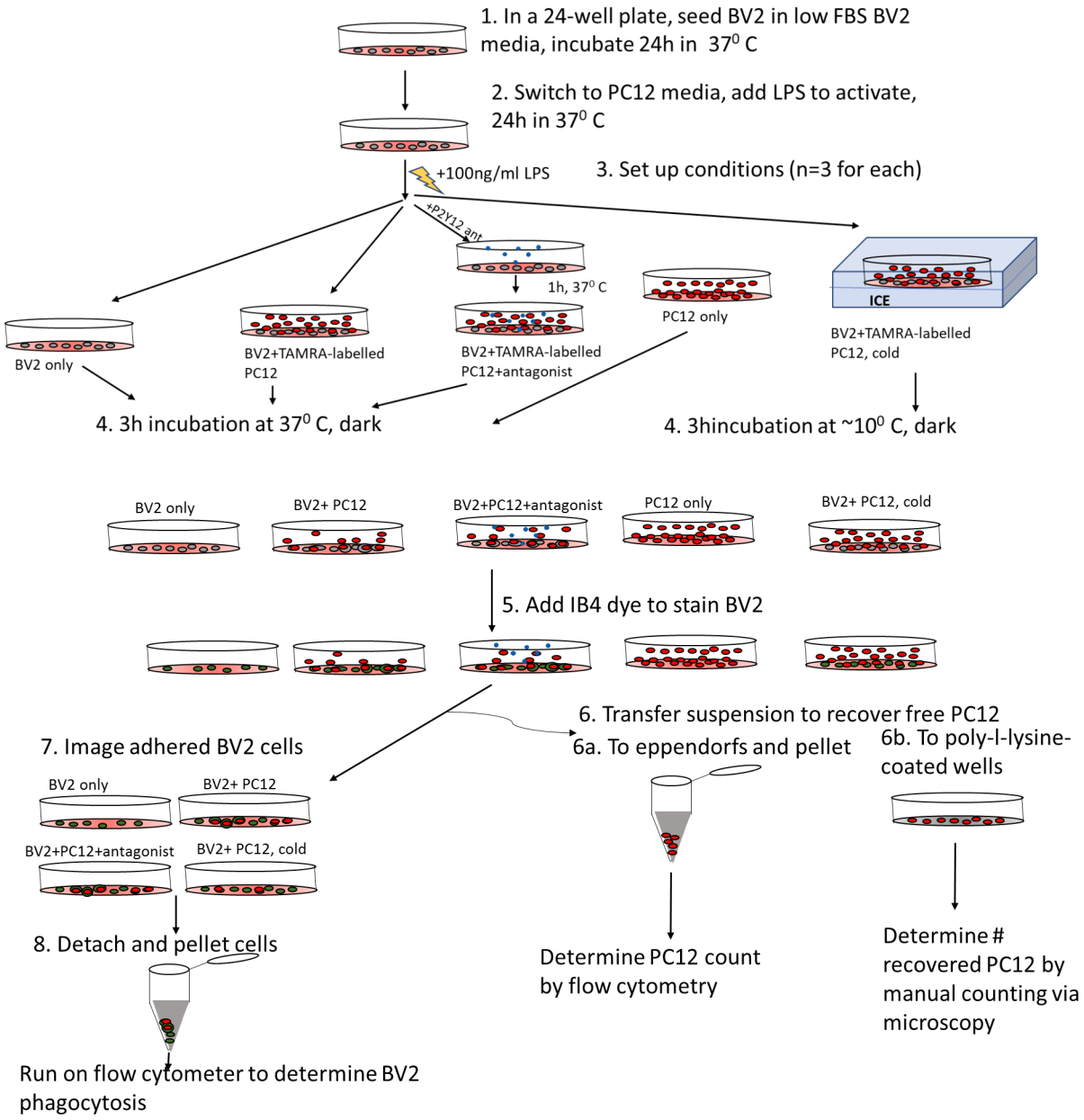

Methods Figure 4. Full Schematic Diagram of PC12-BV-2 Phagocytosis Assay under LPS stress.

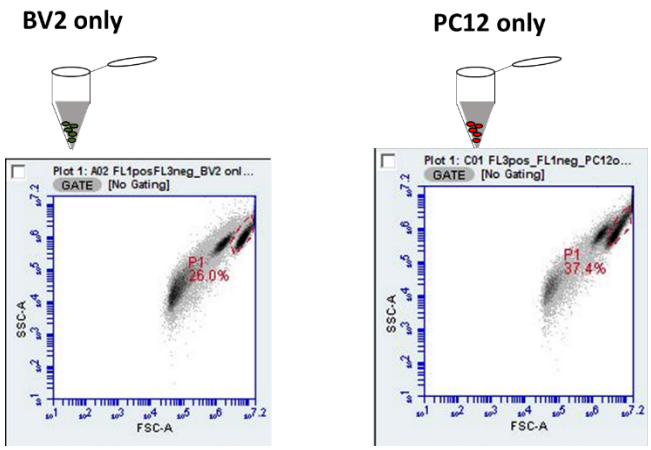

Methods Figure 5. FSC vs. SSC plots for BV-2 only and PC12 only samples

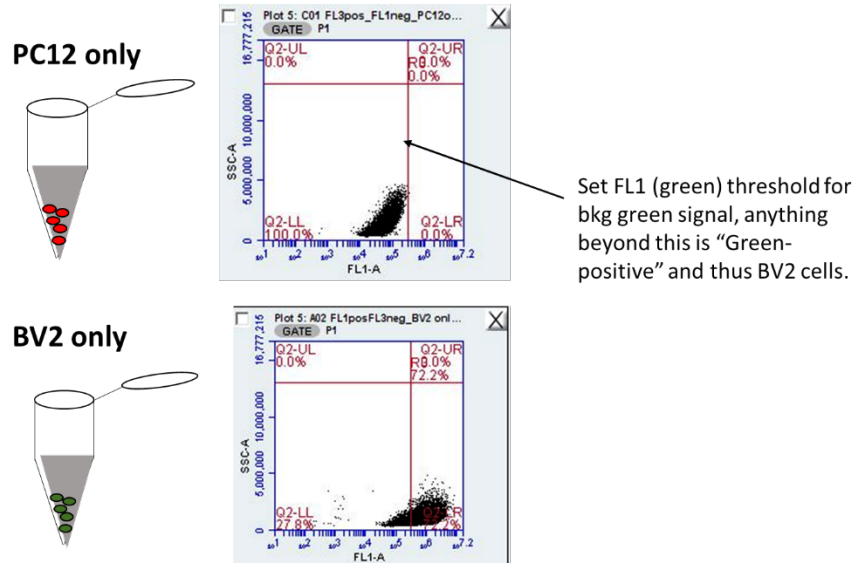

Methods Figure 6. Setting of FL1 (green) threshold for selecting for BV-2 cells.

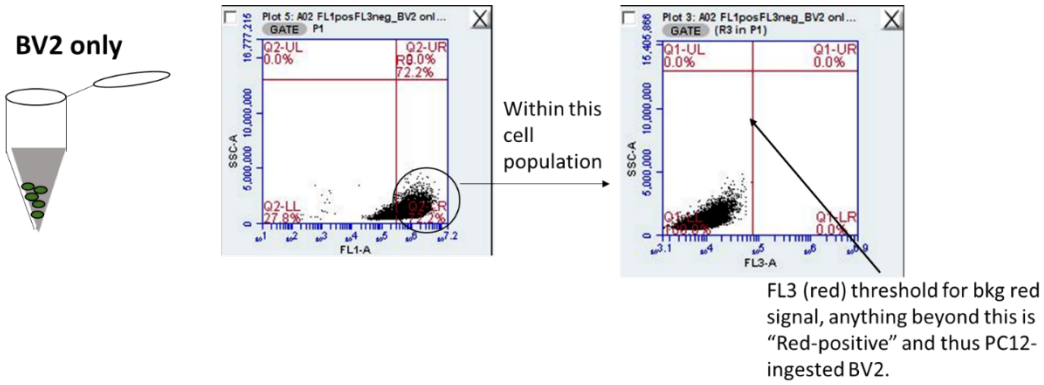

Methods Figure 7. Setting of FL3 (red) threshold for identifying PC12-ingested BV-2.

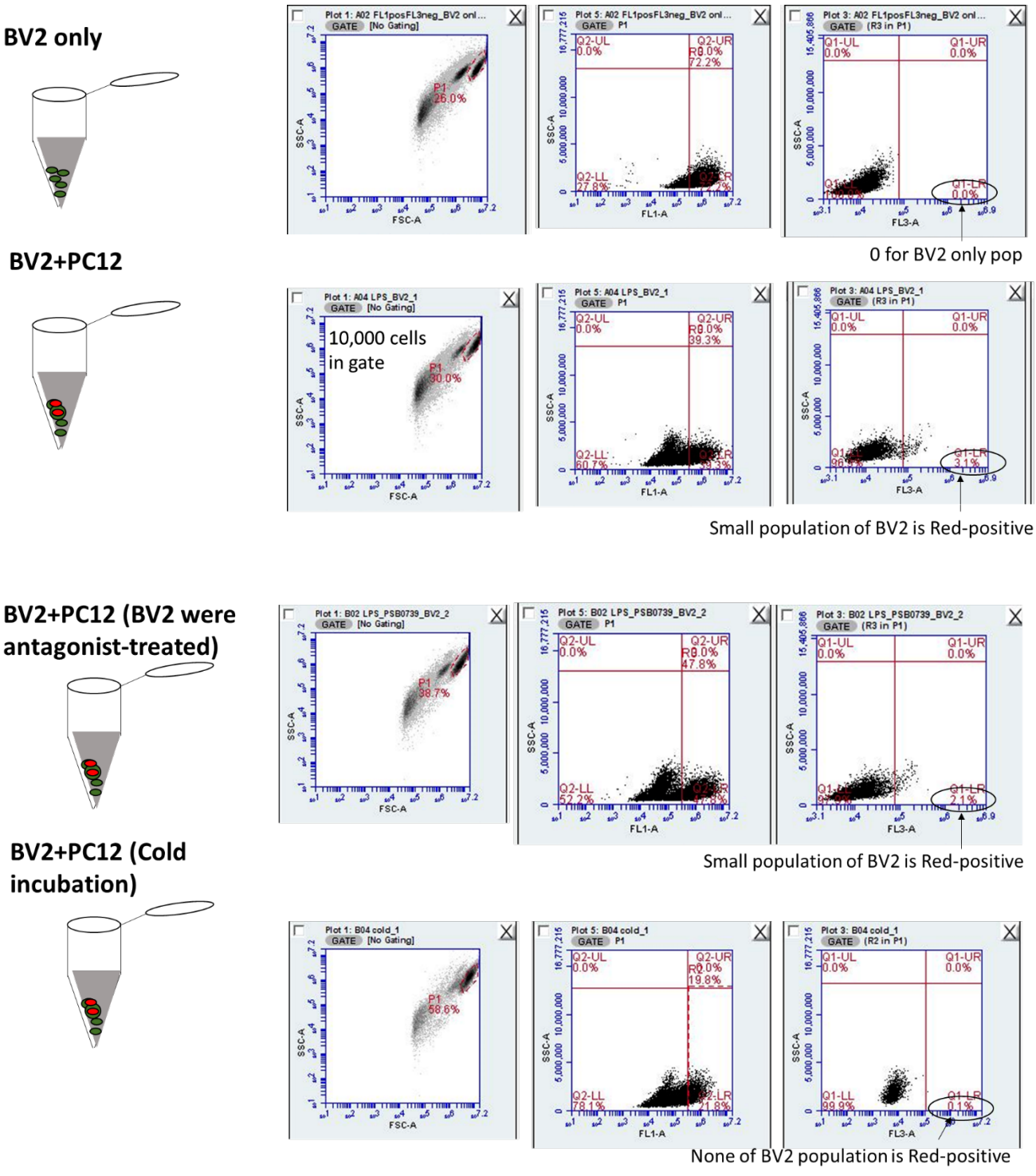

Methods Figure 8. Plots determining the percentage of TAMRA-stained BV-2 for all conditions of experiment, used for final analysis.

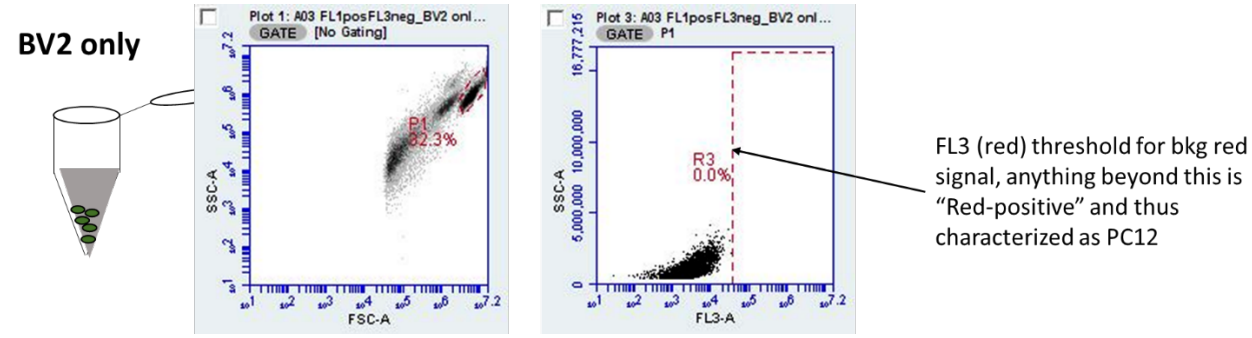

Methods Figure 9. Gating to characterize PC12 cells to use for PC12 recovery analysis by flow cytometry.

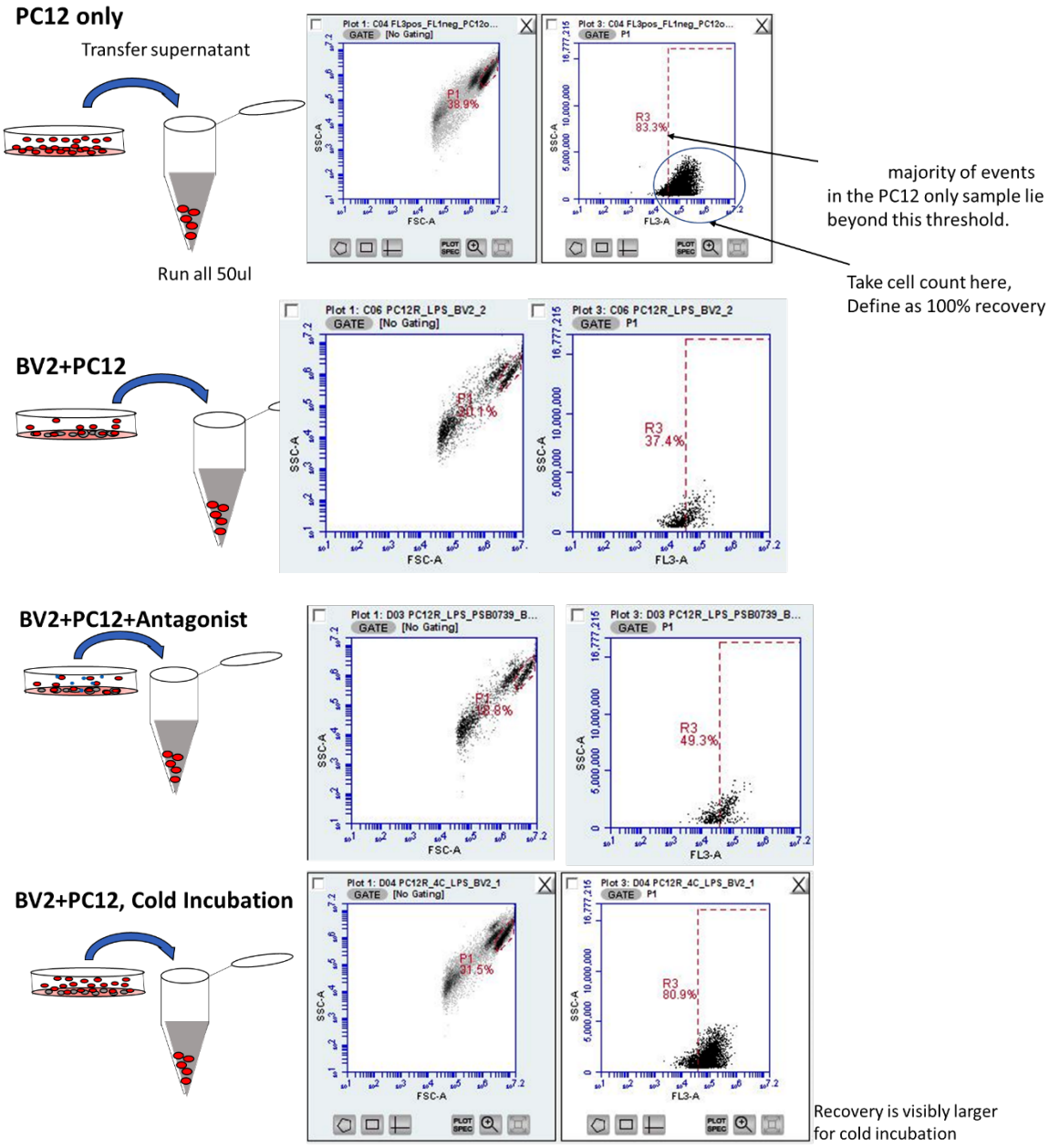

Methods Figure 10. PC12 recovery analysis via flow cytometry for all conditions of the BV-2-PC12 phagocytosis assay.

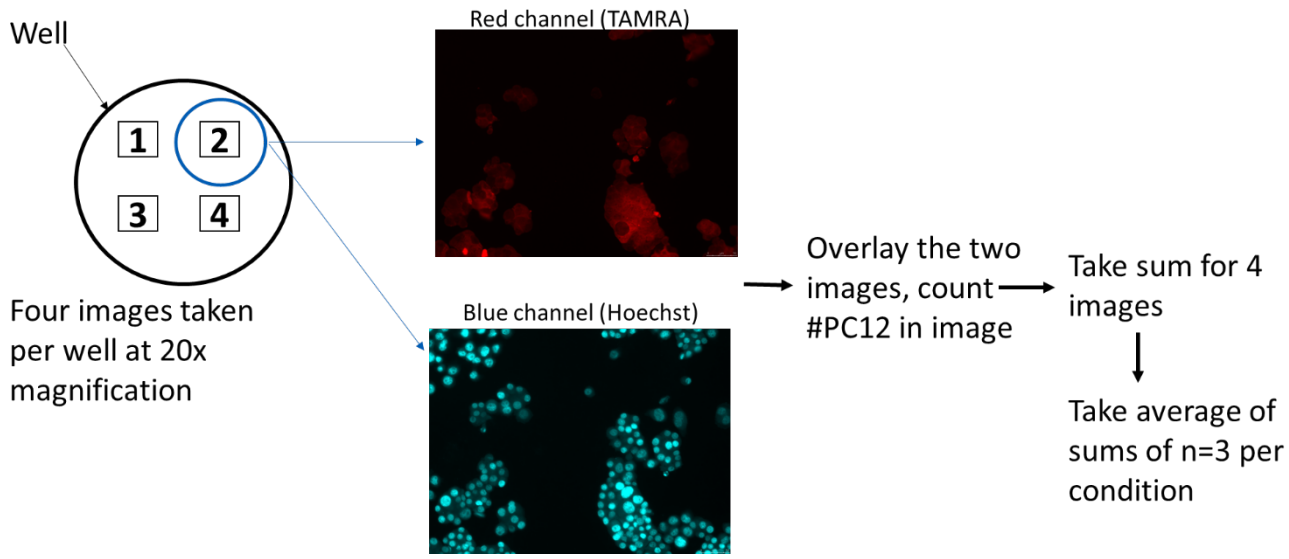

Methods Figure 11. Method of analysis for PC12 recovery via microscopy for the BV-2-PC12 phagocytosis assay.

Statistical analysis

All results are represented as means ± SEM. Statistical tests were conducted using GraphPad PRISM (version 5.03). Where there were two groups compared and one independent variable, statistical significance was analysed using unpaired two-tailed Student's t test. Where there were multiple comparisons and one independent variable, one-way analysis of variance (ANOVA) followed by Tukey's post-hoc test was used. Where there were multiple comparisons and two independent variables, two-way ANOVA followed by Tukey's post-hoc test was conducted. All p values below 0.05 were considered significant and degree of significance is represented as *p<0.05, **p<0.01, ***p<0.001, and ****p<0.0001.

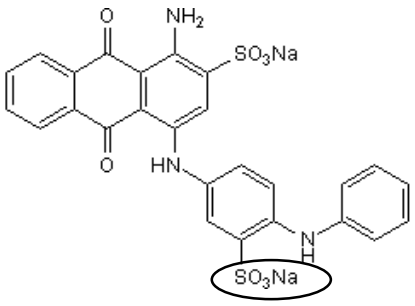

Methods Figure 12. Structure of PSB0739. PSB0739 is understood to be the most potent antagonist of human P2Y12, with a Ki=24.9nM (Hoffman et al., 2009). It is an analogue of the non-nucleotide antagonist reactive blue-2 (RB-2), and targets specifically Arg256 (one of the important amino acids making up the ADP binding pocket) of human P2Y12 via one of its sulfonic acid residues (circled), acting as a competitive and reversible

inhibitor with a short duration of action. Non-nucleotide antagonists are understood to be beneficial as they have a longer plasma half-life compared to nucleotide-derived compounds. It does not require bioactivation. Although it was designed to target human P2Y12, Arg256 in human appears to correspond to Arg262 in mouse, also in transmembrane 6 region (Pausch et al., 2004). Thus, it is likely that PSB0739 interacts with mouse P2Y12 in the same manner. It has indeed been used in experimental studies on P2Y12 function in mouse microglial chemotaxis (Takayama et al., 2016; Madry et al., 2018). It is presently not a clinically sold medication.

Results

The main aim of the thesis was to determine if the P2Y12 receptor promotes microglial phagocytosis and, if so, whether inhibition of the P2Y12 receptor could in principle be neuroprotective in stressed conditions, where inflammatory stimuli such LPS or Aβ induce excessive microglial phagocytosis of live neurons. Additionally, I sought to examine whether the expression P2Y12 is dependent on ADP-mediated activation of the P2Y12 receptor itself.

The P2Y12 receptor is expressed in BV-2 microglia at higher level than in PC12 cells but at a lower level than in primary microglia

Since these experiments utilize the immortalized murine microglial cell line BV-2, which exhibit genome-wide alterations compared to primary microglia, as a preliminary step, I wanted to confirm that these BV-2 cells expressed P2Y12 at levels that could be detected by RT-qPCR. I ran cDNA isolated from BV-2 cells alongside cDNA isolated from the rat neuroblast-like cell line PC12 as a negative control, as well as cDNA from primary mouse microglia for comparison of expression levels. Although I found that P2Y12 is transcriptionally expressed 5-fold less in BV-2 than in primary microglia, the expression level detected through the RT-qPCR analysis was enough to yield a clear distinction in signal between the positive P2Y12 expression in BV-2 compared to the lack of expression in PC12 neurons (Figure 1).

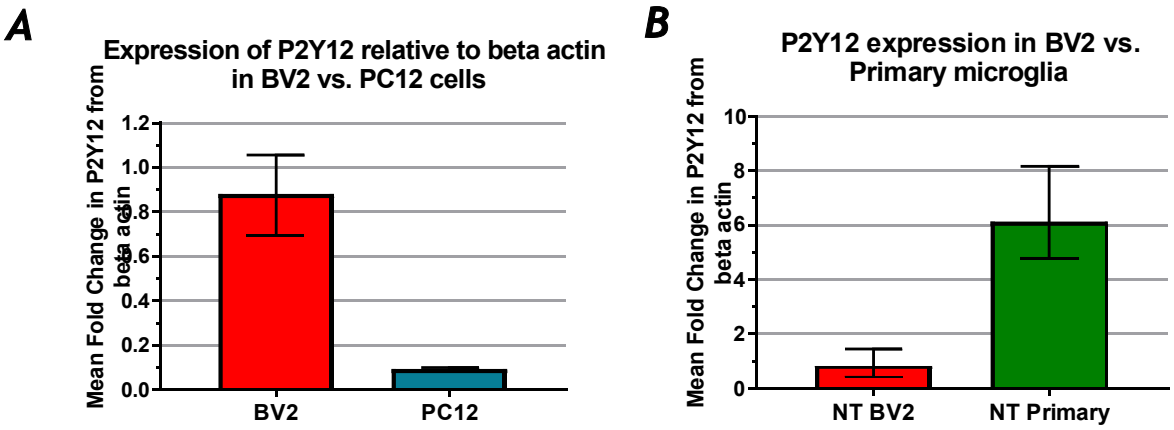

Figure 1. P2Y12 mRNA expression level is higher in BV-2 than PC12, but is lower compared to primary microglia. A: RT-qPCR was performed for untreated BV-2 and PC12 cells to check for expression of P2Y12 at the RNA level in the two cell types with respect to beta-actin. Data = mean with range (3 technical replicates). **B:** P2Y12 expression relative to beta-actin for BV-2 cells and primary mouse microglia, both 48h post-transfection with non-target siRNA. Data = mean with range (3 technical replicates).

The P2Y12 receptor agonist ADP causes a calcium transient in BV-2 microglia

As another preliminary question, I wanted to determine the optimal concentration of ADP treatment to BV-2 cells to ensure P2Y12 activation in these cells. Downstream of P2Y12 ligand binding, intracellular calcium release occurs in microglia, and thus measurement of calcium response is one strategy to examine P2Y12 activation. I conducted a calcium assay to determine whether 100µM or 1mM ADP concentrations were capable of inducing an intracellular calcium response (via P2Y12). 100µM ADP treatment immediately induced a calcium response in BV-2 cells, and the intensity of the response was unchanged when the concentration of ADP treatment was increased to 1mM (Figure 2). Thus, I concluded that 100µM ADP was enough to activate the P2Y12 receptor in BV-2 cells.

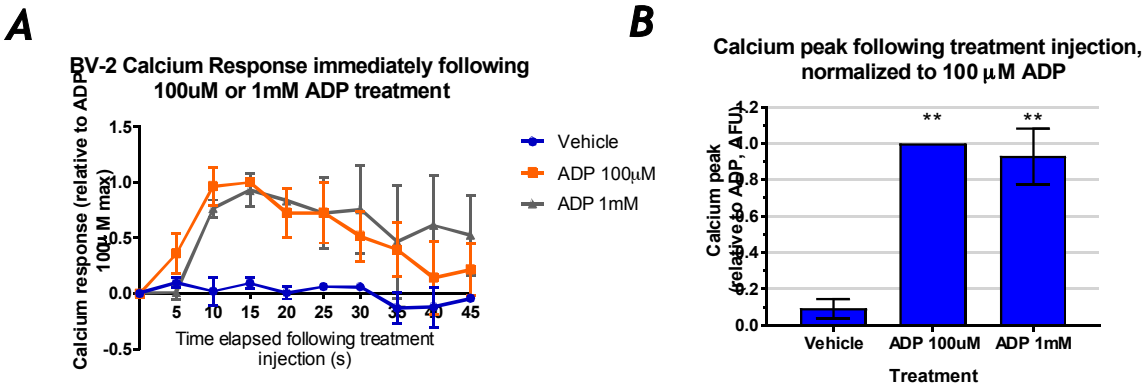

Figure 2. ADP induces an immediate calcium response in BV-2 cells. A: BV-2 microglia were treated with PBS (vehicle, blue), 100µM ADP (orange), or 1mM ADP (grey), and the calcium response (as measured by fluorescence emitted due to indicator activation) was recorded every 5s immediately following treatments using FlexStation. All data are normalized to the peak fluorescence value corresponding to the 100µM ADP condition of the respective independent experiment. Data = mean ± S.E.M. (standard error), n = 3. **B:** Maximum values indicating maximum calcium response obtained for each condition. Data = mean ± S.E.M., n = 3, ** $p<0.01$ versus vehicle, 1-way ANOVA with Tukey's HSD post-hoc test.

Addition of ADP does not change microglial phagocytosis of beads

A central aim of this research was to determine whether P2Y12 regulates microglial phagocytosis, so I initially tested whether the P2Y12 agonist ADP could increase microglial phagocytosis of beads. To determine whether addition of ADP alters microglial phagocytosis of beads, either 100µM ADP or PBS was added together with 1µm red-fluorescent latex beads to BV-2 cell cultures for 1 h incubation at 37 ^{o}C. After the incubation, the cells were pelleted for flow cytometry analysis to measure phagocytosis. When the cell-bead cultures were imaged immediately following the incubation, in both ADP-added and control conditions, the cells exhibited rounded morphologies and appeared viable, with a range of 0-4 beads internalized per cell (Figure 3).

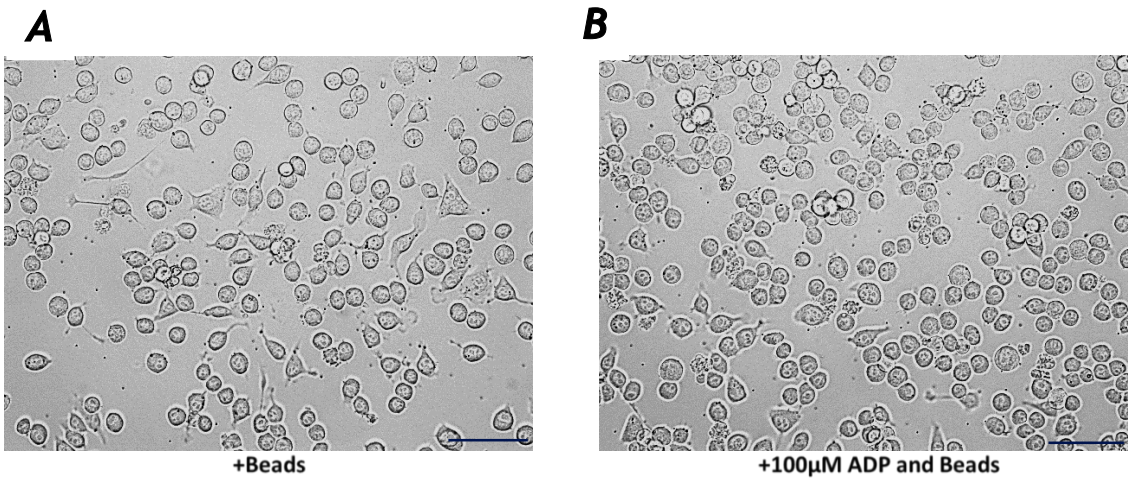

Figure 3. BV-2 cells appear viable even after 1h of exogenous ADP and bead addition. 100,000 BV-2 were seeded in 0.5% FBS DMEM overnight, then treated with either **A:** 0.0012% w/v 1 µm fluorescent beads, or **B:** 0.0012% w/v beads and 100 µM ADP together, for 1 h in 37°C. Images are of the bead-BV-2 co-cultures taken immediately following the incubation. Both treatments yielded round cell morphologies even though all cells showed process ramifications after the overnight incubation before treatments, which suggested that the addition of beads, not the ADP treatment, had an activating effect on the microglia. It appears 0-4 beads are ingested per cell for both conditions. Scale bar represents 75µm (BV-2 diameter is ~12 µm).

For both ADP-added and control conditions, parallel incubations were performed on ice. Under cold conditions, adherence properties of microglia remain unaffected but phagocytosis is perturbed. Indeed, the cold incubation (as shown for the control condition for three independent replicates here) yielded lower positive signals than the 37°C counterparts, both in terms of mean FL3 (mean fluorescence intensity of events within FL3+ gating, indicative of the number of beads ingested per cell) and fraction of events in FL3+ gating (indicative of fraction of total BV-2 that have ingested at least one bead) (Figure 4).

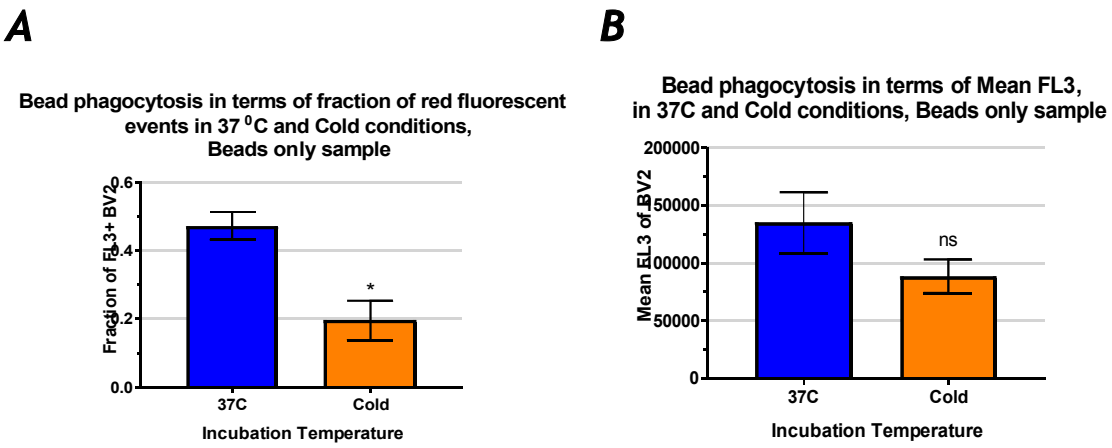

C

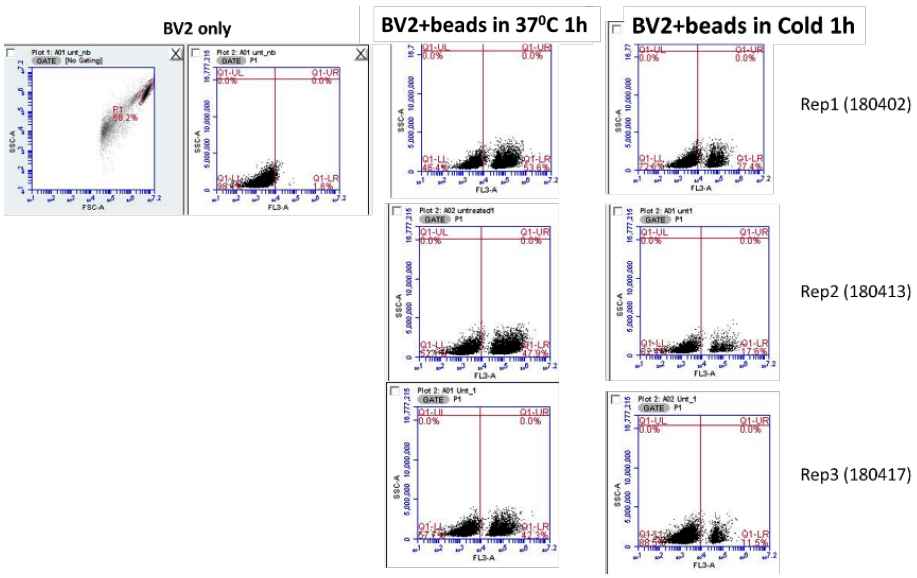

Figure 4. Cold incubation on ice consistently yields lower bead phagocytosis compared to 37^{0}C condition. BV-2 were seeded in 0.5% FBS DMEM overnight, then treated with 0.0012% w/v 1 µm red-fluorescent beads for 1 h either in 37^{o}C or on ice. Samples were run on the flow cytometer. **A:** Fraction of red-fluorescent events among BV-2 cells, and **B:** mean FL-3 values among FL3-positive BV-2 were obtained as measures of bead phagocytosis. Data = mean ± S.E.M., n = 3, * $p < 0.05$ versus 37^{o}C condition, unpaired two-tailed Student's t test. **C:** The initial gating to distinguish BV-2, as well as representative images from each independent experiment of the 37^{o}C and cold conditions are shown. The number of events past the FL-3 threshold, as well as the spread (mean FL3) is clearly affected by the cold incubation.

In order to examine only phagocytosis as separate from adhesion, the difference in the fraction of FL3+ events between the 37^{O}C condition and corresponding cold conditions for the same treatments can be calculated, and these values can be used to quantify for "true" ingestion. Thus, for subsequent phagocytosis analyses, phagocytosis as measured by % FL3+ events was determined by calculating this difference.

Upon making these calculations for the untreated and ADP-added conditions, the addition of 100µM exogenous ADP was found to maintain equivalent levels of bead phagocytosis as the untreated condition (Figure 5).

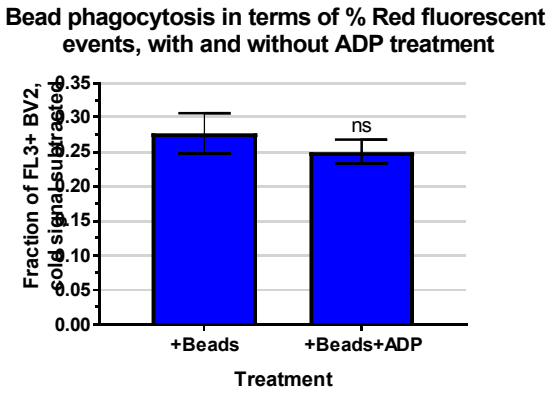

Figure 5. Bead phagocytosis is unchanged with the addition of exogenous ADP treatment. BV-2 cells were treated with either 0.0012% w/v beads or 0.0012% w/v beads with 100µM ADP and incubated for 1 h at 37°C in 0.5% FBS DMEM. The cells were run on the flow cytometer and the fraction of FL3+ (red-fluorescent) events, as an indication of bead phagocytosis, were determined. Fraction of FL3+ events corresponding to identical samples incubated over ice were subtracted from that obtained from 37 °C. Data = mean ± S.E.M., n=3, ns = not significantly different to beads only condition, $p > 0.05$, unpaired two-tailed Student's t test.

To address the possibility of ADP degradation over the 1h incubation period, the same experiment was repeated, in which the bead-BV-2 co-incubation with or without ADP was decreased to 30 min. As expected, the shorter incubation yielded less phagocytosis as demonstrated by fraction of FL3+ events, but the ADP added condition still remained unchanged in relation to the untreated samples (Figure 6).

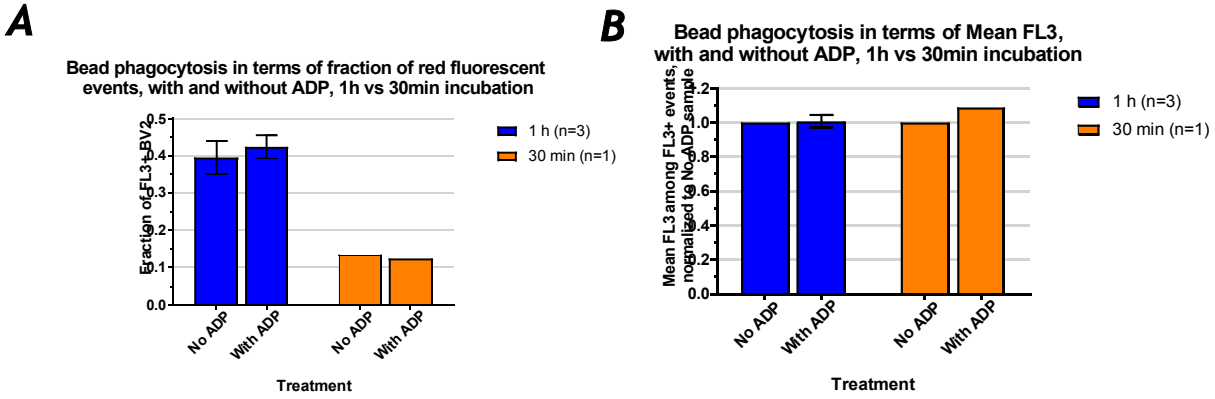

Figure 6. Shortening incubation to 30min still yields equivalent levels of bead phagocytosis between untreated and ADP added conditions. BV-2 cells were treated with either 0.0012% w/v beads or 0.0012% w/v beads with 100µM ADP and incubated for 30 min or 1 h at 37°C in 0.5% FBS DMEM. **A:** Fraction of red-fluorescent events among BV-2, and **B:** mean fluorescence intensities recorded among all red-fluorescent BV-2 were determined as measures of phagocytosis. For 1h incubation (blue): Data = mean ± S.E.M., n=3. For 30min incubation (orange): data = mean (3 technical replicates).

P2Y12 antagonist PSB0739 inhibits the ADP-induced calcium transient in microglia in a time dependent manner

To explore the possibility that the "untreated" BV-2 had activated P2Y12 due to self-released ADP, maintaining phagocytosis at a level unaffected with additional exogenous ADP, I decided to test whether microglial phagocytosis was affected by addition of P2Y12-specific competitive inhibitor, PSB0739. Previous studies have used this antagonist at 10µM concentration for in vitro primary microglia studies, but the optimal incubation times noted in the literature are variable, ranging from 10 min to 1 h, and clear optimization with BV-2 cells has not been established.

First, the viability of BV-2 in response to 10µM PSB0739 treatment for 1 h, the longest incubation time indicated in other reports, was examined by imaging. The cells were incubated in 0.5% FBS (low serum) DMEM. From this preliminary experiment, I was able to establish that the cells appeared viable with the 1 h treatment. Note, however, that the PSB0739-treated BV-2 may have

less process extension than the cells treated with PBS in the low-serum environment (Figure 7), consistent with the known regulation of microglial process extension by P2Y12.

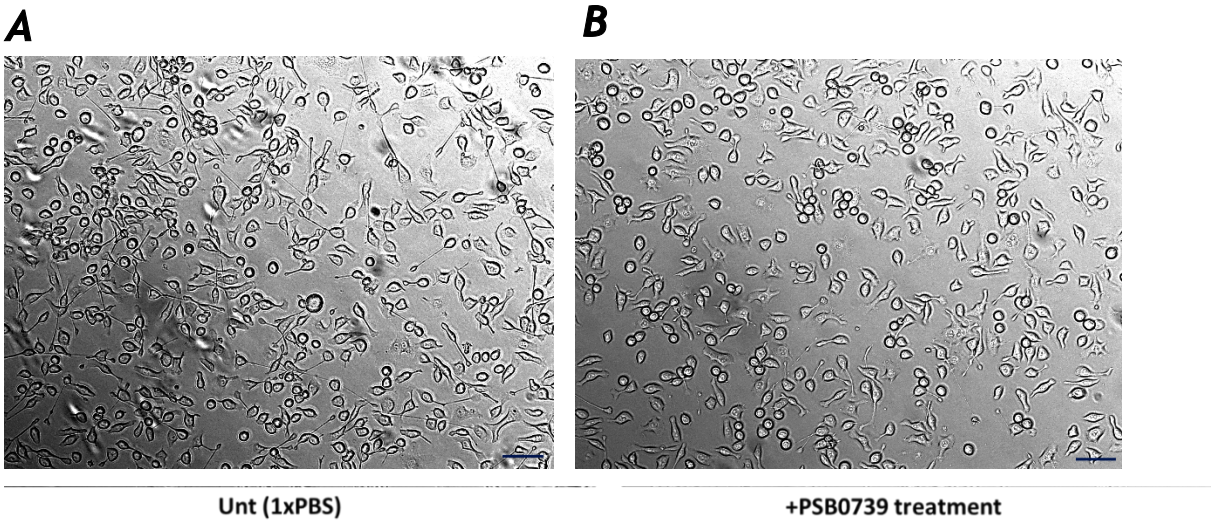

Figure 7. 1h 10 µM PSB0739-treated BV-2 are viable. BV-2 cells were seeded in 0.5% FBS DMEM overnight at a density of 300,000 cells in two wells of a six-well plate, then the following day one well was treated with **A:** PBS and the other with **B:** 10µM PSB0739. The plate was incubated in 37°C for 1 h and imaged on brightfield setting. Scale bar represents 75µm.

Upon establishing that the cells survive even with the longest incubation time indicated in the literature, next I sought to determine the optimal time course for PSB0739 incubation and its efficiency in blocking P2Y12 at 10µM concentration. I conducted a calcium assay time course, testing the ability of PSB0739 to inhibit the ADP-induced calcium response in BV-2 cells. BV-2 cells were treated with the inhibitor for 1 h 20 min, 20 min, or 10 min prior to, or at the same time as, 100µM ADP treatment. Cells treated with the inhibitor and ADP simultaneously yielded a clear response, unchanged from the ADP-only condition, and 1 h 20 min-incubated cells also showed a clear, although delayed, ADP-induced response (Figure 8). In comparison, 10 min and 20 min pre-treated cells showed an attenuation in calcium response to ADP, suggesting that 10 min to 20 min preincubation is the optimal length for efficient PSB0739-mediated P2Y12 inhibition.

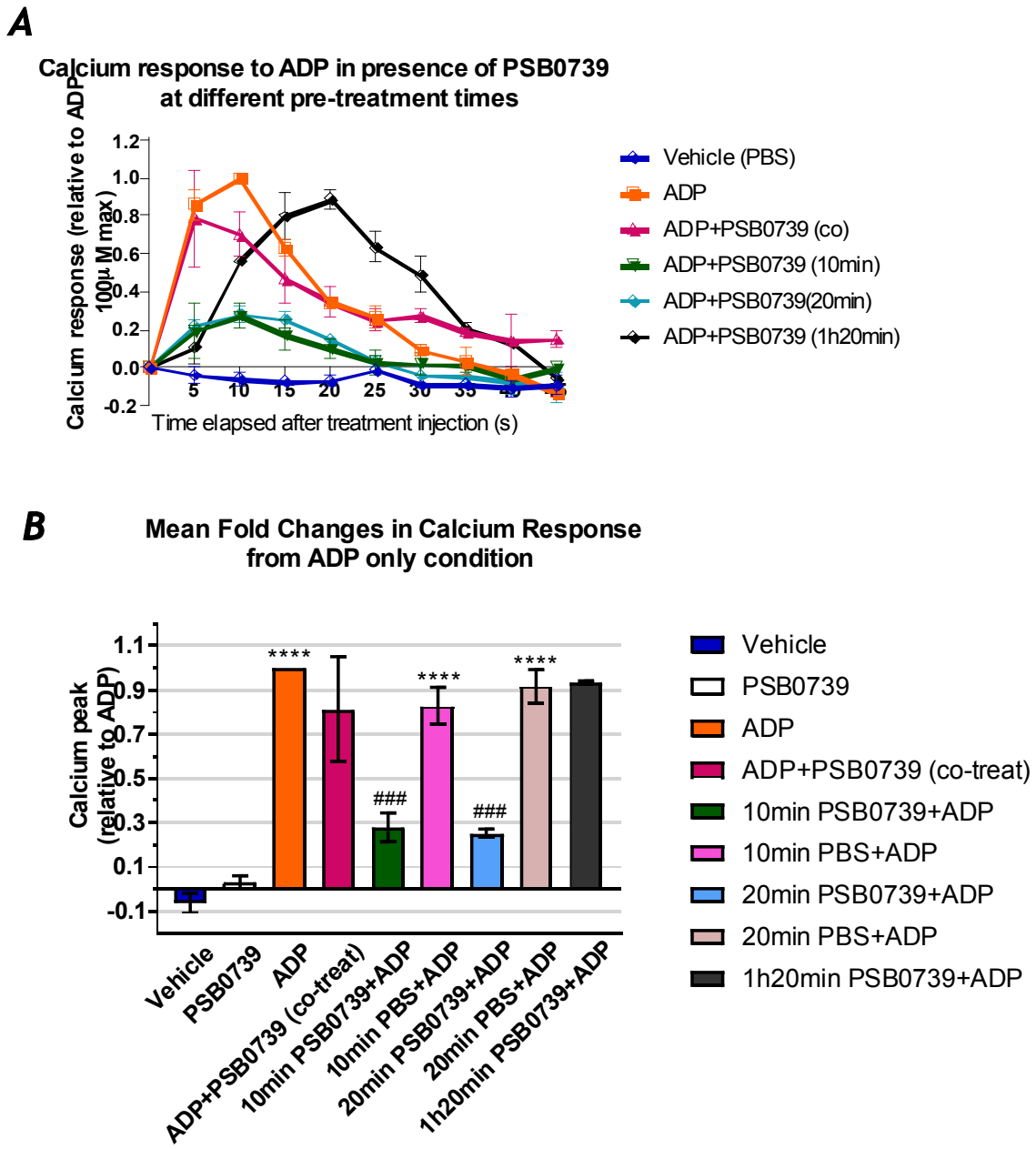

Figure 8. Attenuation of ADP-induced calcium response using P2Y12 inhibitor PSB0739 is time-dependent. A: Calcium response curves of untreated BV-2 following injection with PBS (dark blue), 100µM ADP (orange), ADP and 10 µM PSB0739 together (magenta). Additionally, calcium responses to ADP injection in 10min PSB0739-treated (green), 20min PSB0739-treated (light blue) and 1h 20min PSB0739-treated (black) BV-2 are overlayed. All data are normalized to the peak fluorescence value corresponding to the 100µM ADP condition. Data = mean ± S.E.M., n=3 (except for co-treatment and 1h20min curves where data = mean with range, n=2). **B:** Maximum values indicating level of calcium responses for each condition normalized to ADP condition. Data for untreated BV-2 injected with 10 µM PSB0739 only (white), for 10min PBS-treated BV-2 injected with ADP (control for 10min PSB0739 time point, pink), and for 20min PBS-treated BV-2 injected with ADP (control for 20min PSB0739 time point, light pink) are added. Data = mean ± S.E.M., n=3, **** $p < 0.0001$ versus vehicle, ### $p < 0.001$ versus ADP, 1-way ANOVA with Tukey's HSD post-hoc test (except for co-treatment and 1h 20min conditions where data = mean with range, n=2).

P2Y12 inhibitor decreases unstimulated microglial phagocytosis of beads

To determine if P2Y12 inhibition alters the phagocytic capacity of BV-2 to beads, BV-2 were incubated with PSB0739 for 10 min, then treated with 1µm beads for 1 h. To further examine whether the addition of exogenous ADP has an effect on phagocytosis in P2Y12-inhibited cells, the addition of beads was accompanied with or without 100µM ADP treatment. In terms of the fraction of microglia taking up beads (fraction of FL3+ event values), phagocytosis was reduced significantly by PSB0739 in the absence of ADP, but not in the presence of ADP (Figure 9). The effect of PSB0739 was less clear when measuring bead uptake per cell (mean FL3 values) due to large variability among experiments.

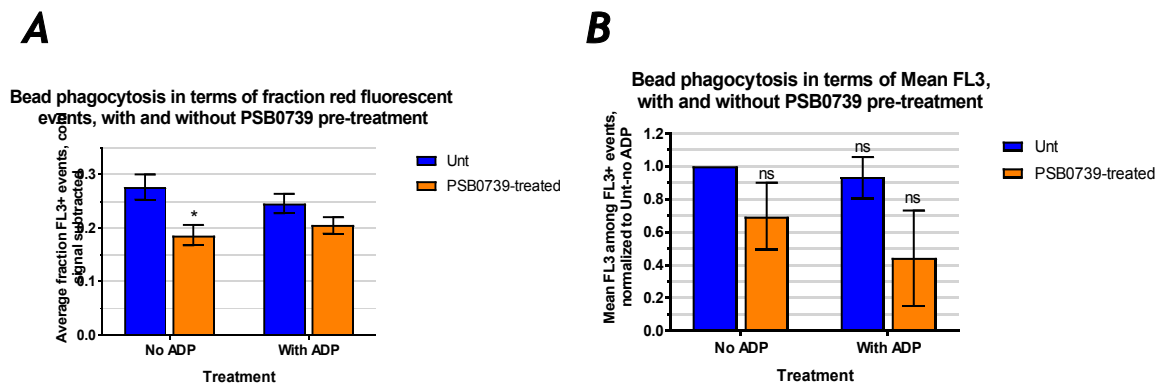

Figure 9. P2Y12-inhibited cells show decreased bead phagocytosis which is slightly recovered with the presence of exogenous ADP, as measured by fraction of red-fluorescent events. Untreated and 10-min 10µM PSB0739 pre-incubated BV-2 cells were treated with either 0.0012% w/v beads or 0.0012% w/v beads with 100µM ADP for 1 h at 37°C in 0.5% FBS DMEM. **A:** Fraction of red-fluorescent BV-2 with data corresponding to cold condition subtracted, and **B:** mean fluorescence intensities recorded among all red-fluorescent BV-2 were determined as measures of phagocytosis. Data = mean ± S.E.M., n = 3, * $p < 0.05$ versus Unt no ADP condition, 2-way ANOVA with Tukey's post-hoc HSD test.

siRNA knockdown of P2Y12 blocks the ADP-induced calcium transient in microglia

The above findings supported the idea that BV-2 are releasing ADP themselves, which may be activating P2Y12 without addition of any exogenous ADP. The inhibitor perhaps competes directly for the binding site of P2Y12, but exogenous ADP addition shifts the balance toward greater ADP binding to P2Y12, leading to slight recovery of the baseline phagocytosis. In short, the results suggest that P2Y12-ADP binding does indeed play a role in microglia phagocytic function, but at baseline levels, and the ADP is mainly supplied by the BV-2 itself.

To probe the functional role of P2Y12 further, I knocked down expression of P2Y12 in BV-2 by transient transfection with a specific siRNA. 48 h following each transfection performed (all experiments using genetic knockdown cells were conducted 48-h after transfection), RNA was extracted from these BV-2 cells and their P2Y12 expression levels were measured, to determine the knockdown efficiency of each transfection. The results of the RT-qPCR conducted for each transfection suggested that the siRNA used does effectively downregulate P2Y12 expression,

although the knockdown efficiencies were highly variable among the five transfections performed. The efficiencies ranged from 35% to 90% reduction in P2Y12 expression, compared to BV-2 transfected with a non-target siRNA performed in parallel (Figure 10). The viability of the BV-2 48 h post-transfection appeared to be unaffected by the knockdown as indicated by imaging, but the P2Y12 siRNA-transfected cells appeared to exhibit less process extension compared to the non-target siRNA transfected cells (Figure 11).

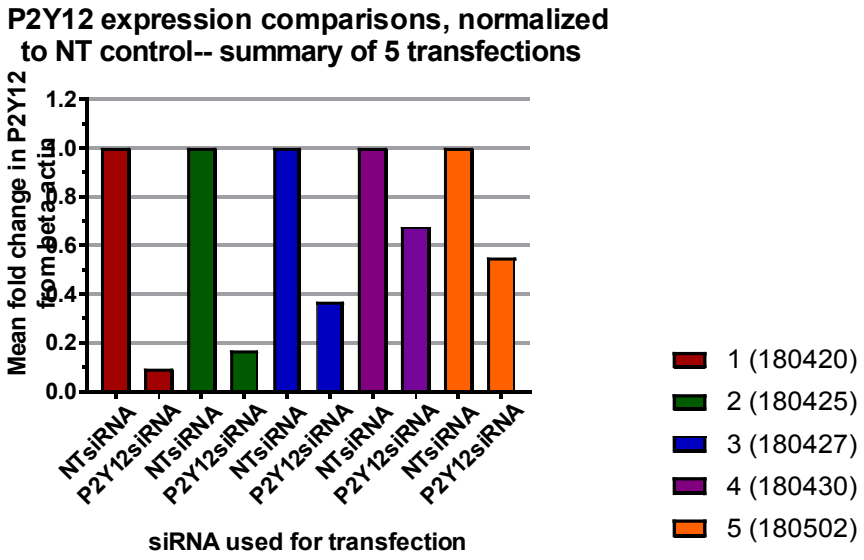

Figure 10. P2Y12 transient knockdown cells were established, demonstrating 35-90% knockdown efficiency. BV-2 cells were transfected with either a non-target siRNA or P2Y12-targeting siRNA on five different days. For each transfection, 48 h later, the RNA of these cells were extracted and the P2Y12 expression relative to beta-actin was determined by RT-qPCR. It should be noted that Lipofectamine 2000 was used for the first three transfections, and Lipofectamine 3000 for the last two transfections, which could explain the drops in reduction efficiency. All data indicated are normalized to the non-target transfection for the corresponding day of transfection. Data = means (3 technical replicates).

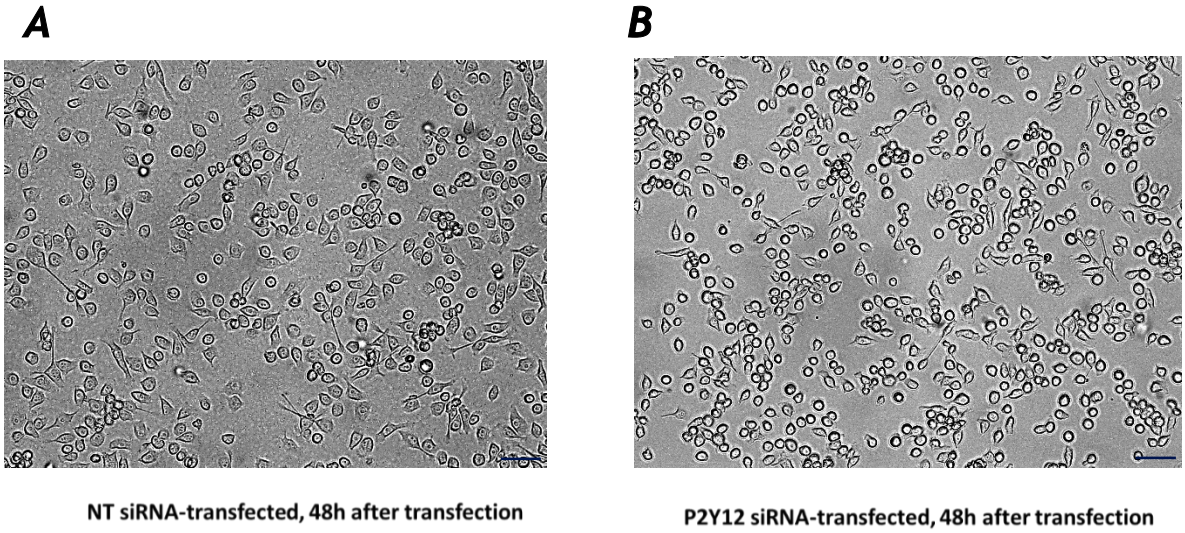

Figure 11. P2Y12 siRNA-transfected cells remain viable. BV-2 cells were transfected with either a non-target siRNA or P2Y12-targeting siRNA, and 48h later cells were imaged on the brightfield setting. Cells were

incubated in 10% FBS DMEM. This sample corresponds to Transfection 1, for which RT-qPCR analysis indicated 90% knockdown efficiency. Scale bar represents 75µm.

To test functional knockdown in the P2Y12 siRNA-transfected cells, for two experiments, these knockdown cells were subjected to ADP treatment and the calcium response was recorded. For both replicates, the knockdown cells exhibited attenuated calcium responses compared to the non-target control, further suggesting that the expression of P2Y12 had been reduced as a result of the transfection. These results also indicated that P2Y12 is the main receptor responsible for ADP-mediated calcium signalling in BV-2 (Figure 12).

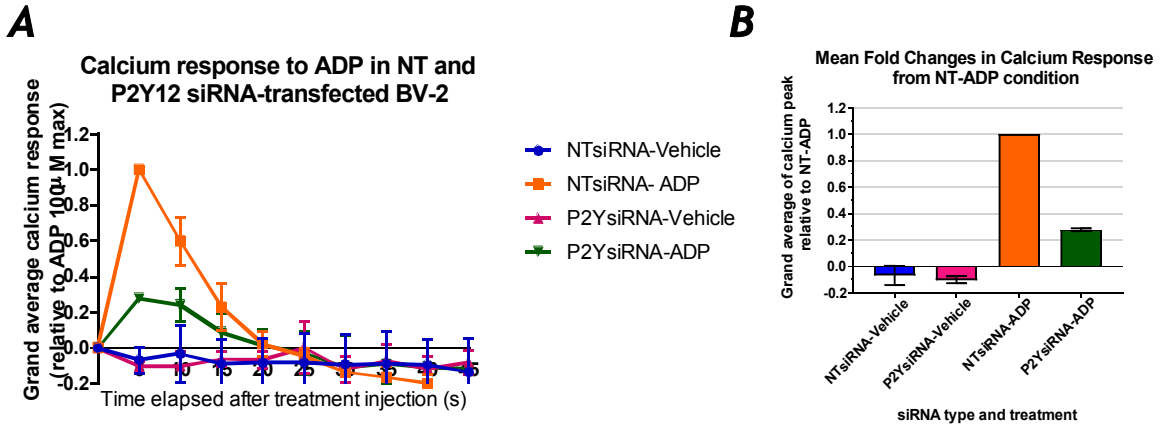

Figure 12. P2Y12 knockdown cells exhibit attenuated calcium response to ADP. Non-target siRNA and P2Y12 siRNA-transfected cells (transfections 1 and 5), were subjected to either PBS or 100µM ADP treatment injection and calcium responses were obtained 48h post-transfection. **A:** Calcium response curve as a function of time following treatment injection, where all data are normalized to the peak fluorescence value corresponding to the 100µM ADP condition. Data = mean with range, n = 2. **B:** Maximum fluorescence values indicating level of calcium responses for each condition normalized to 100µM ADP. Data = mean with range, n = 2. The method of analysis is unchanged from other calcium assays, but the arrival to the calcium maximum point is faster for this experiment (5s post-injection) compared to other experiments (i.e. for PSB0739 time course, most curves reach maximum at 10s). This observation indicates that siRNA-transfected cells react more readily to ADP than untransfected BV-2.

siRNA knockdown of P2Y12 does not lead to significant decreases in bead phagocytosis

Upon repeating the bead phagocytosis assay with P2Y12-knockdown cells, I found that P2Y12 knockdown cells do not show significant changes in bead phagocytosis, in terms of Mean FL3 and fraction of FL3+ events (overall phagocytic counts). In the presence of added ADP, there was no clear effect of knockdown due to variability between experiments (Figure 13). The lack of significant differences in phagocytosis may be related to the low transfection efficiencies of the knockdown cells used in the experiment.

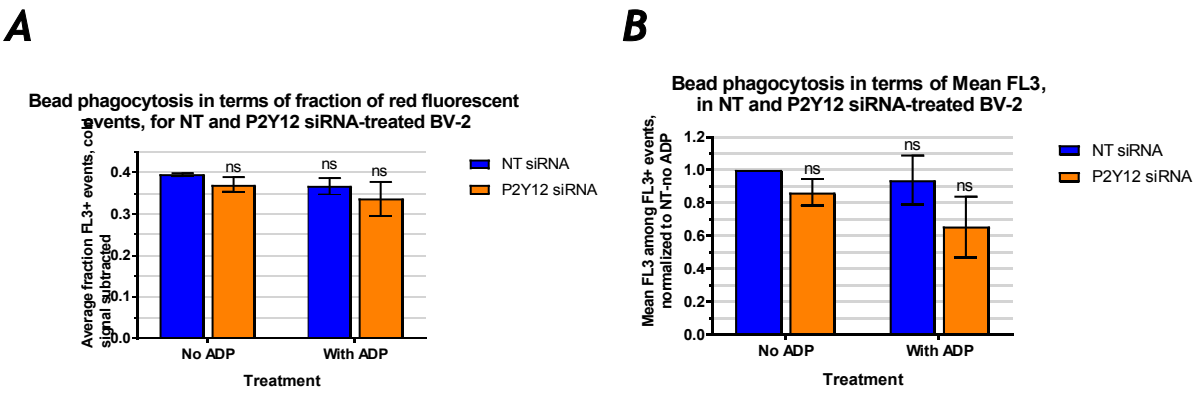

Figure 13. P2Y12 knockdown cells do not show significant decreases in bead phagocytosis. Non-target and P2Y12 knockdown BV-2 cells (transfections 3-5) were treated with either 0.0012% w/v beads or 0.0012% w/v beads with 100µM ADP for 1 h at 37°C in 0.5% FBS DMEM. **A:** Fraction of red-fluorescent BV-2 with data corresponding to cold condition subtracted, and **B:** mean fluorescence intensities among all red-fluorescent BV-2 were determined, as measures of phagocytosis. Data = mean ± S.E.M., n = 3, ns= not significantly different to Unt no ADP condition , p>0.05, 2-way ANOVA with Tukey's post-hoc HSD test.

LPS activates microglia, and PSB0739 decreases bead phagocytosis by LPS-activated BV-2

To address more directly the original question of the role of P2Y12 in stress-induced excessive microglial phagocytosis, I decided to examine the role of P2Y12 in the phagocytic activity of BV-2 in the presence of LPS.

First, to determine that 100ng/ml LPS treatment was sufficient to activate BV-2 cells, I confirmed that this treatment upregulated mRNA expression of the pro-inflammatory cytokine IL-6, measured by qPCR for BV-2 treated with LPS for 24 h compared to an untreated control (Figure 14). BV-2 cells treated with 100ng/ml LPS for 24 h also exhibited a change to a round cell morphology in comparison to untreated controls, further indicating a response to LPS (Figure 15). Moreover, LPS-stressed BV-2 phagocytosed more beads during a 1 h incubation period compared to unstressed BV-2, particularly in terms of mean FL3 (Figure 16). Taken together, these observations established that 100ng/ml LPS treatment for 24 h is sufficient to induce an inflammatory response in BV-2 cells.

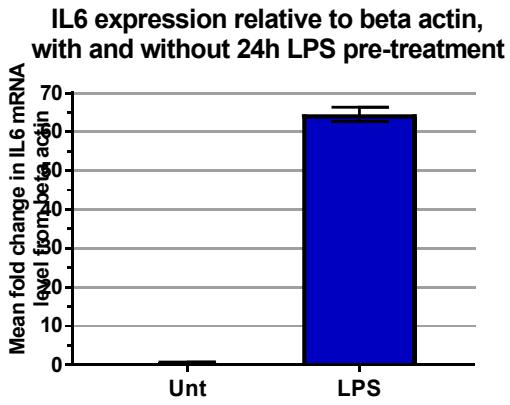

Figure 14. LPS treated cells have upregulation of IL-6. cDNA from BV-2 cells treated with 100ng/ml LPS or left untreated for 24h in 0.5% FBS DMEM were obtained and IL-6 mRNA expression levels relative to beta-actin were determined. Data = mean with range (3 technical replicates).

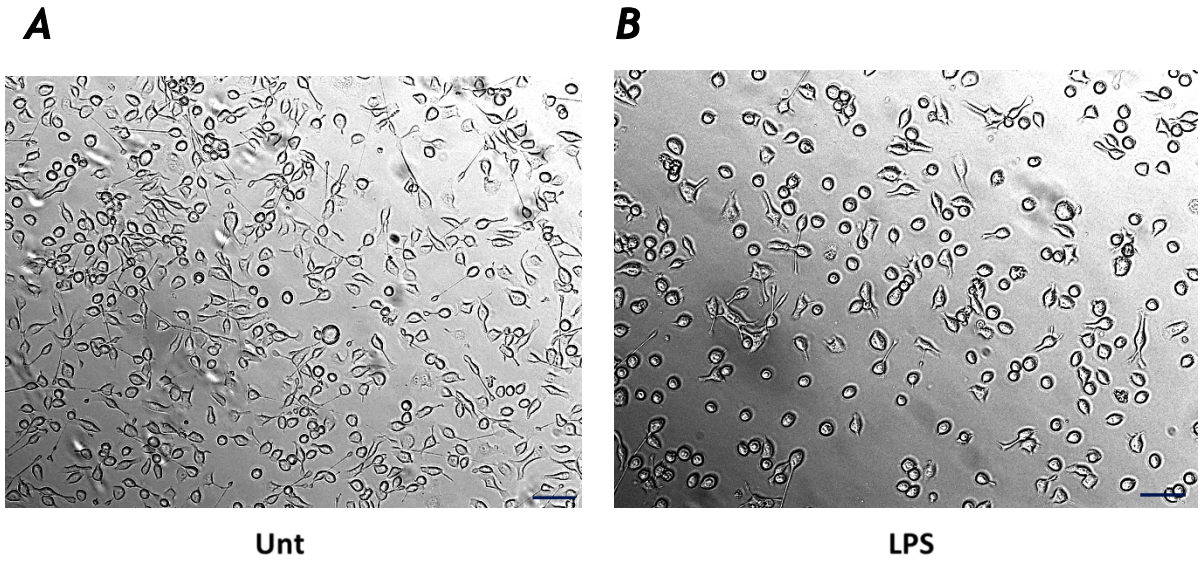

Figure 15. 24h LPS activated BV-2 are viable and exhibit a round cell shape. BV-2 treated with 100ng/ml LPS or left untreated for 24h in 0.5% FBS DMEM were imaged on brightfield setting following incubation to check cell morphology. Scale bar represents 75µm.

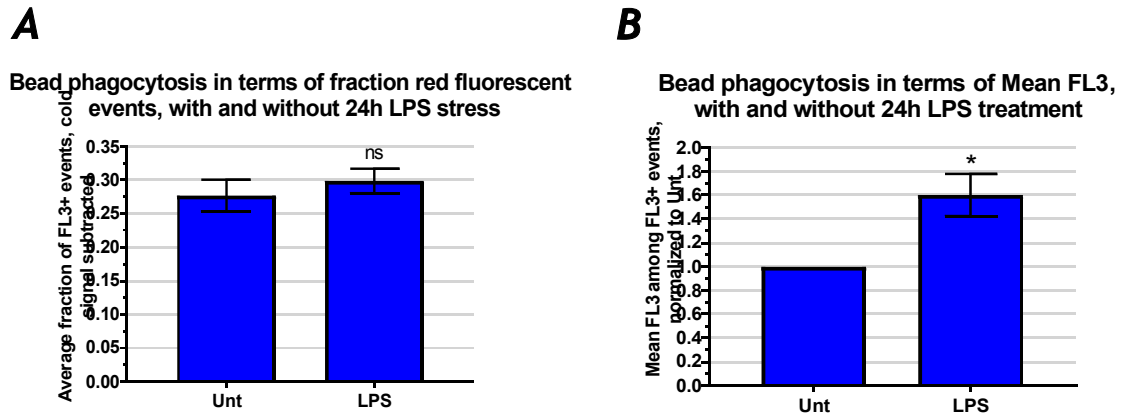

Figure 16. LPS-activated cells show an increase in bead phagocytosis in terms of Mean FL3 (extent of bead phagocytosis per cell). BV-2 were either treated with 100ng/ml LPS or left untreated for 24h incubation in 0.5% FBS DMEM in 37°C. 0.0012% w/v red-fluorescent, 1µm beads were added to all BV-2 samples and cultures were incubated for 1h at 37°C. **A:** Fraction of red-fluorescent BV-2 with data corresponding to cold condition subtracted, and **B:** mean fluorescence intensities recorded among all red-fluorescent BV-2, as measures of phagocytosis. Data = mean ± S.E.M., n = 3, * $p < 0.05$, ns = not significantly different versus untreated condition, unpaired two-tailed Student's t test.

To determine if PSB0739 treatment reduces bead phagocytosis by LPS-activated BV-2, I conducted a bead phagocytosis assay using LPS pre-activated BV-2 with or without a 10-min PSB0739 treatment prior to the addition of beads, with or without 100µM exogenous ADP for a 1 h incubation. LPS-activated BV-2 treated with PSB0739 before the addition of beads phagocytosed less beads, in terms of % events, compared to LPS-activated BV-2 without the inhibitor treatment (Figure 17). The decrease was lessened when ADP was added together with the beads for the 1 h incubation.

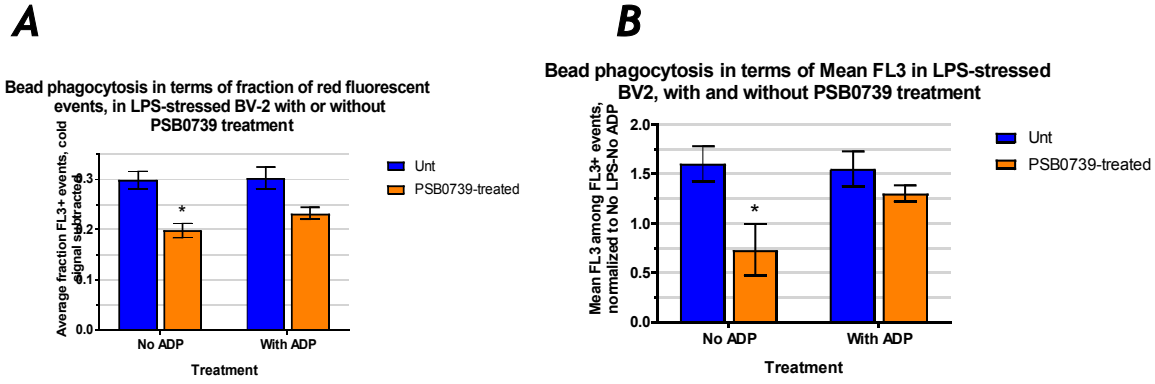

Figure 17. LPS-activated BV-2 treated with P2Y12 inhibitor show significantly reduced bead phagocytosis which is recovered slightly when exogenous ADP is present. BV-2 activated with 100ng/ml LPS for 24h were either left untreated or treated with 10µM PSB0739 for 10min in 0.5% FBS DMEM. Then, these cells were either treated with 0.0012% w/v beads or 0.0012% w/v beads with 100µM ADP for 1 h at 37°C. **A:** Fraction of red-fluorescent BV-2 with data corresponding to cold condition subtracted, and **B:** mean fluorescence intensities recorded among all red-fluorescent BV-2 were determined as measures of phagocytosis.

Data = mean ± S.E.M., n = 3, * $p < 0.05$ versus untreated condition, 2-way ANOVA with Tukey's post-hoc HSD test.

P2Y12 antagonist PSB0739 has no effect on LPS-induced microglial phagocytosis of PC12 cells

To explore the more physiologically relevant question of the role of P2Y12 in specifically microglia phagocytosis of neurons, I proceeded to test the effect of inhibition on LPS-induced phagocytosis of PC12 cells by BV-2 cells. Flow cytometry analyses suggested that LPS-stressed BV-2 had higher phagocytic capacity toward PC12 neurons compared to unstimulated BV-2, although a conclusion on difference cannot be made due to variability in the LPS sample (Figure 18). I performed a PC12 phagocytosis assay using LPS-pretreated BV-2 with or without 1 h PSB0739 treatment prior to the addition of TAMRA (red)-stained PC12 neurons on top of the cells for a 3-h incubation period in 0.5% FBS (low serum) DMEM. At the end of the co-incubation, the uningested PC12-rich supernatant was run on the flow cytometer, by which the number of PC12 neurons recovered from the co-culture was determined (from the count of red-fluorescent cells detected by the cytometer). Simultaneously, the adhered microglia on the surface of the wells were stained with IB4-Alexa 488 (green) label, then detached, pelleted, and run on the flow cytometer to detect the proportion of red-fluorescent cells among the green-labelled microglia population.

It should be noted that 1 h 20 min PSB0739-treated BV-2 exhibited a restoration of a calcium response to ADP in a previous experiment (Figure 8), which appeared to suggest that the inhibitory action of the antagonist becomes ineffective after approximately 1 h. However, it may also suggest the compensatory mechanism of another calcium-related protein while the P2Y12 receptor remains inhibited by PSB0739 (see discussion). Furthermore, P2Y12-mediated calcium activation may serve a function separate from that of phagocytosis.

Both the analysis of adhered BV-2 and PC12 recovery counts indicated that phagocytosis was maintained at equivalent levels between PSB0739-treated, LPS-activated cells and LPS-activated cells which were not treated with the inhibitor (Figure 19). In this experiment, the cold incubation was only performed for the LPS-stressed BV-2 co-incubated with PC12 condition (and not the inhibitor added condition), and so % FL3+ events analyses do not include subtraction of the cold signal. The cold incubation substantially reduced apparent phagocytosis measured by both methods, indicating that these methods were indeed measuring phagocytosis rather than binding of cells.

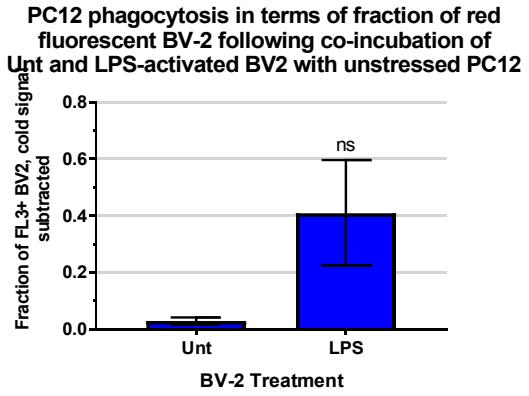

Figure 18. LPS activation of microglia does not significantly increase phagocytosis of PC12 neurons. 50,000 BV-2 were either activated with 100ng/ml LPS or left untreated for 24h incubation in 0.5% FBS DMEM in 37°C. 300,000 PC12 cells labelled with 50µM TAMRA (red-fluorescent), were added directly on top of the seeded BV-2 for 3h incubation in 37°C. Fraction of red-fluorescent events with data corresponding to cold condition subtracted was determined as a measure of phagocytosis. As it was assumed that BV-2 are unlikely to ingest multiple PC12 over the 3h period, mean fluorescence was not used as a measurement for phagocytosis of PC12s. Data = mean ± S.E.M., n = 3, ns = not significantly different to untreated sample, $p > 0.05$, unpaired two-tailed Student's t test.

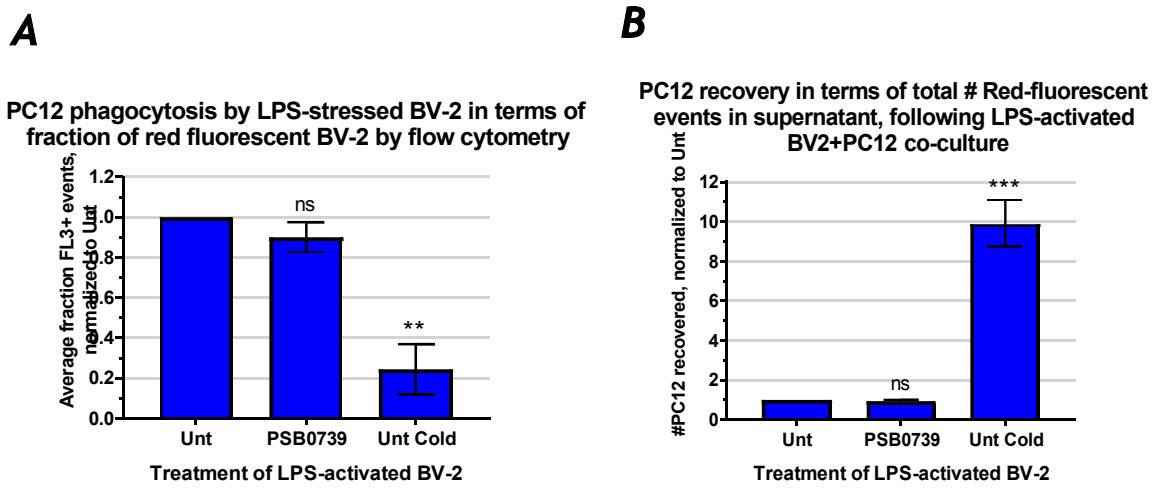

Figure 19. LPS-activated BV-2 treated with P2Y12 inhibitor exhibit the same level of phagocytosis of PC12 neurons as those without inhibitor treatment, and there is a clear attenuation of phagocytosis in cold incubation. 50,000 BV-2 activated with 100ng/ml LPS for 24h were either treated with 10µM PSB0739 or water (untreated) for 1h in 0.5% FBS DMEM in 37°C. 300,000 PC12 cells labelled with 50µM TAMRA (red-fluorescent), were added directly on top for 3h incubation in 37°C. In parallel, LPS-activated BV-2 (no PSB0739 treatment) with PC12 seeded on top were incubated on ice. **A:** Fraction of red-fluorescent BV-2, and **B:** uningested PC12 cells recovered in suspension following the 3h incubation counted by flow cytometry, were used as measures of phagocytosis. Data = mean ± S.E.M., n = 3, **/*** $p < 0.01/0.001$ versus untreated sample, ns = not significantly different to untreated sample, 1-way ANOVA followed by Tukey's post-hoc HSD test.

Since I was aiming to examine BV-2 phagocytosis of specifically live-but-stressed neurons, as opposed to injured or dying neurons, I wanted to ensure that the PC12 cells in the experiment remained viable over the course of the 3 h incubation. To address this concern, the phagocytosis assay was repeated for four additional experiments, in which the co-incubation was performed in PC12 media, composed of 5% FBS, 10% HS in RPMI (thus containing greater concentration of serum).

Furthermore, post-3-h incubation, the PC12-rich supernatants were transferred to poly-l-lysine coated plates, and cell counts were obtained by microscopy instead of flow cytometry to ensure better accuracy of analysis. These experiments led to the same result that LPS-induced PC12 phagocytosis is maintained with and without inhibitor treatment (Figure 20). As additional negative controls, for one experiment, the cells were treated with the general actin inhibitor cytochalasin D, or cylo(Arg-Gly-Asp-D-Phe-Val) (cRGDfV), an inhibitor of the vitronectin receptor, one of the receptors known to facilitate microglial phagocytosis. An inhibition of phagocytosis was demonstrated in the cytochalasin D-treated cells, but not cRGDfV-treated cells, further establishing that phagocytosis is detected using these methods, but also indicating that LPS-induced phagocytosis of PC12 cells likely does not involve the vitronectin receptor (Figure 20).

Still, imaging of the inhibitor pre-treated and untreated BV-2 and PC12 co-cultures following the co-incubation indeed showed instances of red fluorescence enclosed within green-labelled cells, indicating phagocytosis of PC12 by BV-2 (Figure 21a, b). As expected, a clear difference was observed for the cold incubation, which showed red fluorescence being consistently confined to the exterior of the green-stained cells, indicating binding events and not ingesting events (Figure 21c). Similarly, the attenuation of phagocytosis in the cold incubation was demonstrated from images taken of PC12 cells in the recovered supernatant, where the density of PC12 was visibly higher in the cold samples (Figure 22).

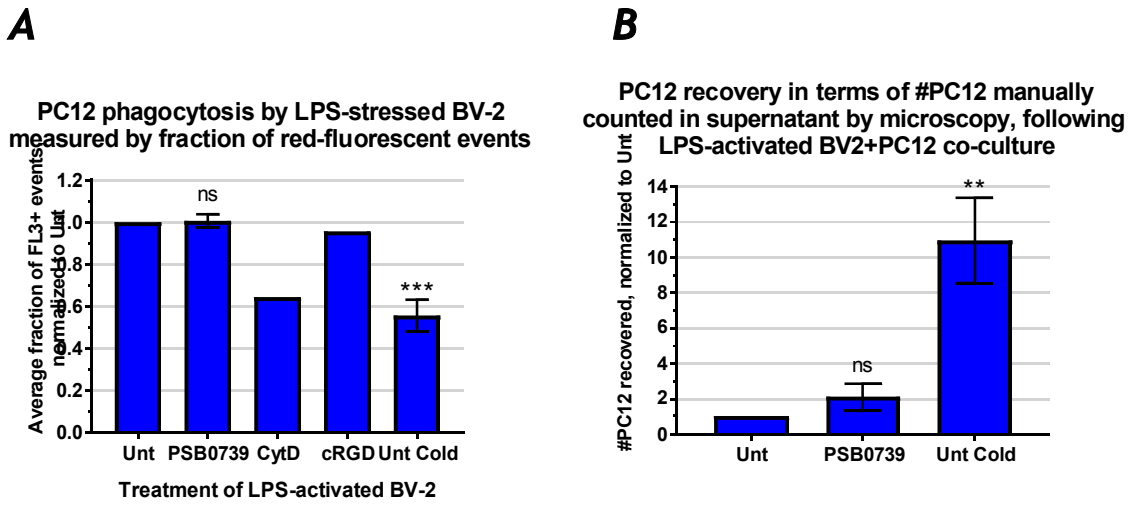

Figure 20. Upon changing the co-culture medium to higher-serum PC12 medium, LPS-activated BV-2 treated with P2Y12 inhibitor still exhibit the same level of phagocytosis of PC12 neurons as those without inhibitor treatment. 50,000 BV-2 activated with 100ng/ml LPS for 24h were either treated with 10μM PSB0739 or water (untreated) for 1h in 10% HS, 5% FBS RPMI in 37°C. For one experiment, 1h cytochalasin D (1μM) and 1h cRGDfV (50 μM) treatment conditions were added. 300,000 PC12 cells labelled with 50μM TAMRA (red-fluorescent), were added directly on top for 3h incubation in 37°C. In parallel, LPS-activated BV-2 (no PSB0739 treatment) with PC12 seeded on top were incubated on ice. **A:** Fraction of red-fluorescent BV-2, and **B:** uningested PC12 cells recovered in suspension counted manually by microscopy, were determined as measures of phagocytosis. Data = mean ± S.E.M., n = 4, **/*** $p < 0.01/0.001$ versus untreated sample, ns = not significantly different from untreated sample, 1-way ANOVA followed by Tukey's post-hoc HSD test. Exception is for CytD and cRGD samples, where data = mean with range (3 technical replicates).

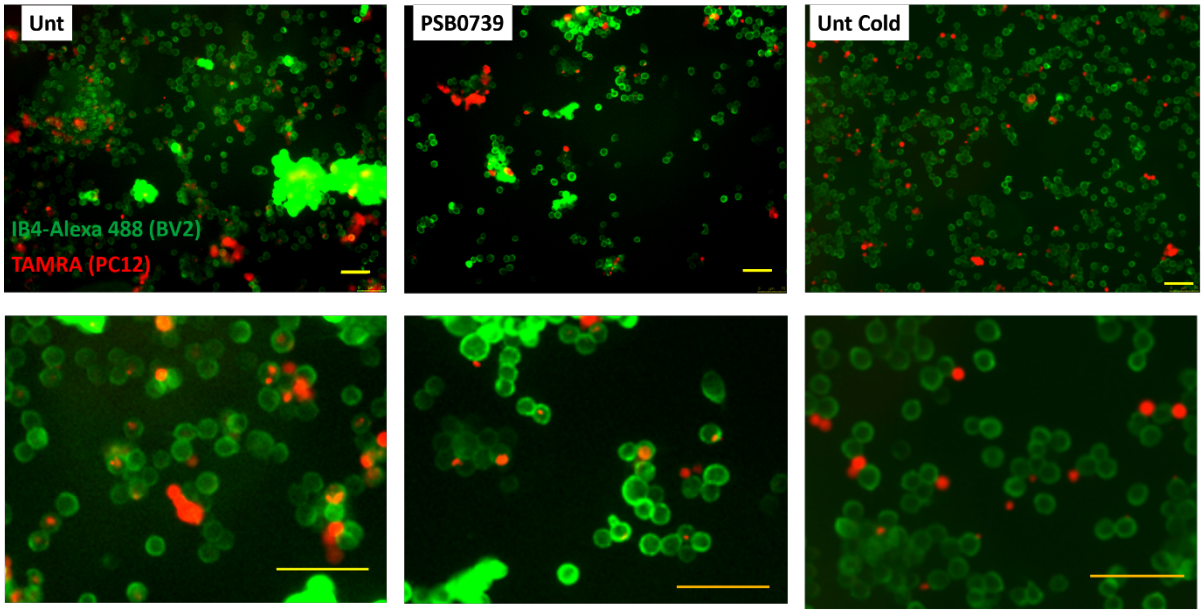

Figure 21. Following 3h co-incubation, PC12-BV-2 co-cultures exhibit evidence of binding and ingesting events for both PSB0739 added and untreated conditions, except untreated cold incubation which shows exclusively binding. 50,000 BV-2 activated with 100ng/ml LPS for 24h were either treated with 10µM PSB0739 (PSB0739) or water (untreated) for 1h in 10% HS, 5% FBS RPMI in 37°C. 300,000 PC12 cells labelled with 50µM TAMRA (red-fluorescent), were added directly on top for 3h incubation in 37°C. In parallel, LPS-activated BV-2 (no PSB0739 treatment) with PC12 seeded on top were incubated on ice (unt cold). Following transfer of supernatant and one wash with PBS, the attached cells in all wells were imaged, showing BV-2 (green) and PC12 (red) for **A:** untreated **B:** PSB0739 inhibitor-added, and **C:** untreated on ice conditions. Representative images from one independent experiment are shown, with close-ups directly below. Scale bars represent 75µm.

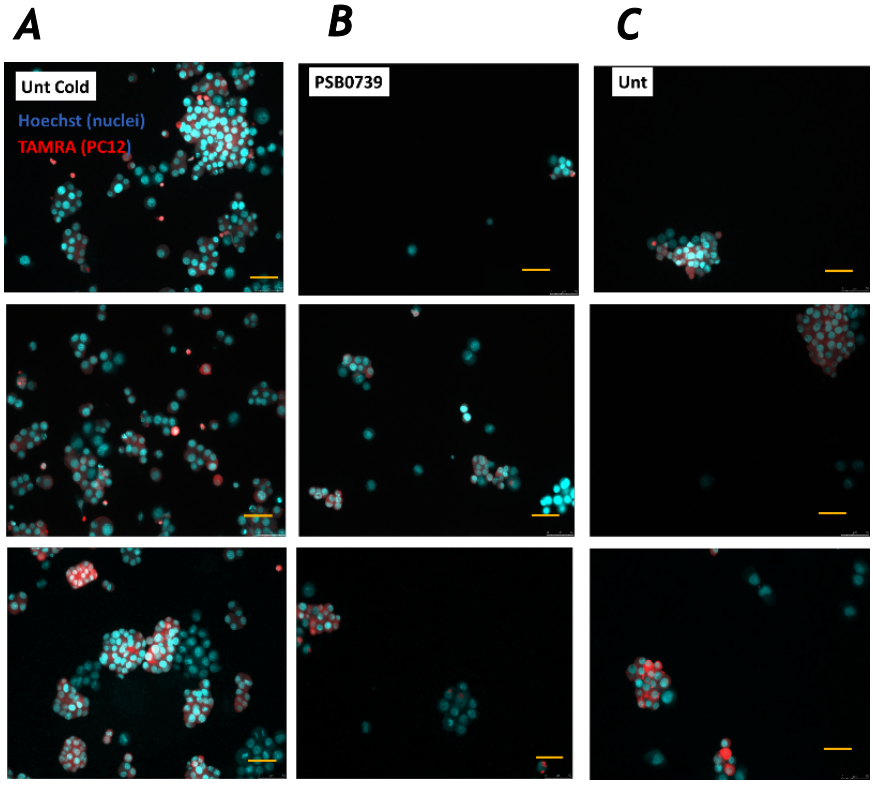

Figure 22. PC12 recovery images show noticeably greater number of uningested PC12 in the cold condition compared to all other conditions, while densities are about equal for inhibitor added and untreated conditions. 50,000 BV-2 activated with 100ng/ml LPS for 24h were either treated with 10μM PSB0739 (PSB0739) or water (untreated) for 1h in 10% HS, 5% FBS RPMI in 37°C. 300,000 PC12 cells labelled with 50μM TAMRA (red-fluorescent), were added directly on top for 3h incubation in 37°C. In parallel, LPS-activated BV-2 (no PSB0739 treatment) with PC12 seeded on top were incubated on ice (unt cold). Uningested PC12-rich suspension was transferred to poly-l-lysine coated plates, incubated 1.5h and all nuclei were stained with 4μg/ml Hoechst 33342 (blue) for counting recovered PC12. Red and blue channel merged images from each independent experiments are shown. Scale bars represent 50μm.

siRNA knockdown of P2Y12 has no effect on phagocytosis of PC12 cells by LPS-activated microglia

Given the possible time sensitivity of PSB0739-mediated P2Y12 inhibition suggested by the earlier calcium response time course experiment, the PC12 experiment was conducted using P2Y12 knockdown and non-target siRNA transfected cells for one replicate in LPS-activated BV-2. The % FL3+ event values were maintained between the P2Y12 knockdown and non-target conditions. Additionally, P2Y12 knockdown cells yielded a large variation in PC12 recovery counts, which overlapped with the phagocytosis by the non-target cells, and thus P2Y12 knockdown has no apparent effect on BV-2 phagocytosis of PC12 in these conditions (Figure 23).

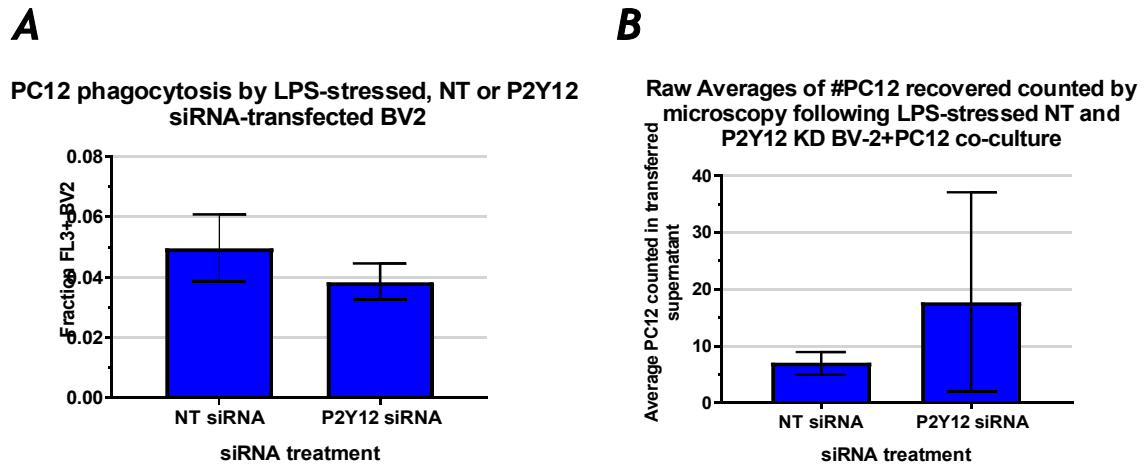

Figure 23. P2Y12 knockdown does not affect phagocytosis of LPS-induced phagocytosis of PC12 neurons. 50,000 non-target and P2Y12 siRNA transfected BV-2 (from Transfection 1) were activated with 100ng/ml LPS for 24h in 10% HS, 5% FBS RPMI in 37°C. 300,000 PC12 cells labelled with 50μM TAMRA (red-fluorescent), were added directly on top for 3h incubation. Note that these cells are 72h post-transfection. **A:** Fraction of red-fluorescent events among attached BV-2, and **B:** uningested PC12 cells recovered in suspension following the 3h incubation counted manually by microscopy, were determined as measures of phagocytosis. Data = mean with range (three technical replicates).

LPS treatment decreases P2Y12 expression in BV-2 microglia

To summarize, although LPS-induced BV-2 phagocytosis of beads was attenuated with inhibitor treatment, LPS-induced phagocytosis of PC12 cells was maintained in both PSB0739-treated

BV-2 as well as P2Y12 knockdown BV-2. These findings suggest that P2Y12 does not play a significant role in the LPS-induced phagocytosis. However, previous studies have reported that LPS may downregulate P2Y12 expression in microglia (Haynes et al., 2006), suggesting the possibility in these last experiments that 24 h LPS treatment to BV-2 itself was causing a reduction in P2Y12, and thus any perturbation of P2Y12 (via knockdown or inhibition) yielded negligible effects on phagocytosis.

As these reports were based on primary microglia, I tested whether LPS changed the expression of P2Y12 in BV-2 cells. Upon extracting RNA from BV-2 treated with LPS for 24-48 h, I found that P2Y12 expression was indeed decreased by 40-70% compared to the untreated condition (Figure 24).

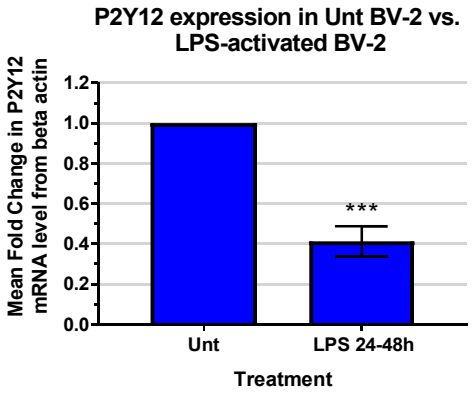

Figure 24. LPS activation leads to decrease in P2Y12 expression in BV-2 cells. cDNA from BV-2 cells treated with 100ng/ml LPS or left untreated for 24-48h in 0.5% FBS DMEM were obtained and P2Y12 mRNA expression levels relative to beta-actin were determined. Data = mean ± S.E.M., n = 4, *** $p < 0.001$ versus untreated sample, unpaired two-tailed Student's t test.

Furthermore, upon performing calcium response assays with 12-16 h LPS-treated BV-2s, I found that these activated BV-2 exhibited an attenuated calcium response to ADP, potentially due to downregulated P2Y12. This attenuation was not observed for cells treated with LPS at the same time as ADP (no preincubation), indicating that the LPS-mediated inhibition or downregulation of P2Y12 is not fast-acting (Figure 25). Furthermore, the calcium assays established that LPS treatment alone does not yield any calcium response.

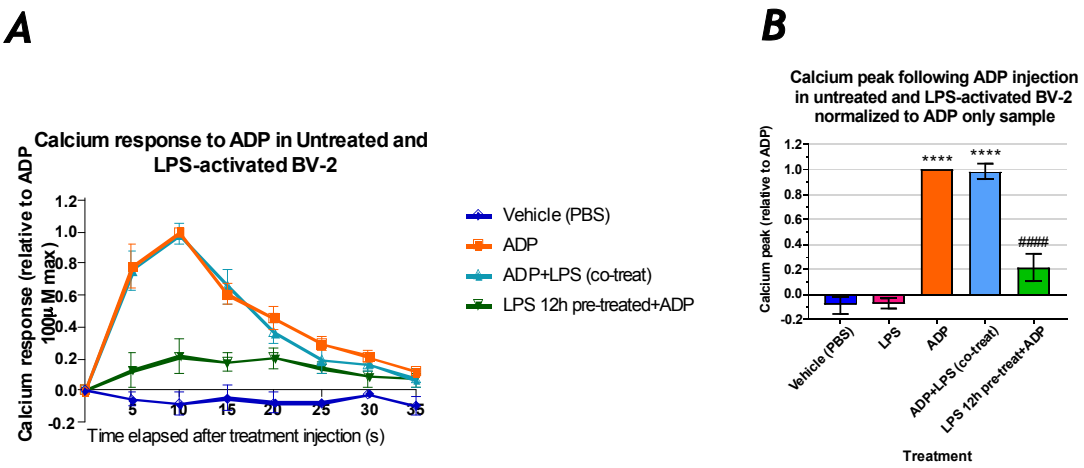

Figure 25. LPS activation attenuates calcium response to ADP. **A:** Calcium response recorded for untreated BV-2 upon injection of PBS (blue), 100µM ADP (orange), 100µM ADP and 100ng/ml LPS together (light blue), or for 100ng/ml LPS pre-treated BV-2 upon injection of 100µM ADP (green). Data = mean ± S.E.M., n = 3. All points are normalized to maximum of 100µM ADP condition. **B:** Maximum calcium response for all conditions tested, normalized to ADP condition. Calcium response of untreated BV-2 to 100ng/ml LPS injection (magenta) is added. Data = mean ± S.E.M., n = 3, **** $p < 0.0001$ versus vehicle, #### $p < 0.0001$ versus ADP, 1-way ANOVA with Tukey's HSD post-hoc test.

Neither PSB0739 nor knockdown significantly attenuates phagocytosis of staurosporine-stressed PC12

This finding that LPS treatment downregulates P2Y12 expression presented a plausible explanation for why knockdown and PSB0739-mediated P2Y12 inhibition yielded little effects on LPS-induced phagocytosis of PC12 by BV-2 cells. For this reason, I decided to observe the effect of PSB0739 inhibition and genetic knockdown on phagocytosis of 10nM staurosporine-stressed PC12 by BV-2, where PC12 are live yet stressed and more liable to be phagocytosed, but does not involve LPS presence. Indeed, I was able to confirm by flow cytometry that BV-2 microglia phagocytose staurosporine-stressed PC12 at higher levels compared to unstressed PC12 (Figure 26). Based on both flow cytometry and microscopy imaging results on PC12 recovery, neither 10-min PSB0739-treated BV-2 nor P2Y12 knockdown cells showed significant changes in phagocytosis of staurosporine-stressed PC12 compared to control (no PSB0739 treatment, non-target siRNA transfected) cells (Figure 27).

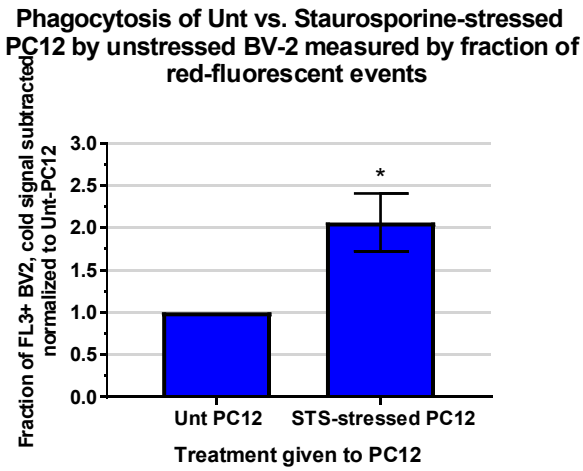

Figure 26. Staurosporine-stressed PC12 are more liable for phagocytosis by microglia than untreated PC12. 300,000 PC12 cells, either stressed with 10nM staurosporine (STS) or treated with PBS (Unt) for 24h, labelled with 50μM TAMRA (red-fluorescent), were added directly on top of 50,000 untreated BV-2 for 3h incubation in 37°C in 0.5% FBS DMEM. In parallel, plates with identical conditions were incubated on ice for 3h. Fractions of red-fluorescent events among BV-2 cells with data corresponding to cold incubation subtracted were determined as measures of phagocytosis. Data = mean ± S.E.M., n = 3, * $p < 0.05$ versus untreated PC12 sample, unpaired two-tailed Student's t test.

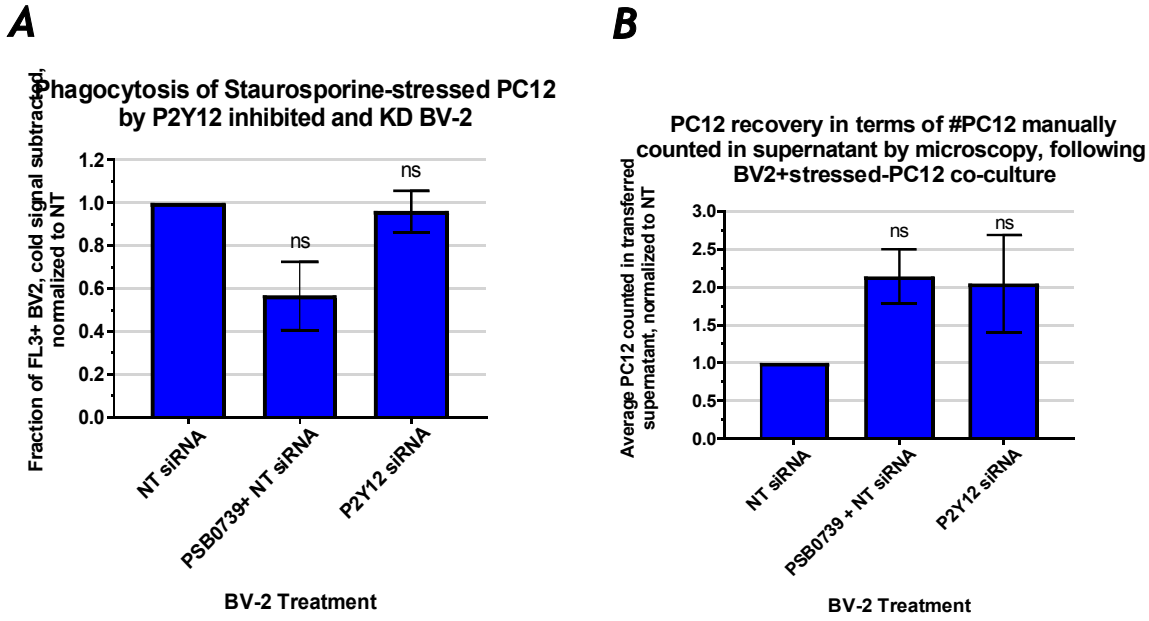

Figure 27. Neither PSB0739 treatment nor P2Y12 genetic knockdown significantly alters phagocytosis of staurosporine-stressed PC12 neurons. 300,000 PC12 cells stressed with staurosporine (10nM) for 24h, labelled with 50μM TAMRA (red-fluorescent), were added directly on top of 50,000 non-target siRNA transfected, P2Y12 siRNA transfected (transfections 3-5), or 10min PSB0739 (10μM) pre-treated BV-2 (that were non-target siRNA transfected for consistency) for 3h incubation in 37°C in 0.5% FBS DMEM. In parallel, plates with identical conditions were incubated on ice for 3h. **A:** Fraction of red-fluorescent events among BV-2 cells with data for corresponding cold incubation subtracted, and **B:** uningested PC12 cells recovered in suspension counted manually by microscopy, were determined as measures of phagocytosis. Data = mean ±

S.E.M., n = 3, ns = not significantly different to non-target siRNA-transfected sample, $p > 0.05$, 1-way ANOVA with Tukey's post-hoc HSD test.

P2Y12-knockdown cells show decreased phagocytosis of unstressed PC12

On the other hand, P2Y12 knockdown cells exhibited less phagocytosis of PC12 neurons that were not stressed with staurosporine, measured either by both flow cytometry (PC12 uptake into BV-2) or PC12 recovery analyses by microscopy (remaining PC12 not phagocytosed) (Figure 28). The effect of PSB0739 on phagocytosis of unstressed PC12 was not examined due to lack of time.

To summarize, P2Y12 pharmacological inhibition decreased phagocytosis of staurosporine-stressed neurons, while P2Y12 knockdown decreased phagocytosis of unstressed PC12, both of which indicated a role of P2Y12 in BV-2 phagocytosis of cells in the absence of LPS.

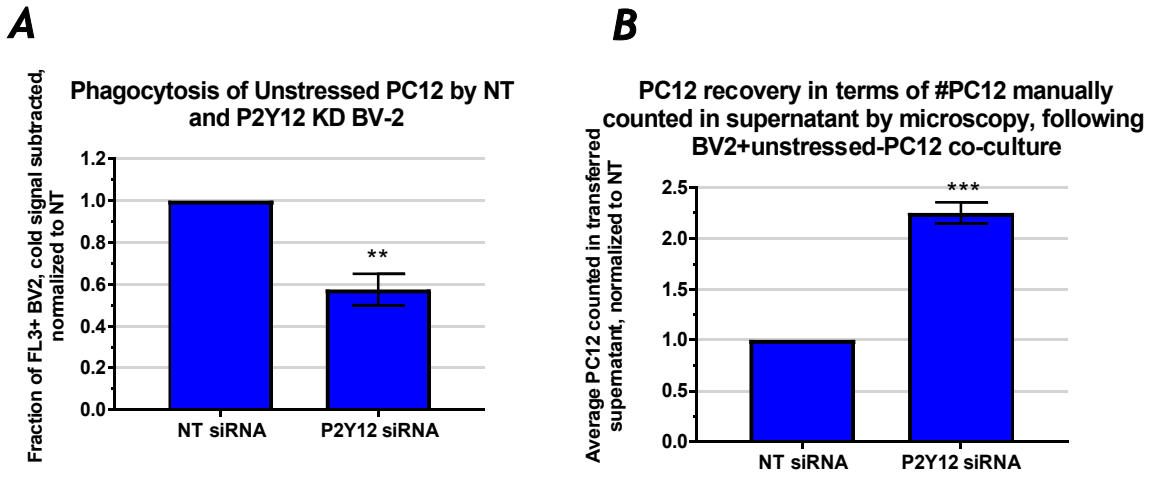

Figure 28. P2Y12 knockdown attenuates phagocytosis of unstressed PC12. 300,000 untreated PC12 labelled with 50µM TAMRA (red-fluorescent), were added directly on top of 50,000 non-target siRNA transfected or P2Y12 siRNA transfected (transfections 3-5) BV-2 for 3h incubation in 37°C in 0.5% FBS DMEM. In parallel, plates with identical conditions were incubated on ice for 3h. **A:** Fraction of red-fluorescent events among BV-2 cells with data for corresponding cold incubation subtracted, and **B:** uningested PC12 cells recovered in suspension counted manually by microscopy, were determined as measures of phagocytosis. Data = mean ± S.E.M., n = 3, **/*** $p < 0.01/0.001$ versus non-target sample, two-tailed unpaired Student's t test.

100µM ADP treatment for 24h decreases P2Y12 expression in BV-2

The finding that LPS treatment causes P2Y12 downregulation raised the additional question of how this is mediated. Considering also the findings that P2Y12 expression is decreased over the course of microglial migration toward target cells releasing ATP/ADP (Haynes et al., 2006; Orr et al.,

2009), I speculated that binding of released ADP by microglia could itself be regulating the expression of P2Y12.

Thus, to test the effect of ADP on P2Y12 expression changes, I performed P2Y12 RT-qPCR of cDNA isolated from BV-2 treated for 24h with 100μM ADP. To probe into the potential concentration-dependency of expression regulation with ADP treatment, I also tested a 10μM ADP-treated condition. From these studies, P2Y12 expression was decreased in response to 100μM ADP, but not 10μM ADP for three experiments (Figure 29).

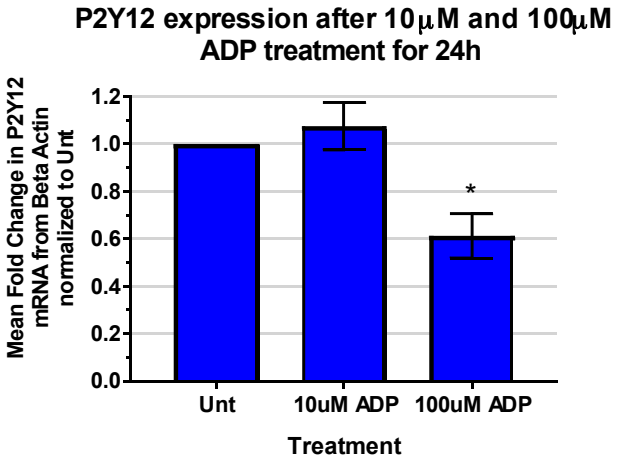

Figure 29. 100μM ADP treatment for 24h decreases P2Y12 expression. cDNA from BV-2 cells treated with 10μM ADP, 100μM ADP or left untreated for 24h in 0.5% FBS DMEM were obtained and P2Y12 mRNA expression levels relative to beta-actin were determined. Data = mean ± S.E.M., n = 3, * $p < 0.05$ versus untreated sample, 1-way ANOVA followed by Tukey's post-hoc HSD test.

PSB0739 treatment alone sustains P2Y12 expression

I wanted to elucidate further whether P2Y12 downregulation is mediated by ADP-binding to P2Y12, and to ask if intercepting ADP-P2Y12 interactions with the addition of PSB0739 prevented downregulation of P2Y12. But, first I asked whether PSB0739 treatment alone has any effect on P2Y12 expression. I extracted RNA from BV-2 following 1 h PSB0739 treatment, as well as that of BV-2 treated with PSB0739 for 24 h. For both samples, P2Y12 expression was maintained, but for the 1 h treated sample, a slight (10%) increase in P2Y12 expression was observed (Figure 30).

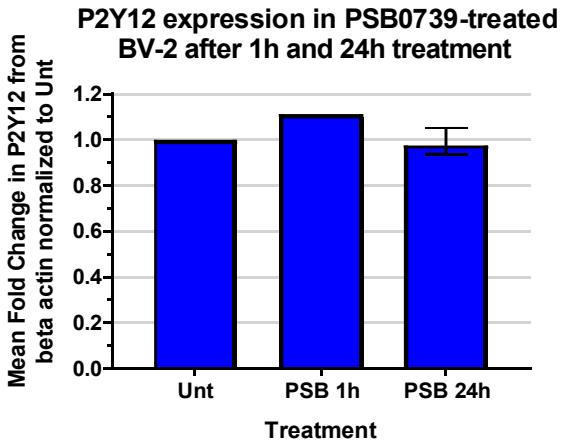

Figure 30. PSB0739 treatment alone maintains P2Y12 expression. cDNA from BV-2 cells treated with 1h 10μM PSB0739, 24h 10μM PSB0739 or left untreated for 24h in 0.5% FBS DMEM were obtained and P2Y12 mRNA expression levels relative to beta-actin were determined. Data = mean with range (three technical replicates).

PSB0739 treatment prior to 24h ADP treatment does not prevent ADP-induced P2Y12 downregulation

Next, I treated BV-2 with PSB0739 inhibitor for 10 min, added 100μM ADP for 24 h, and then extracted RNA from these cells for RT-qPCR analysis. The inhibitor-treated cells still exhibited ADP-mediated downregulation of P2Y12. The level of the downregulation in direct comparison to the ADP treatment only condition was variable, however, with two experiments showing further downregulation, and another yielding slightly higher expression (Figure 31). Thus a definite statement on changes with the inhibitor addition on ADP induced downregulation could not be made.

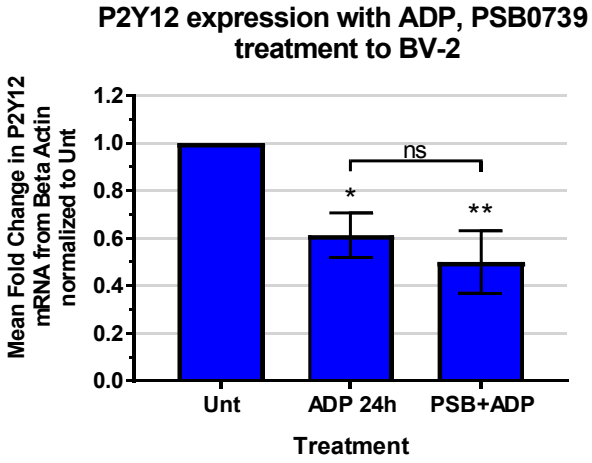

Figure 31. PSB0739 treatment maintains ADP-mediated P2Y12 downregulation. cDNA from BV-2 cells treated with 24h 100μM ADP, treated with 10μM PSB0739 for 10min prior to 24h 100μM ADP treatment, or left untreated for 24h in 0.5% FBS DMEM were obtained and P2Y12 mRNA expression levels relative to beta-actin were determined. Data = mean ± S.E.M., n = 3, */** $p < 0.05/0.01$ versus untreated sample, 1-way ANOVA followed by Tukey's post-hoc HSD test.

PSB0739 and ADP treatments do not affect LPS-induced downregulation of P2Y12

The above results suggested that high concentration of extracellular ADP, but not ADP-P2Y12 binding interactions per se, play a role in the downregulation of P2Y12. In order to examine whether LPS-induced downregulation of P2Y12 would be enhanced with the addition of ADP and PSB0739 treatments, further RT-qPCR experiments were performed in which 24 h LPS-activated BV-2 were treated with 100μM ADP for another 24 h, 10μM PSB0739 for 24 h, or treated with 10μM PSB0739 for 10 min prior to further addition of 100μM ADP for 24 h. Although the downregulation was unchanged with the addition of ADP, LPS-activated cells that were treated with the inhibitor prior to the addition of ADP appeared to exhibit slightly compounded P2Y12 downregulation (Figure 32).

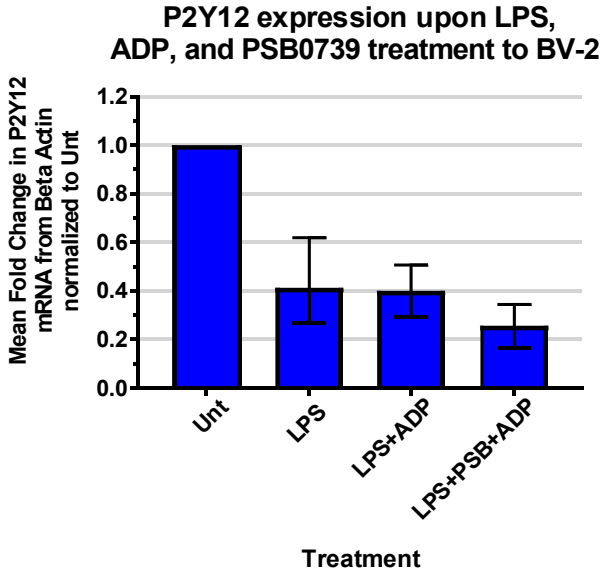

Figure 32. PSB0739 and ADP treatments maintain LPS-mediated P2Y12 downregulation. cDNA from BV-2 cells treated with 24h 100ng/ml LPS, treated with 24h 100ng/ml LPS and 100μM ADP together, or treated with 10μM PSB0739 for 10min prior to 24h 100ng/ml LPS and 100μM ADP treatment, or left untreated for 24h in 0.5% FBS DMEM were obtained and P2Y12 mRNA expression levels relative to beta-actin were determined. Data = mean with range, n = 2.

Discussion

In this thesis, I primarily sought to determine the effect of inhibiting the ADP receptor P2Y12 on microglial phagocytosis of neurons under LPS-stimulated conditions. In addressing this main aim, I found that neither P2Y12 pharmacological inhibition nor genetic knockdown of the P2Y12 receptor was neuroprotective in LPS-induced microglial phagocytosis (Figure 19, 20, 23). This lack of an effect may be explained by the fact that LPS activation decreases the expression of P2Y12, which has previously been reported in primary microglia (Haynes et al., 2006) and was confirmed in the present study in BV-2 microglia (Figure 24).

Despite this apparent "negative" result regarding the original aim, further studies on the P2Y12 receptor explored in this thesis highlighted some novel findings. Here I found that disruption of P2Y12 decreases the phagocytosis of both bead and neuronal targets by unstimulated BV-2 microglia. Secondly, I showed that, consistent with previously reported studies using primary microglia, activation of P2Y12 with ADP immediately induces a calcium transient, which is attenuated drastically when P2Y12 is perturbed in BV-2 cells. In addition through calcium assays, I found that the attenuation of the ADP-mediated calcium response by the P2Y12 antagonist PSB0739 appears to be time-dependent. Finally, I showed that ADP treatment at a high concentration causes marked downregulation of P2Y12 expression. The implications of these results are explored below.

Disruption in P2Y12 causes a decrease in phagocytosis of both neuronal and bead targets under completely unstimulated conditions

In contrast to the phagocytosis assays examining LPS-activated BV-2, the experiments conducted in the absence of LPS yielded changes in phagocytosis upon P2Y12 disruption. Namely, P2Y12 knockdown decreased phagocytosis of unstressed neurons by BV-2 significantly (Figure 28). Additionally, phagocytosis of beads by unstimulated BV-2 was reduced with P2Y12 inhibition to a significant level (Figure 9). However, activating P2Y12 alone by addition of exogenous ADP did not increase this baseline phagocytosis (Figure 5, 6).

With this last point in mind, together these findings suggest that P2Y12 receptor activation neither promotes nor prevents phagocytic ability in a linear fashion; rather, it functions to retain basal phagocytic capacity at a sustained level in unstimulated BV-2 cells, even in the presence of various concentrations of its agonist. This finding supports the current understanding that P2Y12 is a receptor which characterizes homeostatic, non-pathological microglia (Keren-Shaul et al., 2017) which exhibits controlled levels of phagocytosis in the healthy brain (Sipe et al., 2016). Although it is not entirely clear how P2Y12 regulates this phagocytic homeostasis, it appears ADP-mediated P2Y12 activation, and not merely the presence of P2Y12, is involved in the mechanism, as the addition of exogenous ADP gave a slight recovery in bead phagocytosis from the reduction seen when P2Y12 was inhibited or knocked down (Figure 9, 13).

Additionally, the finding that P2Y12 inhibitor treatment significantly decreases bead phagocytosis by unstimulated microglia in the absence of any exogenous ADP (Figure 9) is interesting, as it suggests that the unstimulated microglia itself is releasing ADP (or ATP that is degraded to ADP). Consistent with this idea, constitutive release of ATP from microglia in the resting state has been reported, although the concentration of ATP and whether it is sufficient to activate P2Y12 is vague (Corriden and Insel, 2010; Cisneros et al., 2015). Another study reported that soluble ATP release via connexin hemichannels at microglia functions to maintain baseline motility (Davalos et al., 2005). Thus, microglial P2Y12 receptor activation under resting (not activated by inflammatory stimuli) may in part be self-mediated, and this autocrine signalling could govern the controlled and balanced levels of phagocytosis observed in healthy microglia.

Given that LPS-activated BV-2 did not show any change in PC12 phagocytosis upon P2Y12 inhibition or knockdown, I have focused so far on the implications of the phagocytosis assays conducted for unstimulated microglia. However, it is important to address the discrepancy in results obtained between neuron and bead targets incubated with LPS-activated BV-2. Although there was no effect of P2Y12 inhibition or knockdown found for neuronal targets (Figure 19, 20, 23), there was a significant decrease in bead phagocytosis in response to PSB0739 treatment (Figure 17). It is not clear why this difference is observed only for the LPS-added experiment; nonetheless, this finding suggests that even under P2Y12 downregulated conditions, phagocytosis of beads, but not neurons, is affected by P2Y12 inhibition. But what is the cause for this difference? It should be recognized that neurons and beads differ in many respects, most notably their surface properties which likely largely affect their propensity for binding and being ingested by microglia. Nevertheless, an undeniable difference is their size (1μm bead diameter vs. ~5μm PC12 diameter). Size-selective phagocytosis has been demonstrated and studied in macrophages, for which preference for smaller-sized targets (~0.5-1.7 μm) has been observed (Tabata and Ikada, 1988; Rudt et al., 1993). Remarkably, in another study examining size-dependent phagocytosis in macrophages, elimination of membrane ruffling by induced osmotic swelling caused the macrophages to lose their size selectivity for smaller targets (Champion et al., 2009). Membrane ruffling is a known characteristic of chemotactic microglia and is regulated by P2Y12 (Inoue et al., 1998; Honda et al., 2001). Thus, this discrepancy between targets in the LPS-added phagocytosis experiments potentially highlights the role of P2Y12 in regulating membrane ruffling for the purpose of not only cell movement, but also for selective phagocytosis of smaller particles over whole cells, in homeostatic microglia.

To reiterate, P2Y12-mediated membrane ruffling could underlie size selectivity in basal phagocytic mechanisms; a possibility is that unstimulated microglia exhibit appropriate and controlled phagocytosis at the right levels as they possess the ability to distinguish, by size, what can be eaten or not, and this mechanism is facilitated by P2Y12. This speculation, together with the established role of P2Y12 in process extension, gives support to the suggestions of P2Y12's involvement in the

ingestion of parts of neurons, including synapses to regulate synaptic pruning and plasticity, instead of whole cells in healthy microglia (Sipe et al., 2016; Maeda et al., 2010).

Activation of P2Y12 with ADP induces a calcium transient which is attenuated by LPS, P2Y12 inhibition and P2Y12 knockdown

Results from the calcium response assays confirmed the fact that ADP mediates P2Y12 activation, followed by intracellular calcium signalling. Namely, 100μM ADP treatment of BV-2 induced a strong calcium transient, which was drastically attenuated when P2Y12 was disrupted by 10-20 min inhibitor pre-treatment (Figure 8), P2Y12 knockdown (Figure 12), or LPS-mediated activation (Figure 25). These results are consistent with previous studies on primary mouse and human microglia; addition of 2-methylthio-ADP (2MeSADP) was found to evoke a calcium increase in cultured mouse microglia (Moller et al., 2000), and P2Y12 antagonism using the same inhibitor, PSB0739, was shown to block the ADP-mediated calcium response in human microglia (Moore et al., 2015). In addition, the calcium transient that was observed in the present study could be described as a fast initial peak and quick decay, a trend which is indicative of calcium release from endoplasmic reticulum (ER)-mediated internal stores (Moller et al., 2002). Thus, using BV-2 cells, my findings confirm that P2Y12 is the main regulator of ADP-mediated calcium signalling in microglia.

These results also highlighted the ability of P2Y12 to respond immediately to acute changes in ADP concentration in the extracellular environment. Specifically, the peak in calcium response to ADP was observed just 5-10s following treatment injection on a consistent basis across all independent experiments conducted. This immediate sensing of a sharp rise in ADP levels likely underlies cases of quick microglia responses to acute stress in the healthy brain, such as sudden injury. Indeed, homeostatic microglia exhibit rapid process extension mediated by P2Y12 upon sensing ATP leakage by injured neurons (Madry et al., 2018). Moreover, the rapidity of microglial process movement has been captured by time-lapse confocal imaging, where retinal microglia were found to extend their processes in response to acute injury on a scale of seconds (Lee et al., 2008).

Connected to this topic, the activity of P2Y12 in facilitating process extension in response to sites of large nucleotide release is another interesting question to explore, as the mechanism is not fully clarified. Perhaps this point can be studied through use of fetal bovine serum (FBS), which at high concentrations, is shown to cause a decrease and shortening of microglial processes (Bohlen et al., 2017). Bovine serum albumin (BSA), a major component of FBS, has been found to lower the potency of ATP binding to the receptor P2X7, as ATP binds to BSA instead (Michel et al., 2001). These observations indicate that perhaps the attenuation of process extension in high serum environments is due to BSA binding similarly to ADP, lowering instances of ADP-P2Y12 interactions. Through the use of FBS at different concentrations to disrupt ADP-P2Y12 binding to varying extents, it may be possible to probe into the mechanism of P2Y12-mediated process extension by examining

how P2Y12 senses extracellular ADP, and upon doing so, whether P2Y12 itself translocates to a different region of the cell membrane to facilitate process extension.

The implications so far discussed are illustrated in the schematics below. In summary, my findings from the phagocytosis and calcium response assays indicate that P2Y12 can be tied to the basal phagocytic capacity in untreated, healthy microglia, which is activated in part by self-released ATP (Figure 33). Binding of the antagonist PSB0739 blocks P2Y12-mediated signalling, which interferes with basal phagocytosis. However, when a high concentration of extracellular ADP is added, ADP and PSB0739 compete for the binding site of P2Y12, and P2Y12 activation is partially restored (although not completely, as PSB0739 still has higher affinity for P2Y12 than ADP) (Figure 34). Nevertheless, high concentration of ADP treatment to untreated cells does not affect phagocytosis, perhaps due to a quick feedback loop regulated by intracellular calcium and potassium mobilization, which restores the level of P2Y12 activation (Figure 35). In terms of more real-life applications of these mechanisms, P2Y12 activation may be mediating microglia process extension and membrane ruffling in instances of synaptic pruning or small pathogen elimination in the non-pathological, healthy brain (Figure 36).

Another intriguing aspect of the calcium assays was the apparent time-dependency of PSB0739 on inhibiting the ADP-mediated calcium response (Figure 8), which suggests intricacies in the mechanism of P2Y12 activation. Specifically, the calcium response was attenuated only for cells treated with the inhibitor for 10-20 min prior to the assay, but not for the 1h 20min pre-treatment condition. A possible explanation is that following ligand binding, P2Y12 activates another receptor which essentially takes over the role of P2Y12 by resuming calcium signalling in response to ADP. Studies have shown that different G protein-coupled receptors (GPCRs) are capable of direct interaction and receptor crosstalk, via formation of heterodimers (Ferre et al., 1991). Interestingly, it has been found that P2Y12 can couple with the ADP-binding P2Y1 receptor to form a heterodimer in human tsA201 cells, a modified HEK293 cell line (Davis., 2017). This report presents the possibility that upon P2Y12 ligand binding (whether it is PSB0739 or ADP), within approximately 1.5 h following binding, P2Y12 couples with P2Y1. ADP binding to P2Y1 following this heterodimer formation could initiate a pathway which feeds back into the P2Y12-signalling sequence, resuming calcium release (Figure 37). However, why this coupling would occur with a reversibly-binding antagonist, and why it would take 1.5 h for heterodimer formation to occur while ADP binding immediately initiates the calcium signalling pathway in a matter of seconds, seems rather unusual and the kinetics underlying interactions between P2Y12 and other GPCRs require further study.

High concentration of ADP downregulates P2Y12 expression

Studies of P2Y12 expression regulation produced the novel finding that high-concentration ADP treatment (100μM but not 10μM) for 24h lead to a significant decrease in P2Y12 expression in

microglia, which was not prevented with the addition of PSB0739 (Figure 29, 31). These results suggest that high extracellular ADP concentration regulates P2Y12 expression, but the mechanism is not via ADP-P2Y12 binding. Additionally, I found that ADP and PSB0739 treatments do not affect LPS-mediated P2Y12 downregulation (Figure 32), which also suggests that LPS-mediated downregulation does not involve ADP-P2Y12 interaction.

Given that the P2Y12 downregulation was observed only for the higher concentration of ADP treatment tested, expression regulation may be governed by the concentration of extracellular nucleotides on the microglial cell surface. One possible mechanism is presented below (Figure 37), where downregulation is initiated by the activation of adenosine receptors. It is reasonable to speculate that an accumulation of ADP at the surface leads to greater ADP degradation, resulting in large production of adenosine at the surface. In addition, the role of adenosine receptors in LPS-mediated P2Y12 downregulation has been suggested; Gs-coupled A2A adenosine receptor activation is associated with LPS, TNF-α, or aggregated Aβ-mediated activation of microglia along with concurrent downregulation of P2Y12 receptors (Orr et al., 2009). Extracellular adenosine accumulation and subsequent activation of adenosine receptors is understood to increase rapidly intracellular AMP concentrations, which upregulates 5' AMP-activated protein kinase (AMPK), as studied in a rat epithelial line (Aymerich et al., 2006). Several factors downstream of AMPK activation (i.e. Sirtuin 1 (SIRT1), Peroxisome proliferator-activated receptor gamma coactivator 1-alpha (PGC-1α), p53) are known to mediate inhibition of NF-κB signalling (Salminen et al., 2011). In platelets, NF-κB has been found to bind directly to the promoter of the P2Y12 gene (Rauch et al., 2010), and thus, NF-κB inhibition would yield reduced P2Y12 expression.

Still, there are other transcription factors implicated in the mechanism of P2Y12 transcriptional regulation which suggests that the pathway is much more complex. Interferon regulatory factor 8 (IRF8) and transcription factor PU.1 have been found to bind together at the P2Y12 gene and remain constitutively bound at this locus in resting microglia (Mancino et al., 2015). This finding suggests that the mechanism of P2Y12 maintenance at basal conditions is controlled by IRF8 and PU.1 activity. Moreover, IRF8 is recognized as a transcriptional regulator of a wide range of genes, including P2Y12, underlying microglial motility (Masuda et al., 2014; Masuda et al., 2012). IRF8 has also been found to act in concert with NF-κB to regulate iNOS expression in myeloid cells (Simon et al., 2015). Thus, P2Y12 expression is likely regulated by not only NF-κB , but also PU.1, and IRF8.

The finding that 100μM ADP treatment for 24h leads to a downregulation of P2Y12 expression could prompt further examinations the regulation of extracellular nucleotide levels at the microglia cell surface. The implication from this study is that in healthy microglia, where P2Y12 is constitutively expressed at high levels, the extracellular nucleotide concentrations are in balance and

regulated in some way. Does this mean that a certain ratio of extracellular ATP : ADP : AMP : adenosine is necessary for microglia to maintain regular levels of phagocytosis? The requirement of a maintained nucleotide gradient across the microglial cell membrane for healthy neurological function has been suggested in studies on aging. Namely, a significant depletion of purines in the blood has been found in association with aging (Abraham et al., 2003). Together with the finding that a downregulation of P2Y12 is related to aging (Galatro et al., 2017), these observations suggest that perhaps a low concentration of extracellular ADP outside of microglia, also presents a deviation from the baseline-maintained nucleotide gradient and affects P2Y12 expression with age. Interestingly, purine deficiencies have been associated with neurological dysfunction, such as in Lesch-Nyhan disease (Nyhan, 1997), which further indicate the importance of extracellular nucleotide balance in the brain.

Furthermore, different lengths of treatment time on P2Y12 expression can be explored, as an additional implication is that it is not just an imbalance of the concentration of extracellular nucleotides that is causing downregulation, but it is the fact that the imbalance is prolonged over a few h that is causing this transcriptional change. This point brings up the fact that P2Y12 is perhaps capable of handling acute perturbations in the extracellular environment, but is vulnerable to being depleted when encountering persistent imbalance of extracellular nucleotides.

Examination of the functional significance of downregulation in relation to microglial cell states is also necessary. Given that 24h ADP treatment causes P2Y12 downregulation to the same levels as LPS treatment, it is worth asking if this 24h ADP treated microglia have changed into a different cell state, namely an inflammatory, chronically activated one. Perhaps prolonged ADP treatment at high concentration induces effects on microglia similar to LPS. If so, molecular pathways of LPS-mediated and ADP-mediated downregulation likely converge.

To summarize, my findings suggest that P2Y12 is an important player in maintaining the controlled phagocytic capacity characteristic of homeostatic, unstimulated microglia. On the other hand, P2Y12 is not majorly involved in microglia function in inflammation-activated microglia. P2Y12 is capable of responding to acute stressors in the form of sudden changes in extracellular ADP concentration. Upon sensing these changes, they activate an immediate calcium response, facilitating process extension and membrane ruffling, perhaps not only for the purpose of cell movement toward targets, but also as a way to distinguish small targets, such as pathogens or parts of neurons which are appropriate for ingestion, from whole cells. Upon inflammatory activation by LPS or Aβ, however, P2Y12 expression is downregulated in microglia, which leads to a loss of this size-selectivity, and potentially the loss of this ability underlies the heightened, non-specific phagocytosis exhibited by activated microglia. The mechanism of downregulation of P2Y12 upon inflammatory activation could

involve prolonged exposure to an imbalance in extracellular nucleotide concentrations across the microglial cell membranes.

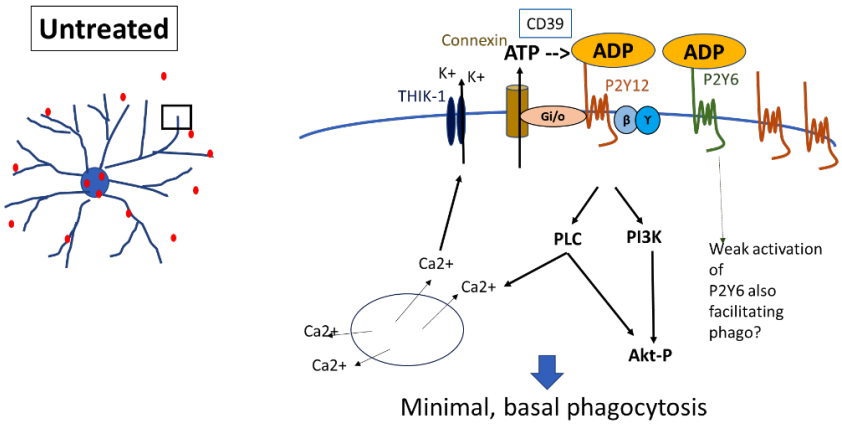

Figure 33. Proposed mechanism for P2Y12-mediated basal phagocytic capacity in untreated, healthy microglia, via self-release of ATP. Under unstimulated conditions, microglial P2Y12 is active at low levels, mediated by self-release of ATP via connexin channels. This minimal level of activation facilitates baseline phagocytosis, which could in part be also mediated by weak P2Y6 activation (as ADP is a weak agonist of P2Y6 as well). There is a low level of calcium mobilization and potassium release through the P2Y12-coupled THIK-1 potassium channel.

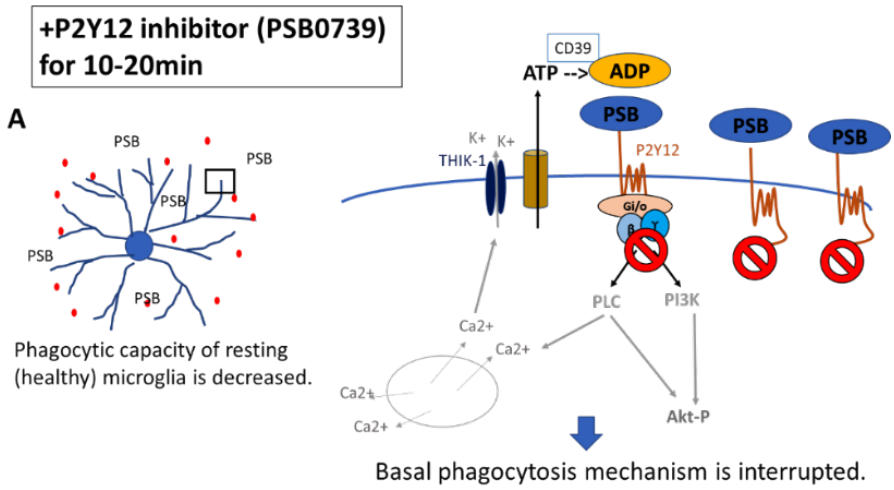

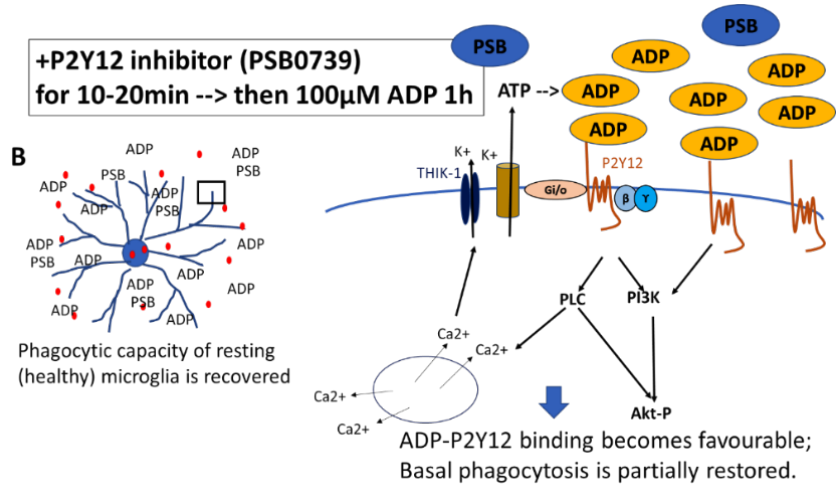

Figure 34. PSB0739 competes with extracellular ADP directly for P2Y12 binding site, which may explain partial restoration of phagocytosis of P2Y12-inhibited cells in the presence of high concentrations of ADP. **A)** Addition of the highly potent PSB0739 blocks P2Y12 activity and reduces the basal phagocytosis levels by inhibiting the PI3K, PLC pathways and stopping calcium and potassium release. **B)** Adding a high concentration of extracellular ADP to P2Y12-inhibited cells results in direct competition between PSB0739 and ADP for the P2Y12 binding site. However the high concentration of ADP shifts the balance slightly toward ADP-P2Y12 binding (instead of PSB0739-P2Y12 binding), partially restoring basal levels of phagocytosis. The recovery may be partial because PSB0739 is still much more potent to P2Y12 than ADP.

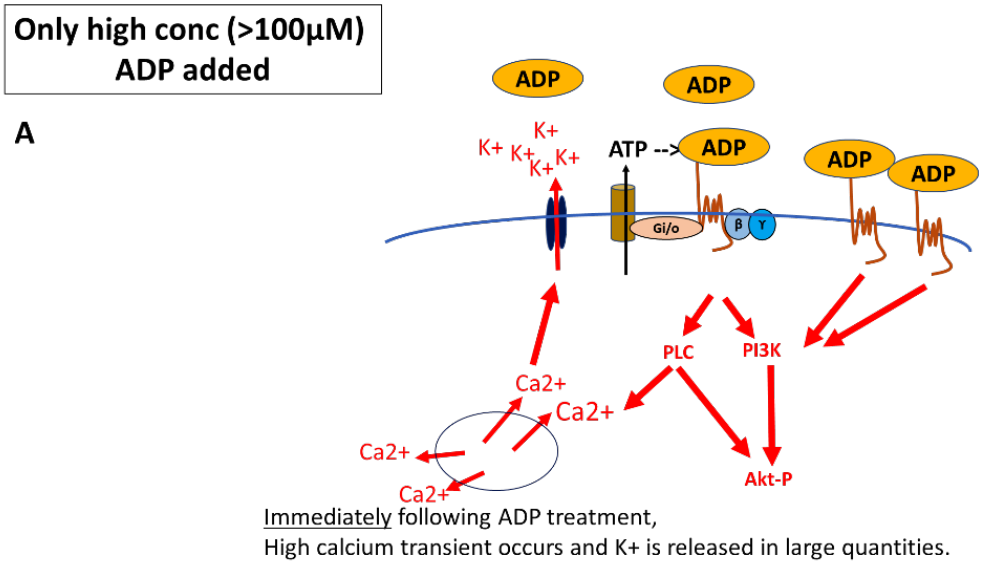

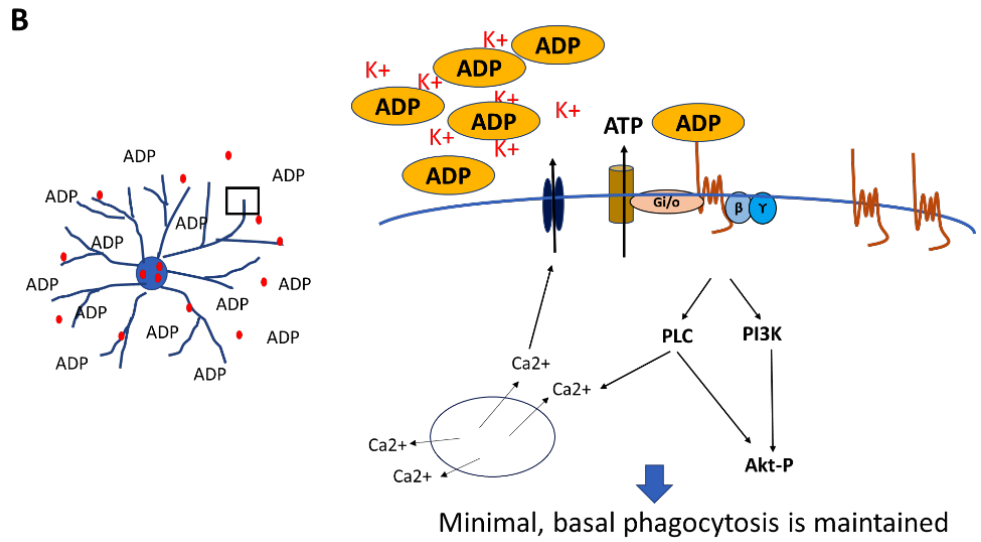

Figure 35. Possible mechanism for maintenance of basal phagocytosis upon high concentration of ADP treatment by calcium and potassium ion-mediated feedback loop. A) High concentration of ADP addition to untreated microglia causes immediate P2Y12 activation and strong calcium release downstream. Strong intracellular calcium release leads to strong potassium efflux from the cell. **B)** The strong release of potassium ions results in potassium ion accumulation on the outside of the cell, and these ions reduce the potency of extracellular ADP to the P2Y12 receptor due to their attraction to the negatively-charged phosphate groups of ADP. This effect of potassium ions could lead to the restoration of basal activation levels of P2Y12.

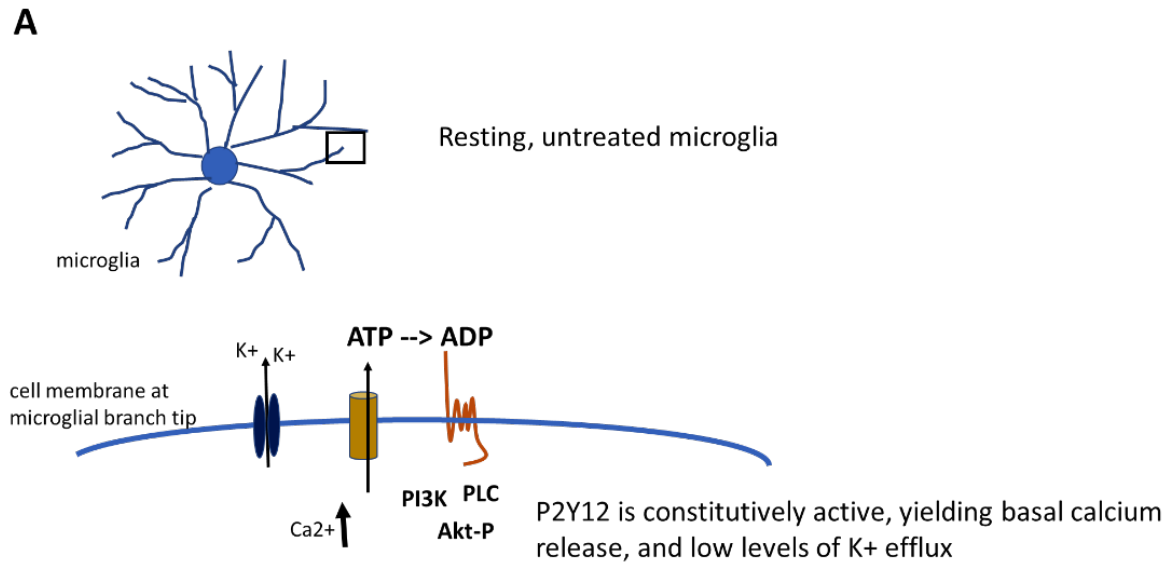

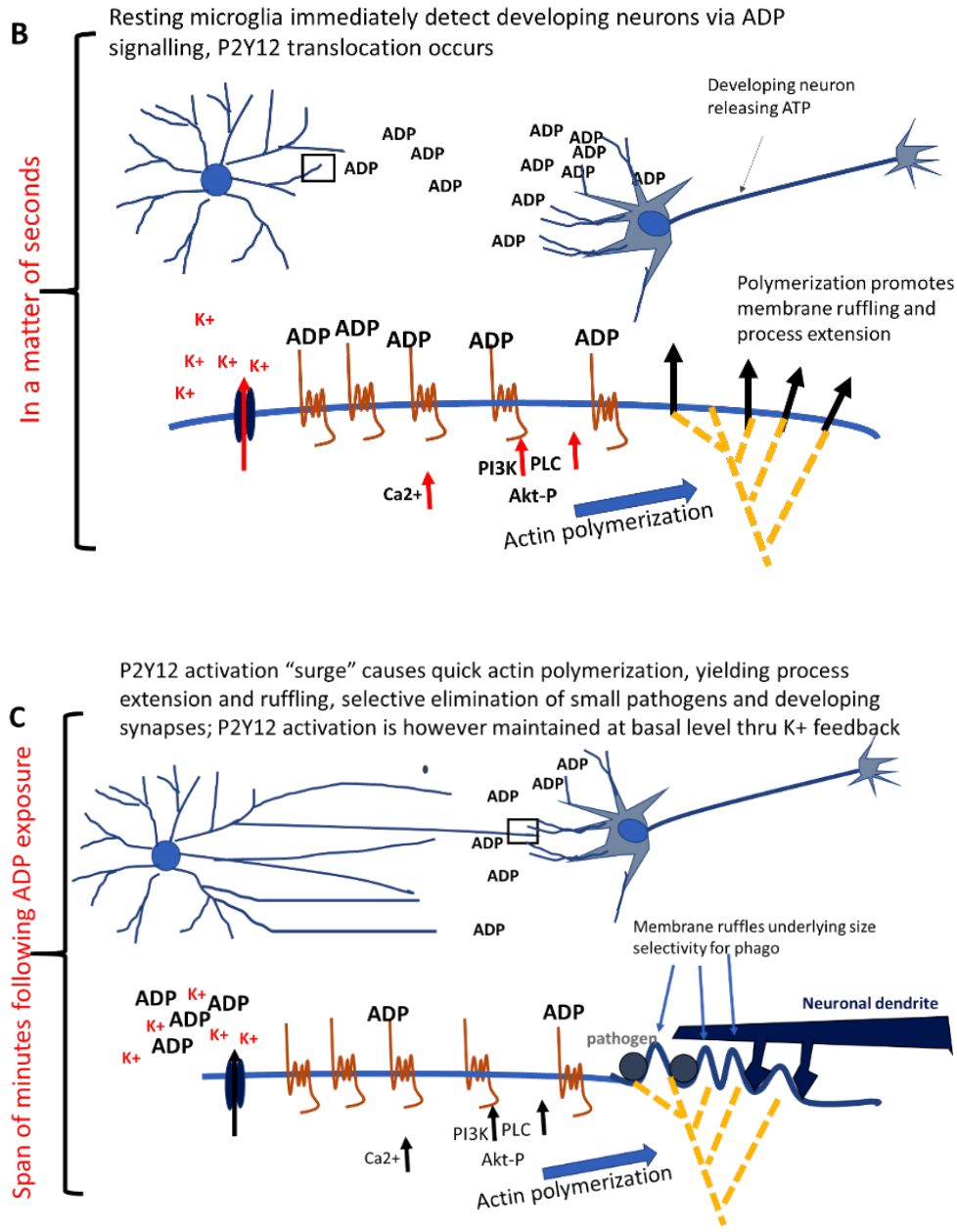

Figure 36. Possible model for P2Y12-mediated process extension and membrane ruffling for purpose of synaptic pruning and small pathogen elimination in healthy microglia. A) Unstimulated microglia likely have constitutively active P2Y12 regulated by self-released ATP which facilitates low release of intracellular calcium and potassium ion efflux. P2Y12 is distributed equally throughout the microglial cell membrane. **B)** However, when the microglia encounters a developing neuron which is releasing ATP (then quickly degraded to ADP), P2Y12 receptors on the microglia congregate at the tips of the microglia processes closest to the ADP source. P2Y12 congregation and activation at this localized position on microglia processes leads to membrane ruffling and process extension. More specifically, where there are high amounts of P2Y12 translocation and activation, there are high amounts of actin polymerization and integrin activation, and thus for this region of the branch, there is elongation and ruffling due to aggregation of polymerized actin within the cytoplasm. **C)** The level of P2Y12 activation may be regulated by calcium and potassium mobilization. Meanwhile, the processes extended help to make the microglia closer in proximity to targets, and ruffling allows for selectivity for smaller targets, such as dendritic spines of developing neurons for synaptic pruning. Additionally, this mechanism of selective phagocytosis of smaller targets mediated by P2Y12 may be applicable to the engulfment of small pathogens by healthy microglia.

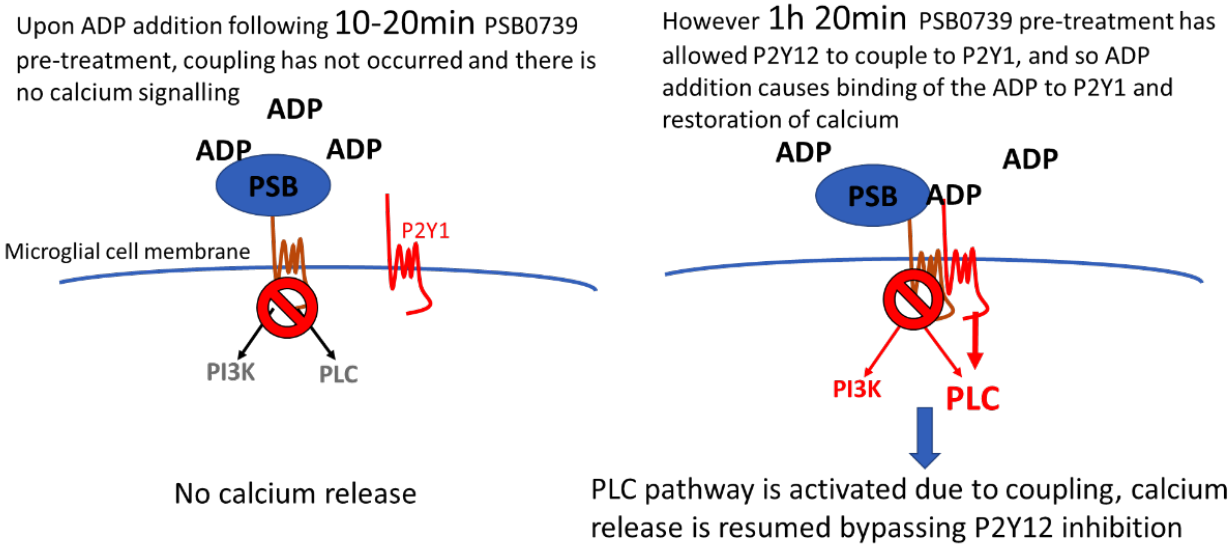

Figure 37. Schematic of possible P2Y1-P2Y12 coupling to explain time-dependency of attenuated calcium response from PSB0739 treatment. The coupling of P2Y12 with another ADP receptor, P2Y1, has been proposed in platelets (P2Y1 is expressed in brain tissue as well). 10-20 min of PSB0739 treatment may not be enough time to allow this coupling to occur, but within 1h 20min of ligand binding to P2Y12, the coupling may occur, such that ADP binding to P2Y1 feeds into the P2Y12 pathway, bypassing inhibition and resumes downstream calcium signalling.

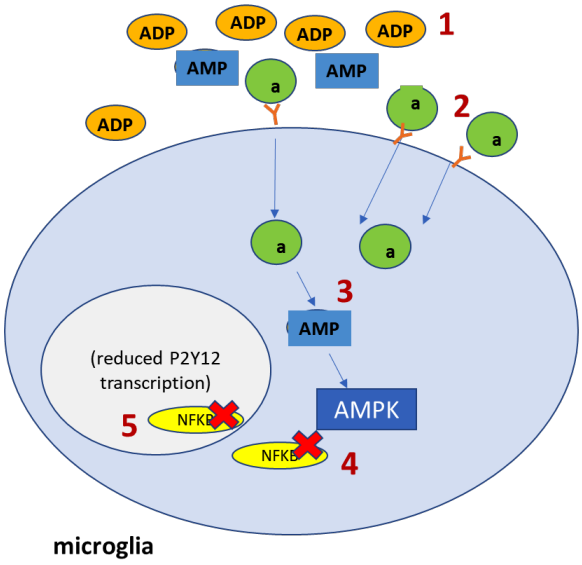

Figure 38. Possible mechanism for prolonged extracellular ADP exposure leading to downregulation of P2Y12 expression. 1) Addition of high concentration ADP causes accumulation of unbound ADP, leading to greater ADP degradation. **2)** ADP degrades to AMP and adenosine via CD73 and CD39; adenosine receptors are activated. **3)** Adenosine is internalized via adenosine receptor, intracellular adenosine is reconverted to AMP, causing increase in intracellular AMP, and activation of AMPK. **4)** AMPK is known to downregulate NF-κB (known to interact directly with P2Y12 promoter in platelets). **5)** In the absence of NF-κB , P2Y12 transcription is halted (which also likely involves IRF8 and PU.1 transcription factors).

Conclusion

In this thesis, I aimed to study the effect of P2Y12 antagonism on LPS-induced microglial phagocytosis of neurons. My findings principally suggest that P2Y12 does not play a significant role in LPS-induced microglia, and inhibition of P2Y12 does not protect neurons from heightened phagocytosis under LPS stimulus. Instead, my results reveal a novel role of P2Y12 in the maintenance of basal phagocytosis observed in homeostatic, unstimulated microglia. The baseline phagocytic capacity is sustained even upon acute changes in extracellular ADP, which seems to be governed by immediate activation of a P2Y12-mediated intracellular calcium signalling pathway. Moreover, this study further shows that high concentration ADP treatment downregulates P2Y12 mRNA expression. Although the exact mechanism of regulation is still unclear, given that LPS mediates a similar downregulation of P2Y12, the possibility emerges that prolonged extracellular nucleotide imbalance is involved in the transformation of microglia to the chronically active, phagocytic state under inflammatory stress. Following these findings, future studies could potentially be directed toward exploring what constitutes extracellular nucleotide imbalance in the brain and seeking ways in which P2Y12 expression can be recovered in diseased microglia to allow re-emergence of homeostatic microglia which will restore normal levels of phagocytosis, with the ultimate aim of treating neurodegenerative disorders.

References Cited

Abbracchio MP and Verderio C. Pathophysiological roles of P2 receptors in glial cells. Novartis Found Symp. 2006; 276:91-103; discussion 103-12, 275-81.

Abraham EH, Salikhova AY, Rapaport E. ATP in the treatment of advanced cancer. Current topics in membranes. 2003; 1:415-52.

Akiyama H, Kawamata T, Dedhar S, McGeer PL. Immunohistochemical localization of vitronectin, its receptor and beta-3 integrin in Alzheimer brain tissue. Journal of neuroimmunology. 1991 Apr 1;32(1):19-28.

Aymerich I, Foufelle F, Ferré P, Casado FJ, Pastor-Anglada M. Extracellular adenosine activates AMP-dependent protein kinase (AMPK). J Cell Sci. 2006 Apr 15;119(8):1612-21.

Bal□Price A, Matthias A, Brown GC. Stimulation of the NADPH oxidase in activated rat microglia removes nitric oxide but induces peroxynitrite production. Journal of neurochemistry. 2002 Jan 1;80(1):73-80.

Blasi E, Barluzzi R, Bocchini V, Mazzolla R, Bistoni F. Immortalization of murine microglial cells by a v-raf/v-myc carrying retrovirus. J Neuroimmunol. 1990; 27:229-237.

Bocchini V, Mazzolla R, Barluzzi R, Blasi E, Sick P, Kettenmann H. An immortalized cell line expresses properties of activated microglial cells. J Neurosci Res. 1992; 31:616-621.

Bohlen CJ, Bennett FC, Tucker AF, Collins HY, Mulinyawe SB, Barres BA. Diverse requirements for microglial survival, specification, and function revealed by defined-medium cultures. Neuron. 2017 May 17;94(4):759-73.

Brown GC, Neher JJ. Microglial phagocytosis of live neurons. Nat Rev Neurosci. 2014; 15:209-216.

Cannon GJ, Swanson JA. The macrophage capacity for phagocytosis. Journal of cell science. 1992 Apr 1;101(4):907-13.

CAPRIE Steering Committee. A randomised, blinded, trial of clopidogrel versus aspirin in patients at risk of ischaemic events (CAPRIE). Lancet. 1996; 348(9038): 1329-39.

Champion JA, Mitragotri S. Shape induced inhibition of phagocytosis of polymer particles. Pharmaceutical research. 2009 Jan 1;26(1):244-9.

Charles JF, Humphrey MB, Zhao X, Quarles E, Nakamura MC, Aderem A, Seaman WE, Smith KD. The innate immune response to Salmonella enterica serovar Typhimurium by macrophages is dependent on TREM2-DAP12. Infection and immunity. 2008 Jun 1;76(6):2439-47.

Chekeni FB, Elliott MR, Sandilos JK, Walk SF, Kinchen JM, Lazarowski ER, Armstrong AJ, Penuela S, Laird DW, Salvesen GS, Isakson BE. Pannexin 1 channels mediate 'find-me'signal release and membrane permeability during apoptosis. Nature. 2010 Oct;467(7317):863.

Cisneros-Mejorado A, Pérez-Samartín A, Gottlieb M, Matute C. ATP signaling in brain: release, excitotoxicity and potential therapeutic targets. Cellular and molecular neurobiology. 2015 Jan 1;35(1):1-6.

Combs CK, Johnson DE, Cannady SB, Lehman TM, Landreth GE. Identification of microglial signal transduction pathways mediating a neurotoxic response to amyloidogenic fragments of beta-amyloid and prion proteins. J Neurosci. 1999; 19:928-939.

Corriden R, Insel PA. Basal release of ATP: an autocrine-paracrine mechanism for cell regulation. Sci. Signal.. 2010 Jan 12;3(104):re1-.

Cunningham CI, Martinez-Cerdeno V, Noctor SC. Microglia regulate the number of neural precursor cells in the developing cerebral cortex. J Neurosci. 2013; 33:4216-4233.

D'amelio M, Cavallucci V, Middei S, Marchetti C, Pacioni S, Ferri A, Diamantini A, De Zio D, Carrara P, Battistini L, Moreno S. Caspase-3 triggers early synaptic dysfunction in a mouse model of Alzheimer's disease. Nature neuroscience. 2011 Jan;14(1):69.

Davalos D, Grutzendler J, Yang G, Kim JV, Zuo Y, Jung S, Littman DR, Dustin ML, Gan WB. ATP mediates rapid microglial response to local brain injury in vivo. Nature neuroscience. 2005 Jun;8(6):752.

Davis S. *Biochemical and Molecular Characterisation of the Proposed P2Y1-P2Y12 Receptor Heterodimer in TsA201 Cells* (Doctoral dissertation).

De Simone R, Niturad CE, De Nuccio C, Ajimone-Cat MA, Visentin S, Minghetti L. TFG- β and LPS modulate ADP-induced migration of microglial cells through P2Y1 and P2Y12 receptor expression. J Neurochemistry. 2010; 115:450-459.

Dewil M, Van Den Bosch L, Robberecht W. Microglia in amyotrophic lateral sclerosis. Acta Neurologica Belgica. 2007 Sep 1;107(3):63.

Dibaj P, Nadrigny F, Steffens H, Scheller A, Hirrlinger J, Schomburg ED, Neusch C, Kirchhoff F. NO mediates microglial response to acute spinal cord injury under ATP control in vivo. Glia. 2010 Jul 1;58(9):1133-44.

Dissing-Olesen L, LeDue JM, Rungta RL, Hefendehl JK, Choi HB, MacVicar BA. Activation of neuronal NMDA receptors triggers transient ATP-mediated microglial process outgrowth. J Neurosci. 2014;34:10511-10527.

Di Virgilio F, Ceruti S, Bramanti P, Abbracchio MP. Purinergic signaling in inflammation of the central nervous system. Trends Neurosci 2009; 32:79-87.

Elliott MR, Chekeni FB, Trampont PC, Lazarowski ER, Kadl A, Walk SF, Park D, Woodson RI, Ostankovich M, Sharma P, Lysiak JJ. Nucleotides released by apoptotic cells act as a find-me signal to promote phagocytic clearance. Nature. 2009 Sep;461(7261):282.

Ferre S, Von Euler G, Johansson B, Fredholm BB, Fuxe K. Stimulation of high-affinity adenosine A2 receptors decreases the affinity of dopamine D2 receptors in rat striatal membranes. Proceedings of the National Academy of Sciences. 1991 Aug 15;88(16):7238-41.

Fitzgerald KA, Rowe DC, Barnes BJ, Caffrey DR, Visintin A, Latz E, Monks B, Pitha PM, Golenbock DT. LPS-TLR4 signaling to IRF-3/7 and NF-κB involves the toll adapters TRAM and TRIF. Journal of Experimental Medicine. 2003 Oct 6;198(7):1043-55.

Foster CJ, Prosser DM, Agans JM, Zhai Y, Smith MD, Lachowicz JE, Zhang FL, Gustafson E, Monsma FJ Jr, Wiekowski MT, Abbondanzo SJ, Cook DN, Bayne ML, Lira SA, Chintala MS. Molecular identification and characterization of the platelet ADP receptor targeted by thienopyridine antithrombotic drugs. J Clin Invest. 2001; 107(12):1591-1598.

Fricker M, Neher JJ, Zhao JW, Théry C, Tolkovsky AM, Brown GC. MFG-E8 mediates primary phagocytosis of viable neurons during neuroinflammation. Journal of Neuroscience. 2012 Feb 22;32(8):2657-66.

Fuller AD, Van Eldik LJ. MFG-E8 regulates microglial phagocytosis of apoptotic neurons. Journal of Neuroimmune Pharmacology. 2008 Dec 1;3(4):246-56.

Galatro TF, Holtman IR, Lerario AM, Vainchtein ID, Brouwer N, Sola PR, Veras MM, Pereira TF, Leite RE, Möller T, Wes PD. Transcriptomic analysis of purified human cortical microglia reveals age-associated changes. Nature neuroscience. 2017 Aug;20(8):1162.

Gao HM, Zhou H, Hong JS. NADPH oxidases: novel therapeutic targets for neurodegenerative diseases. Trends in pharmacological sciences. 2012 Jun 1;33(6):295-303.

Gomez-Nicola D, Perry VH. Microglial dynamics and role in the healthy and diseased brain: a paradigm of functional plasticity. The Neuroscientist. 2015 Apr;21(2):169-84.

Greene L and Tischer A. Establishment of a noradrenergic clonal line of rat adrenal pheochromocytoma cells which respond to nerve growth factor. Proc Natl Acad Sci USA. 1976; 73:2424-2428.

Guerreiro R, Wojtas A, Bras J, Carrasquillo M, Rogaeva E, Majounie E, Cruchaga C, Sassi C, Kauwe JS, Younkin S, Hazrati L. TREM2 variants in Alzheimer's disease. New England Journal of Medicine. 2013 Jan 10;368(2):117-27.

Hanisch UK, Kettenmann H. Microglia: active sensor and versatile effector cells in the normal and pathologic brain. Nature neuroscience. 2007 Nov;10(11):1387.

Haynes SE, Hollopeter G, Yang G, Kurpius D, Dailey ME, Gan WB, Julius D. The P2Y12 receptor regulates microglial activation by extracellular nucleotides. Nat Neurosci. 2006; 9:1512-1519.

Henn A, Lund S, Hedtjärn M, Schrattenholz A, Pörzgen P, Leist M. The suitability of BV2 cells as alternative model system for primary microglia cultures or for animal experiments examining brain inflammation. ALTEX: Alternatives to animal experimentation. 2009;26(2):83-94.

Hickman SE, Kingery ND, Ohsumi TK, Borowsky ML, Wang LC, Means TK, El Khoury J. The microglial sensome revealed by direct RNA sequencing. Nature neuroscience. 2013 Dec;16(12):1896.

Hickman SE, El Khoury J. TREM2 and the neuroimmunology of Alzheimer's disease. Biochemical pharmacology. 2014 Apr 15;88(4):495-8.

Hoffmann K, Baqi Y, Morena MS, Glänzel M, Müller CE, Von Kügelgen I. Interaction of new, very potent non-nucleotide antagonists with Arg256 of the human platelet P2Y12 receptor. Journal of Pharmacology and Experimental Therapeutics. 2009 Nov 1;331(2):648-55.

Hollopeter G, Jantzen HM, Vincent D, Li G, England L, Ramakrishnan V, Yang RB, Nurden P, Nurden A, Julius D, Conley PB. Identification of the platelet ADP receptor targeted by antithrombotic drugs. Nature 2001; 409 (6817):202-207.

Holtman IR, Raj DD, Miller JA, Schaafsma W, Yin Z, Brouwer N, Wes PD, Möller T, Orre M, Kamphuis W, Hol EM. Induction of a common microglia gene expression signature by aging and neurodegenerative conditions: a co-expression meta-analysis. Acta neuropathologica communications. 2015 Dec;3(1):31.

Honda S, Sasaki Y, Ohsawa K, Imai Y, Nakamura Y, Inoue K, Kohsaka S. Extracellular ATP or ADP induce chemotaxis of cultured microglia through Gi/o-coupled P2Y receptors. J Neurosci 2001; 21:1975-1982.

Hornik TC, Vilalta A, Brown GC. Activated microglia cause reversible apoptosis of pheochromocytoma cells, inducing their cell death by phagocytosis. J Cell Sci 2016; 129(1):65-79.

Inoue K. The function of microglia through purinergic receptors: neuropathic pain and cytokine release. Pharmacol Ther. 2006; 109:210-226.

Irino Y, Nakamura Y, Inoue K, Kohsaka S, Ohsawa K. Akt activation is involved in P2Y12 receptor-mediated chemotaxis of microglia. J Neurosci Res. 2008; 86:1511-1519.

Jones BM, Sethi-Dua P, Zhao Y, Bhattacharjee S, Hill JM, Lukiw W. Regulating amyloidogenesis through the natural triggering receptor expressed in myeloid/microglial cells 2 (TREM2). Frontiers in cellular neuroscience. 2014 Mar 31;8:94.

Jonsson T, Stefansson H, Steinberg S, Jonsdottir I, Jonsson PV, Snaedal J, Bjornsson S, Huttenlocher J, Levey AI, Lah JJ, Rujescu D. Variant of TREM2 associated with the risk of Alzheimer's disease. New England Journal of Medicine. 2013 Jan 10;368(2):107-16.

Kaminska B, Gozdz A, Zawadzka M, Ellert□Miklaszewska A, Lipko M. MAPK signal transduction underlying brain inflammation and gliosis as therapeutic target. The Anatomical Record. 2009 Dec 1;292(12):1902-13.

Kanazawa H, Ohsawa K, Sasaki Y, Kohsaka S, Imai Y. Macrophage/microglia-specific protein Iba1 enhances membrane ruffling and Rac activation via phospholipase C-γ-dependent pathway. Journal of Biological Chemistry. 2002 May 31;277(22):20026-32.

Kao AW, Eisenhut RJ, Martens LH, Nakamura A, Huang A, Bagley JA, Zhou P, de Luis A, Neukomm LJ, Cabello J, Farese RV, Kenyon C. A neurodegenerative disease mutation that accelerates the clearance of apoptotic cells. Proc. Natl, Acad. Sci. USA 2011; 108:4441-4446.

Keren-Shaul H, Spinrad A, Weiner A, Matcovitch-Natan O, Dvir-Szternfeld R, Ulland TK, David E, Baruch K, Lara-Astaiso D, Toth B, Itzkovitz S. A unique microglia type associated with restricting development of Alzheimer's disease. Cell. 2017 Jun 15;169(7):1276-90.

Koizumi S, Shigemoto-Mogami Y, Nasu-Tada K, Shinozaki Y, Ohsawa K, Tsuda M, Joshi BV, Jacobson KA, Kohsaka S, Inoue K. UDP acting at P2Y 6 receptors is a mediator of microglial phagocytosis. Nature. 2007 Apr;446(7139):1091.

Koizumi S, Ohsawa K, Inoue K, Kohsaka S. Purinergic receptors in microglia: functional modal shifts of microglia mediated by P2 and P1 receptors. Glia. 2013 Jan 1;61(1):47-54.

Kreutzberg GW. Microglia: a sensor for pathological events in the CNS. Trends in neurosciences. 1996 Aug 1;19(8):312-8.

Lazarowski ER. Vesicular and conductive mechanisms of nucleotide release. Purinergic signalling. 2012 Sep 1;8(3):359-73.

Lee JE, Liang KJ, Fariss RN, Wong WT. Ex vivo dynamic imaging of retinal microglia using time-lapse confocal microscopy. Investigative ophthalmology & visual science. 2008 Sep 1;49(9):4169-76.

Lim HM, Heo W, Han JW, Lee MG, Kim JY. NPP1 is responsible for potent extracellular ATP hydrolysis as NTPDase1 in primary cultured murine microglia. Purinergic signalling. 2018 Jun 1;14(2):157-66.

Madry C, Kyrargyri V, Arancibia-Cárcamo IL, Jolivet R, Kohsaka S, Bryan RM, Attwell D. Microglial ramification, surveillance, and interleukin-1β release are regulated by the two-pore domain K+ channel THIK-1. Neuron. 2018 Jan 17;97(2):299-312.

Madry C, Arancibia-Cárcamo IL, Kyrargyri V, Chan VT, Hamilton NB, Attwell D. Effects of the ecto-ATPase apyrase on microglial ramification and surveillance reflect cell depolarization, not ATP depletion. Proceedings of the National Academy of Sciences. 2018 Jan 30:201715354.

Maeda M, Tsuda M, Tozaki-Saitoh H, Inoue K, Kiyama H. Nerve injury-activated microglia engulf myelinated axons in a P2Y12 signaling-dependent manner in the dorsal horn. Glia. 2010; 58:1838-1846.

Mancino A, Termanini A, Barozzi I, Ghisletti S, Ostuni R, Prosperini E, Ozato K, Natoli G. A dual cis-regulatory code links IRF8 to constitutive and inducible gene expression in macrophages. Genes & development. 2015 Feb 15;29(4):394-408.

Marin-Teva JL, Dusart I, Colin C, Gervais A, van Rooijen N, Mallat M. Microglia promote the death of developing Purkinje cells. Neuron 2004; 41(4):535-47.

Marker DF, Puccini JM, Mockus TE, Barbieri J, Lu SM, Gelbard HA. LRRK2 Kinase inhibition prevents pathological microglial phagocytosis in response to HIV-1 Tat protein. J Neuroinflammation 2012; 9:261.

Masuda T, Nishimoto N, Tomiyama D, Matsuda T, Tozaki-Saitoh H, Tamura T, Kohsaka S, Tsuda M, Inoue K. IRF8 is a transcriptional determinant for microglial motility. Purinergic signalling. 2014 Sep 1;10(3):515-21.

Masuda T, Tsuda M, Yoshinaga R, Tozaki-Saitoh H, Ozato K, Tamura T, Inoue K. IRF8 is a critical transcription factor for transforming microglia into a reactive phenotype. Cell reports. 2012 Apr 19;1(4):334-40.

Michel AD, Xing M, Humphrey PP. Serum constituents can affect 2′□& 3′□O□(4□benzoylbenzoyl)□ATP potency at P2X7 receptors. British journal of pharmacology. 2001 Apr 1;132(7):1501-8.

Möller T, Kann O, Verkhratsky A, Kettenmann H. Activation of mouse microglial cells affects P2 receptor signaling. Brain research. 2000 Jan 17;853(1):49-59.

Möller T. Calcium signaling in microglial cells. Glia. 2002 Nov 1;40(2):184-94.

Moore CS, Ase AR, Kinsara A, Rao VTS, Michell-Robinson M, Leong SY, Butovsky O, Ludwin SK, Seguela P, Bar-Or A, Antel JP. P2Y12 expression and function in alternatively activated human microglia. Neurol Neuroimmunol Neuroinflamm. 2015;2;e80.

Nasu□Tada K, Koizumi S, Inoue K. Involvement of β1 integrin in microglial chemotaxis and proliferation on fibronectin: different regulations by ADP through PKA. Glia. 2005 Nov 1;52(2):98-107.

Nawarskas JJ, Clark SM. Ticagrelor: A novel reversible oral antiplatelet agent. Cardiol Rev 2011; 19:85-100.

N'Diaye EN, Branda CS, Branda SS, Nevarez L, Colonna M, Lowell C, Hamerman JA, Seaman WE. TREM-2 (triggering receptor expressed on myeloid cells 2) is a phagocytic receptor for bacteria. J Cell Biol. 2009 Jan 26;184(2):215-23.

Neher JJ, Neniskyte U, Zhao JW, Bal-Price A, Tolkovsky AM, Brown GC. Inhibition of microglial phagocytosis is sufficient to prevent inflammatory neuronal death. J Immunol 2011;186:4973-4983.

Neher JJ, Neniskyte U, Hornik T, Brown GC. Inhibition of UDP/P2Y6 purinergic signaling prevents phagocytosis of viable neurons by activated microglia in vitro and in vivo. Glia. 2014 Sep;62(9):1463-75.

Neniskyte U, Neher JJ, Brown GC. Neuronal Death Induced by Nanomolar Amyloid β Is Mediated by Primary Phagocytosis of Neurons by Microglia. J of Biological Chemistry. 2011; 286(46):39904-39913.

Neniskyte U, Brown GC. Lactadherin/MFG□E8 is essential for microglia□mediated neuronal loss and phagoptosis induced by amyloid β. Journal of neurochemistry. 2013 Aug 1;126(3):312-7.

Nomura K, Vilalta A, Allendorf DH, Hornik TC, Brown GC. Activated microglia desialylate and phagocytose cells via neuraminidase, galectin-3, and mer tyrosine kinase. The Journal of Immunology. 2017 Jun 15;198(12):4792-801.

Nyhan WL. The recognition of Lesch-Nyhan syndrome as an inborn error of purine metabolism. Journal of inherited metabolic disease. 1997 Jun 1;20(2):171-8.

Ohsawa K, Irino Y, Sanagi T, Nakamura Y, Suzuki E, Inoue K, Kohsaka S. P2Y12 receptor-mediated integrin-β1 activation regulates microglial process extension induced by ATP. Glia. 2010; 58:790-801.

Ohsawa K, Imai Y, Kanazawa H, Sasaki Y, Kohsaka S. Involvement of Iba1 in membrane ruffling and phagocytosis of macrophages/microglia. J Cell Sci. 2000 Sep 1;113(17):3073-84.

Orr AG, Orr AL, Li XJ, Gross RE, Traynelis SF. Adenosine A 2A receptor mediates microglial process retraction. Nature neuroscience. 2009 Jul;12(7):872.

Pankratov Y, Lalo U, Verkhratsky A, North RA. Vesicular release of ATP at central synapses. Pflügers Archiv. 2006 Aug 1;452(5):589-97.

Paolicelli RC, Bolasco G, Pagani F, Maggi L, Scianni M, Panzanelli P, Giustetto M, Ferreira TA, Guiducci E, Dumas L, Ragozzino D, Gross CT. Synaptic pruning by microglia is necessary for normal brain development. Science 2011; 333(6048):1456-8.

Pausch MH, Lai M, Tseng E, Paulsen J, Bates B, Kwak S. Functional expression of human and mouse P2Y12 receptors in Saccharomyces cerevisiae. Biochemical and biophysical research communications. 2004 Nov 5;324(1):171-7.

Perry VH, Holmes C. Microglial priming in neurodegenerative disease. Nature Reviews Neurology. 2014 Apr;10(4):217.

Potucek YD, Crain JM, Watters JJ. Purinergic receptors modulate MAP kinases and transcription factors that control microglial inflammatory gene expression. Neurochem Int 2006; 49:204-214.

Raju NC, Eikelboom JW, Hirsh J. Platelet ADP-receptor antagonists for cardiovascular disease: Past, present and future. Nat Clin Pract Cardiovasc Med 2008; 5(12):766-780.

Ransohoff RM, Perry VH. Microglial physiology: unique stimuli, specialized responses. Annu Rev Immunol. 2009; 27:119-45.

Rauch BH, Rosenkranz AC, Ermler S, Böhm A, Driessen J, Fischer JW, Sugidachi A, Jakubowski JA, Schrör K. Regulation of functionally active P2Y12 ADP receptors by thrombin in human smooth muscle cells and the

presence of P2Y12 in carotid artery lesions. Arteriosclerosis, thrombosis, and vascular biology. 2010 Dec 1;30(12):2434-42.

Reed-Geaghan FG, Savage JC, Hise AG, Landreth GE. CD14 and toll-like receptors 2 and 4 are required for fibrillar A-beta-stimulated microglial activation. J Neurosci 2009; 29:11982-11992.

Rogers, J., Mastroeni, D., Leonard, B., Joyce, J. and Grover, A., 2007. Neuroinflammation in Alzheimer's disease and Parkinson's disease: are microglia pathogenic in either disorder?. *International review of neurobiology*, *82*, pp.235-246.

Rudt S, Müller RH. In vitro phagocytosis assay of nano-and microparticles by chemiluminescence. III. Uptake of differently sized surface-modified particles, and its correlation to particle properties and in vivo distribution. European journal of pharmaceutical sciences. 1993 Mar 1;1(1):31-9.

Salminen A, Hyttinen JM, Kaarniranta K. AMP-activated protein kinase inhibits NF-κB signaling and inflammation: impact on healthspan and lifespan. Journal of molecular medicine. 2011 Jul 1;89(7):667-76.

Saponaro C, Cianciulli A, Calvello R, Dragone T, Iacobazzi F, Panaro MA. The PI3K/Akt pathway is required for LPS activation of microglial cells. Immunopharmacology and immunotoxicology. 2012 Oct 1;34(5):858-65.

Sasaki Y et al. Selective expression of Gi/o-coupled ATP receptor P2Y12 in microglia in rat brain. Glia 2003; 44(3):242-250.

Savi P et al. P2Y12, a new platelet ADP receptor, target of clopidogrel. Biochem Biophys Res Commun 2001; 283(2):379-383.

Schafer DP, Lehrman EK, Kautzman AG, Koyama R, Mardinly AR, Yamasaki R, Ransohoff RM, Greenberg ME, Barres BA, Stevens B. Microglia sculpt postnatal neural circuits in an activity and complement-dependent manner. Neuron 2012; 74(4):691-705.

Schmidt P, Ritscher L, Dong EN, Hermsdorf T, Coster M, Wittkopf D, Meiler J, Schoneberg T. Identification of determinants required for agonistic and inverse agonistic ligand properties at the ADP receptor P2Y12. Molecular pharmacology. 2012 Oct 23:mol-112.

Simon J, Filippov AK, Goransson S, Wong YH, Felin C, Michel AD, Brown DA, Barnard EA. Characterization and channel coupling of the P2Y(12) nucleotide receptor of brain capillary endothelial cells. J Biol Chem 2002; 277 (35):31390-31400.

Sipe GO, Lowery RL, Tremblay ME, Kelly EA, Lamantia CE, Majewska AK. Microglial P2Y12 is necessary for synaptic plasticity in mouse visual cortex. Nature Communications. 2016; 1-15.

Stadelmann C, Brück W, Bancher C, Jellinger K, Lassmann H. Alzheimer disease: DNA fragmentation indicates increased neuronal vulnerability, but not apoptosis. Journal of Neuropathology & Experimental Neurology. 1998 May 1;57(5):456-64.

Swiatkowski P, Murugan M, Eyo UB, Wang Y, Rangaraju S, Oh SB, Wu LJ. Activation of microglial P2Y12 receptor is required for outward potassium currents in response to neuronal injury. Neuroscience. 2016 Mar 24;318:22-33.

Tabata Y, Ikada Y. Effect of the size and surface charge of polymer microspheres on their phagocytosis by macrophage. Biomaterials. 1988 Jul 1;9(4):356-62.

Takayama F, Hayashi Y, Wu Z, Liu Y, Nakanishi H. Diurnal dynamic behavior of microglia in response to infected bacteria through the UDP-P2Y 6 receptor system. Scientific reports. 2016 Jul 21;6:30006.

Von Kugelgen, I. Pharmacological profiles of cloned mammalian P2Y-receptor subtypes. Pharmacology & Therapeutics 2006; 110(3): 415-432.

Wallentin L, Becker RC, Budaj A, Cannon CP, Emanuelsson H, Held C, Horrow J, Husted S, James S, Katus H, Mahaffey KW. Ticagrelor versus clopidogrel in patients with acute coronary syndromes. New England Journal of Medicine. 2009 Sep 10;361(11):1045-57.

Wyss-Coray T, Rogers J. Inflammation in Alzheimer disease-a brief review of the basic science and clinical literature. Cold Spring Harb Perspect Med. 2012; 1.

Zhang Y, Chen K, Sloan SA, Bennett ML, Scholze AR, O'Keeffe S, Phatnani HP, Guarnieri P, Caneda C, Ruderisch N, Deng S. An RNA-sequencing transcriptome and splicing database of glia, neurons, and vascular cells of the cerebral cortex. Journal of Neuroscience. 2014 Sep 3;34(36):11929-47.

Zhao Y, Wu X, Li X, Jiang LL, Gui X, Liu Y, Sun Y, Zhu B, Piña-Crespo JC, Zhang M, Zhang N. TREM2 is a receptor for β-amyloid that mediates microglial function. Neuron. 2018 Mar 7;97(5):1023-31.